Biosorption of Hexavalent Chromium Cr(VI) from Synthetic Waste Solutions by Novel Modified and Raw Lignocellulosic Biosorbents

A Dissertation submitted to the
Indian Institute of Technology Guwahati
for the Award of the Degree of

Doctor of Philosophy

Submitted by

Abhishek Ajmani

Roll No: 146106015

Under the supervision of

Dr. Selvaraju Narayanasamy

Department of Biosciences and Bioengineering

Indian Institute of Technology Guwahati

Assam

March 2020

Dedicated to my parents

INDIAN INSTITUTE OF TECHNOLOGY GUWAHATI

DEPARTMENT OF BIOSCIENCES AND BIOENGINEERING

GUWAHATI-781039

DECLARATION

I, hereby declare that the matter embodied in this thesis entitled "**Biosorption of Hexavalent Chromium Cr(VI) from Synthetic Waste Solutions by Novel Modified and Raw Lignocellulosic Biosorbents**" is the result of investigations carried out by me under the supervision of **Dr. Selvaraju Narayanasamy**, Department of Biosciences and Bioengineering, Indian Institute of Technology Guwahati, Guwahati, India for the award of degree of Doctor of Philosophy. This work has not been submitted elsewhere for any degree, diploma, associateship or membership etc. of any Institute or University to the best of my knowledge and belief.

IIT Guwahati — Abhishek Ajmani

March 18, 2020 — Roll No. 146106015

INDIAN INSTITUTE OF TECHNOLOGY GUWAHATI

DEPARTMENT OF BIOSCIENCES AND BIOENGINEERING

GUWAHATI-781039

Dr. Selvaraju Narayanasamy
Assistant Professor
Department of Biosciences and Bioengineering

Tel. No.: +91-361-2583210
Fax No.: +91-361-2582249
E-mail: selva@iitg.ac.in

CERTIFICATE

This is to certify that the thesis entitled "**Biosorption of Hexavalent Chromium Cr(VI) from Synthetic Waste Solutions by Novel Modified and Raw Lignocellulosic Biosorbents**" being submitted to the **Indian Institute of Technology Guwahati** by **Abhishek Ajmani** for the award of the degree of **Doctor of Philosophy** in **Biosciences and Bioengineering,** is a bona fide record of research work carried out by him. The contents of this thesis have not been submitted to any other University or Institute for the award of any degree or diploma.

IIT Guwahati

March 18, 2020

Dr. Selvaraju Narayanasamy

(Thesis supervisor)

ACKNOWLEDGMENT

I express my sincere gratitude to my research advisor ***Dr. Selvaraju Narayanasamy*** *for his guidance, patience, valuable discussion, tolerance and continuous moral support encouragement and help in all possible ways. I am humbled and grateful to have him as my Thesis supervisor. I am indebted by his kind, positive attitude and placing confidence and trust in me to be his student. I am also grateful to him for letting me pursue my own ideas and I am privileged to work in his lab.*

I have no words for expressing gratitude to ex Dean of Students' Affairs ***Prof. Chandan Mahanta*** *and ex Department HOD* ***Prof. Kannan Pakshirajan*** *for their administrative capability and problem solving attitude. It is by their cooperation only that I am able to complete my Ph.D.*

I would like to thank my Doctoral committee: ***Dr. Senthil Sivaprakasam****, Chairman of Doctoral Committee and members* ***Professor Kannan Pakshirajan****,* ***Dr. Prabhu Vairakannu*** *for their intellectual support, encouragement and valuable suggestions.*

I would like to thank ex HOD ***Prof. V. V. Dasu, Prof. Kannan Pakshirajan*** *and the current HOD* ***Prof. Latha Rangan*** *for providing Departmental facilities.*

I would like to thank MHRD and IIT Guwahati for financial support.

I owe my gratitude to Central Instrument Facility and Department Central Instrument Facility and the respective technical staff for providing the Instrument facility. I want to express my thanks to our non-technical staff members for their help and support.

I would like to acknowledge my friends ***Dr. Radhakrishna Gattu****,* ***Dr. Arun Dhillon****,* ***Dr. Rakesh Kumar****,* ***Dr. Ramanjaneyulu Unnava****,* ***Dr. Nand Kishore Roy****,* ***Dr. Anuj Kumar Singh, Mr. Jagath and Mr. Vivek Prakash*** *for their valuable suggestions,*

moral support, assistance and contribution through the thick and thin of Ph.D. journey. I am obliged to have ***Amit Kumar Rohillan***, ***Adarsh Kumar Chiranjivi***, ***Bapi Mandal***, ***Anil P Bidkar*** *and* ***Kamalesh Verma*** *as my friends and for their love, advice, sympathy throughout the Ph.D.*

I am grateful to my labmates ***Shravan Kumar***, ***Chandi Patra***, ***Tasrin Shahnaz***, ***Rajmohan Naidu*** *and* ***Vivek Sharma*** *for being nice, cooperative, positive and creating a peaceful and healthy working environment in the lab.*

I wish to acknowledge all the research scholars of Department of Biosciences and Bioengineering, IIT Guwahati for their help and endless support.

Last but not the least, I am deeply grateful to my parents, brother and relatives for their unconditional love, support, patience and motivation to carry out Ph.D.

Above all, I am grateful to God for finding me capable of fulfilling this extremely difficult task and providing me continuous motivation, positive energy and support during the course of Ph.D. I am also thankful to God for blessing me with the completion of Doctoral work.

Abhishek Ajmani

List of Figures

List of Tables

Nomenclature

q_t	Biosorption capacity at time 't' (mg/g)
q_e	Biosorption capacity at equilibrium (mg/g)
C_o	initial metal concentration (mg/L)
C_e	metal concentration at equilibrium (mg/L)
C_t	metal concentration at *t* time (mg/L)
V	volume of the metal solution (L)
m	weight of the biosorbent (g)
Q_o	maximum biosorption capacity from Langmuir model or Thomas model (mg/g)
K_L	Langmuir isotherm constant (L/mg)
R_L	separation factor (dimensionless)
K_F	Freundlich isotherm constant (mg/g) $(L/mg)^{1/n}$
n_F	Freundlich exponent (dimensionless)
Q_m	maximum biosorption capacity from Dubinin–Radushkevich model (mg/g)
K	constant related to the mean free energy of biosorption (mol^2/kJ^2)
ε	Polanyi potential of Dubinin–Radushkevich model (kJ/mol)
R	universal gas constant (8.314 J/mol/K)
T	temperature (K)
E	Apparent adsorption energy (kJ/mol)
k_1	pseudo-first-order constant (min^{-1})
k_2	pseudo-second-order constant (g/mg/min)
k_{id}	intra-particle diffusion rate constant ($mg/g/min^{1/2}$)
C	Intercept of intraparticle diffusion model
$\Delta G°$	free energy change (kJ/mol)
$\Delta H°$	enthalpy change (kJ/mol)
$\Delta S°$	entropy change (kJ/mol/K)
K_c	distribution coefficient
K_{RP}	Redlich Peterson model constant (L/g)
α_{RP}	Redlich Peterson constant (L/mg)
β	exponential term
v	volume of molecules or gas adsorbed at random
v_m	volume of molecules or gas adsorbed for a monolayer (constant)
c	ratio of heat of adsorption of the first layer and second layer

x	relative pressure expressed as P/P_o
E_a	activation energy
A	pre-exponential factor
k_{TH}	adsorption rate constant (Thomas) (mg/L/min)
W	quantity of adsorbent used in column experiment
N_{AB}	saturation concentration (mg/L)
k_{AB}	kinetic constant (Adams Bohart) (L/mg min)
Z	bed height (cm)
P	probability of molecule to get adsorbed
k	constant related to Yoon Nelson model
k_{YN}	Yoon Nelson rate constant
τ	time duration for 50% adsorbate breakthrough (min)
t	service time (min) at breakthrough time
u	linear flow velocity (cm/min)
N_o	adsorption capacity of the bed (mg/L)
K_a	rate constant (BDST model) (L/mg min)
C_{des}	concentration of chromium desorbed at time 't'
C_{ads}	concentration of chromium adsorbed at time 't'
C	intercept (Intraparticle diffusion model)

Contents

Abstract

Clean water is a basic need of all organisms including humans. However, due to industrial and human activities of human, there is release of toxic pollutants in unprecedented amounts into the water sources. One such toxic pollutant is hexavalent chromium. Hexavalent chromium has been found to cause many ailments including cancer. WHO has set the safe limit of hexavalent chromium in drinking water as 0.05 mg/L and for other purposes as 0.1 mg/L. Conventional methods of removal of hexavalent chromium have various drawbacks such as use of toxic chemicals, generation of toxic by-products. On the other hand, adsorption, particularly biosorption is a method which is eco-friendly, does not involve the use of toxic chemicals. Lignocellulosic plant materials are cheap, available in plenty amount, biodegradable, eco-friendly and have been found to be good material for biosorption of toxic pollutants including hexavalent chromium.

In the present work, we have explored three different lignocellulosic plant materials namely *Pinus kesiya*, *Senna siamea* and *Phanera vahlii* and activated carbon prepared from these materials for the abatement of hexavalent chromium from synthetic waste solutions. All materials were characterized using FESEM, EDX, FTIR, BET and TGA. Parameters influencing adsorption process such as pH, biosorbent dose, contact time, temperature and initial metal concentration were optimized. Further, adsorption isotherms such as Langmuir, Freundlich and others were fitted to the experimental data to determine important parameters such as maximum adsorption capacity. Kinetic models were also applied to infer the mechanism of adsorption process. Thermodynamics studies were conducted to determine the spontaneity and other important parameters. We conducted regeneration and reuse investigations to find the recyclability of the adsorbent materials. Among the investigated biosorbents, we find the *Phanera vahlii* zinc chloride activated carbon (PVZCAC) to possess the highest adsorption capacity of approx. 300 mg/g. The surface area of the PVZCAC was also maximum among the explored materials with a value of 1673.0 m^2/g.

Having explored the various materials in batch mode and found the best material, we conducted continuous column studies for further determining the capability of the prepared material PVPZAC. Various parameters influencing adsorption process in

continuous mode such as bed height, initial metal concentration and flow rate were modulated for determining the best conditions. The experimental data of breakthrough curves was fitted to various theoretical models such as Thomas, Yoon Nelson, Adams Bohart and Bed Depth Service time to establish and determine vital parameters such as maximum adsorption capacity. We find that low initial metal concentration and flow rate and high bed depth showed high magnitude removal of hexavalent chromium. We find that the PVZCAC has adsorption capacity at par with other materials investigated so far.

Chapter 1
Introduction and Literature Review

1.1 Background

Clean water is an indispensable need of all organisms including humans. Besides drinking, water is needed for other purposes as well such as domestic, industrial and irrigation etc. With the beginning of human civilization, man explored the treasure hidden in the womb of earth in the form of ores, petroleum and natural gas. As a result, industrial revolution occurred in many domains which further led to increase in mining and chemical production activities. Civilization made huge developments, however, meanwhile, it did not have proper solution for tackling the toxic chemicals, byproducts generated as a result of these industrial activities. This led to the release of huge amounts of toxic chemicals, heavy metals, dyes and other such substances directly into the landfill or rivers etc. In conclusion, we, human beings were not left with any other option but to create pollution. Pollution is the addition of undesired/unwanted toxic substances into the environment such as dyes, heavy metals, chemicals, plastic materials etc.

The definition of heavy metals is quite ambiguous and comprises of 10 different criteria to comply with most of heavy metals. An easy definition of heavy metal is metal with a density of more than 5 g/cm^3. On the basis of this definition, the list of heavy metals comprises of Gold, Copper, Iron, Platinum, Chromium and many more (Moore and Stanitski, 2014). Among these metals, chromium has been given more attention due to its scale of use, release into environment and substantial health hazards including cancer.

1.2 Chromium

1.2.1 Status of chromium in World and India

Chromium is the 7^{th} most abundant metal on earth. Chromium ranks 2^{nd} on the list of metals frequently found in the polluted sites. India stands 2^{nd} in the annual production of chromite worldwide. India produced 4.9 million tons, 4.1 million tons and 3.4 million tons of chromite in the year 2007–2008, 2008–2009 and 2009–2010, respectively (Dhal et al., 2013).

1.2.2 Tolerance limit of Chromium

World health organization (WHO) has prescribed safe limit of Cr(VI) in potable water as 0.05 mg L^{-1} and in water for other purpose as 0.1 mg L^{-1} (*Guidelines for Drinking-water Quality*, 2011). The typical concentration of total chromium

concentration in potable water is less than 2 µg/L, however, amount as big as 120 µg/L has been reported (*Guidelines for Drinking-water Quality*, 2011).

1.2.3 Sources of chromium (VI)

1.2.3.1 Natural sources

a) Terrestrial sources

Chromium occurs in nature primarily in two forms: chromite and crocoite. Chromite ore is usually hard, shining and has a steel gray color. Chromite ore is composed of varying amount of chromium ranging from 40 to 68%. Chromite exists in two types: pod-shaped and stratiform (or layered). Majority of the chromite ore occurs in stratiform. The chromite ore is spread across South Africa, Cuba, India, Pakistan, Yugoslavia, Greece, Brazil and New Caledonia. Crocoite, commonly known as lead chromate ($PbCrO_4$). Crocoite is shining, orange-red colored mineral and is less hard as compared to chromite. Chromium element was originally produced from crocoites (Saha et al., 2011).

b) **Aquatic sources**

Chromium is present in trace quantities in natural waters due to the very low mobility of chromium(III) which is the main form of chromium found in nature. Chromium can also exist in hexavalent form as CrO_4^{2-}, however, chromates in nature are rare (Saha et al., 2011).

c) Atmospheric sources

The atmosphere related chromium originates primarily from two phenomenona: wind blowing and volcanic eruption. The atmospheric persistence of chromium can be estimated by the worldwide settling of the chromium to soil is approximately 4.6×10^4 metric ton Y^{-1} (Saha et al., 2011).

1.2.3.2 Anthropogenic sources

The anthropogenic sources of chromium are contaminated soils, airborne sources (industrial processes) and ground water. Chromium is used in various industries such as ink, dyes, pigments, glass, ceramics, textiles, metal finishing, leather tanning, welding, electroplating, electronic and metallurgy industries (Bertagnolli et al., 2014) (Sibi, 2016), nuclear power plants (Mona et al., 2011), wood preservation and pulp production facilities (Moussavi and Barikbin, 2010), petroleum refining processes (Hou et al., 2012), cooling towers (Rai et al., 2016) and corrosion inhibitors. Due to these activities,

chromium leaches out to landfill sites and gets released to atmosphere as suspended particles (Saha et al., 2011). The tanning industry is the primary contributor of chromium pollution at world level.

1.2.4 Chemistry of Chromium

Naturally occurring chromium has three stable isotopes ^{52}Cr, ^{53}Cr and ^{54}Cr. Chromium can exist in valencies of -2 to +6 (Mishra and Doble, 2008), however, it is found mainly in its trivalent, Cr(III) and hexavalent, Cr(VI) forms. Trivalent and hexavalent chromium have different physicochemical properties as well as effect on living organisms.

The trivalent chromium is relatively nontoxic and exists as cation Cr^{3+} below pH 3.8 and $Cr(OH)^{2+}$ from pH 3.8 to 6.3. Trivalent chromium exists as $Cr(OH)_3$ at pH 6.3 to 11.5 (Rai et al., 1989). Further, trivalent chromium is present in $Cr(OH)^{4-}$ hydroxocomplex form above pH 11.5 (Lukman et al., 2014). Trivalent chromium is the most prevalent form found in natural water (González Bermúdez et al., 2012). The solubility of Cr(III) compounds is usually less. Below pH 5.0, oxides formed from Cr(III) are slightly soluble in water, however, above pH 5.0 hydrated compounds produced from Cr(III) are relatively less soluble in water.

Hexavalent chromium exists in different soluble species form with the variation of pH from 1 to 14 such as CrO_4^{2-}, CrO_2^{4-}, $HCrO_4^{1-}$, H_2CrO_4 and $Cr_2O_7^{2-}$ (Yang and Chen, 2008). At low pH (pH < 1), the predominant species is H_2CrO_4 and tri- and tetra-chromates are also formed. Between pH 1 and 7, $HCrO^{4-}$ and $Cr_2O_7^{2-}$ are the dominate anions (Albadarin et al., 2011). Beyond pH 7, CrO_4^{2-} ions is the primary species occuring in the solution (Neagu, 2009). Chromate (CrO_4^{2-}) is the main occuring species of Cr(VI) in natural water habitats and is also the primary contaminant resulting from chromium-related industries.

1.2.5 Chromium Health effects

Trivalent chromium is required as micronutrient in human diet for the proper metabolism of glucose, lipids and proteins. Trivalent chromium deficiency as well as excess is problematic to humans.

As opposed to trivalent chromium, hexavalent chromium is highly toxic even when present in small amount. Chromium (VI) imposes its toxicity owing to the

negatively charged Cr(VI) complexes that easily traverse cell membrane through the sulphate ionic channel followed by rapid reduction reactions with ascorbate and glutathione resulting in the formation of numerous harmful reactive intermediates (Mona et al., 2011) (Mondal et al., 2017). The hazardous effect of hexavalent chromium ranges from causing allergic reactions, respiratory disorders, lung cancer to damaging kidney, liver and digestive organs (Mona et al., 2011). Inhalation of Cr(VI) containing materials can cause various respiratory diseases such as bronchitis, asthma including bronchogenic carcinoma (Sari and Tuzen, 2009).

1.3 Conventional methods of chromium removal

A number of methods have been used traditionally for the abatement of hexavalent chromium from wastewater such as chemical oxidation, membrane process, filtration, ion exchange, membrane separation, electrochemical treatment, chemical precipitation, evaporation and sorption, desalination, direct reduction, electrolysis, electrocoagulation and catalytic reduction etc.

1.3.1 Liquid-liquid extraction

Liquid-liquid extraction is a method which is based on the disproportionate distribution of the metal ion between two immiscible solvents. The distribution ratio is the ratio of metal ion in the organic phase to aqueous phase and is a good estimator of the efficiency of process. Hexavalent chromium has been separated from waste water by liquid liquid extraction using the positively charged amine groups on the extractant in organic phase (Someda et al., 2005) (Senol, 2004). Tributylphosphate $PO(C_4H_9O)_3$ (TBP) (Ouejhani et al., 2003), Alamine 336/kerosene (El-Hussaini et al., 2012), 2-octylaminopyridine (2-OAP) in xylene (Mane et al., 2016), Tricaprylmethylammonium chloride in isoamylalcohol (Kalidhasan et al., 2010) have also been investigated for liquid-liquid extraction of hexavalent chromium from wastewater and found to be efficient for removal of hevalent chromium. However, this process has drawbacks such as use of harmful chemicals and generation of toxic byproducts.

1.3.2 Chemical reduction

This is a popular method of chromium treatment in effluent and involves the reduction of hexavalent chromium to less toxic trivalent chromium by the use of bisulfate followed by precipitation of trivalent chromium using lime. The precipitated chromium is recovered by dissolution in sulphuric acid (Boast, 1988). Various chemicals and materials

have been used for chemical reduction of hexavalent chromium viz. $FeSO_4$ (Franco et al., 2009), scrap iron (Prasad et al., 2011), ascorbic acid (Xu et al., 2004) and found these materials to be useful. Kang and group compared the removal efficiency of micro/nanostructured zero valent iron with commercial zero valent iron and found the former to posses more removal capacity of upto 330.0 mg g^{-1} which was thrice than that of commercial zero valent iron (Kang et al., 2017). Qin and coworkers conducted pilot-scale study using $FeSO_4$ for the removal/reduction of hexavalent chromium and found $FeSO_4$ to be highly productive (Qin et al., 2005).

1.3.3 Ion exchange

Ion exchange has also been used conventionally for the treatment of hexavalent chromium. Specifically, ammonium ions have good utility to remove negatively charged hexavalent chromium ions from the wastewater. Various materials have been developed for ion exchange of hexavalent chromium from wastewater viz. Modified zeolites (Figueiredo and Quintelas, 2014), IRN77 and SKN1 (Rengaraj et al., 2001), Lewatit FO36 (Rafati et al., 2010), Ceralite IRA 400 (P. S. Kumar et al., 2008) and metal organic resin–alginic acid composite (Rapti et al., 2016) and were found to be effective at removing hexavalent chromium. Purolite C106 (Petruzzelli et al., 1995) and styrene-divinylbenzene-based macroporous sulphonate, Amberjet 1200Na (Cetin et al., 2013) have been investigated at the pilot-scale level and found to be highly beneficial for the elimination of hexavalent chromium. The demerits of this process are high cost, chemical process and not environment friendly.

1.3.4 Electrocoagulation

Electrocoagulation has been widely used for the abatement of hexavalent chromium from wastewater. This method involves the coagulation of hexavalent chromium with in-situ generated electrons or ions from a sacrificial electrode. Various electrocoagulation studies have been conducted for removal of hexavalent chromium from wastewater individually (El-Taweel et al., 2015) or in combination with lead (Sharma et al., 2019) or arsenic (Parga et al., 2005) using Iron electrode and were found to be successful. Further, aluminum, stainless steel and combination of both electrode were used to investigate the effect of electrodes and aluminium was found to have best performance among all electrodes (Prasetyaningrum et al., 2018). Al-Al electrodes were also investigated in electrocoagulation process for removal of hexavalent chromium and

were found to be productive (Bhatti et al., 2009). The demerit of this process is the long duration and generation of toxic substances.

1.3.5 Coagulation/flocculation

This process is based on the coagulation/flocculation of various pollutants by inorganic chemical reagents such as $Al_2(SO_4)_3$, $Fe_2(SO_4)_3$, $FeCl_3$ and other related substances. Aluminium sulphate and ferric chloride were used for the coagulation of hexavalent chromium from tannery effluent and were found to be productive in removal of hexavalent chromium (Song et al., 2004).

1.3.6 Precipitate flotation

Precipitate flotation involves the flotation of the precipitates formed by the chemical reagents and pollutants by the adhesion with air droplets which are removed from the effluent. Rhamnolipid was investigated for the removal of hexavalent chromium using the precipitate flotation technique (Salmani Abyaneh and Fazaelipoor, 2016). Sodium dodecylsulfate and ethanol were used for the precipitate flotation of trivalent chromium and 96% removal was achieved (Medina et al., 2005). Sodium laurylsulfate was investigated for the precipitate flotation of hexavalent chromium in a three stage process and was found to be efficient (Bhattacharyya et al., 1971).

All of these conventional techniques suffer from one or other demerits such as high operational cost, huge energy requirements, secondary waste generation. These methods work only when high metal concentration is present. Further, conventional processes are complex due to the different intensive sub-processes and use of chemicals and generation of toxic sludges.

1.4 Adsorption

Adsorption is defined as the transfer of liquid, gas or solid molecules on a surface involving either physical or chemical bonds (Artioli, 2008). Adsorption has been investigated/used in many processes such as heterogenous catalysis, chromatography including environmental remediation. Adsorption is an easy, low cost procedure which does not involve the use of toxic chemicals with no or less sludge generation. Various types of biosorbent, living as well as dead have been investigated. Further, various types of adsorbents have been synthesized using natural and synthetic polymer, chemicals etc.

1.5 Types of adsorbents reported

1.5.1 Microbial biomass

Microorganisms have been investigated for the elimination of Cr(VI) from wastewater in dead state. The surface of the microorganism contains various biomolecules which have functional groups for the adsorption of hexavalent chromium. The mechanism involves adsorption, reduction, complexation etc.

1.5.1.1 Algal biomass

Various investigators have investigated dried algae biomass (microalgae and macroalgae) for the abatement of hexavalent chromium from effluent. *Enteromorpha intestinalis* and *Microspora amoena* (Al-Homaidan et al., 2018), *Ceramium virgatum* (Sari and Tuzen, 2008), *Macrocystis pyrifera* and *Undaria pinnatifida* (Cazón et al., 2012), *Oedogonium hatei* (Gupta and Rastogi, 2009), Dunaliella spp. (Dönmez and Aksu, 2002), *Ulva lactuca* (El-Sikaily et al., 2007), *Rhizoclonium hieroglyphicum* (Onyancha et al., 2008), *Rhizoclonium hookeri* (Kayalvizhi et al., 2015) were studied for the adsorption of hexavalent/trivalent chromium and *Rhizoclonium hookeri* was found to have the highest biosorption capacity of 67.3 mg/g. Lee and coworkers screened various species of red, brown and green marine algae on the east cost of Korea and found a novel red marine alga (Pachymeniopsis sp.) (Lee et al., 2000) to have maximum biosorption capacity of 225.0 mg/g among the screened algae. Many researchers have investigated various species of Spirulina algae viz. Spirulina sp. (Rezaei, 2016), *Spirulina fusiformis* (Pandi et al., 2009), fresh and spent *Spirulina platensis* biomass (Gokhale et al., 2008) in batch mode and immobilized *Spirulina platensis* (Gokhale et al., 2009) in packed column mode and found them to be productive. Further, Spirulina sp. possessed high biosorption capacity of 90.9 mg/g. Also, many Cladophora algae viz. *Cladophora glomerata* (Al-Homaidan et al., 2018), *Cladophora albida* (Deng et al., 2009), *Cladophora crispate* (Aksu et al., 1996) have been thoroughly investigated by various authors and found to be promising for removal of hexavalent chromium. Dried *Spirogyra condensata* biomass (Onyancha et al., 2008) and filamentous algae Spirogyra sp. (Gupta et al., 2001) were investigated for hexavalent chromium removal.

1.5.1.2 Fungal biomass

A large number of dead fungal biomasses *Mucor meihi* (M. Tobin and C. Roux, 1998), *Agaricus bisporus* (Ertugay and Bayhan, 2008), *Neurospora crassa* (Tunali et al.,

2005), *Termitomyces clypeatus* (Ramrakhiani et al., 2011), *Arthrinium malaysianum* (Majumder et al., 2017) and *Saccharomyces cerevisiae* (Park et al., 2005) have been studied for the biosorption of hexavalent chromium from wastewater. Among them, *Arthrinium malaysianum* was found to have the highest biosorption capacity of 100.6 mg/g. Trichoderma sp. BSCR02 (Benila Smily and Sumithra, 2017), and *Trichoderma viride* immobilized fungal biomass (Bishnoi et al., 2007) were used to study the adsorption of hexavalent chromium and found to be highly productive. Aspergillus fungus has been studied thoroughly by numerous researchers involving many strains viz. *Aspergillus* niger (Park et al., 2005), Aspergillus *niger* (Mungasavalli et al., 2007), *Aspergillus niger* (Mondal et al., 2017), *Aspergillus niger* (R. Kumar et al., 2008), *Aspergillus sydoni* (R. Kumar et al., 2008) in various forms, treated and untreated and found the biosorption capacity to be approx. 15.0 mg/g. However, Khambhaty and coworkers isolated a marine fungus *Aspergillus niger* (Khambhaty et al., 2009) and found its biosorption capacity to be 117.3 mg/g. *Rhizopus oryzae* (Park et al., 2005) and *Rhizopus arrhizus* (Aksu and Balibek, 2007) were considered for the biosorption of hexavalent chromium and *Rhizopus arrhizus* was found to have high biosorption capacity of 78.0 mg/g. Bai and Abraham studied the biosorption of hexavalent chromium using *Rhizopus nigricans* in its raw form (Bai R and Abraham, 2001) and chemically modified forms (Bai and Abraham, 2002) viz. NaOH, ammonia solution, formaldehyde, CTAB, polyethylenimine, APTS and after immobilization in various polymeric matrices (Bai and Abraham, 2003) viz. calcium alginate, polyvinyl alcohol (PVA), polyacrylamide, polyisoprene and polysulfone and found that the APTS modified *Rhizopus nigricans* yielded high biosorption capacity of 51.2 mg/g. Prakasham and group compared Stirred tank and Fluidized bed adsorption of hexavalent chromium using *Rhizopus nigricans* biomass and found the Fluidized bed to be better. Artist's Bracket (AB) fungi was studied for biosorption of hexavalent chromium from wastewater and maximum biosorption capacity was found to be 200 mg/g (Pourkarim et al., 2017). Various strains of fungi Penicillium viz. *Penicillium griseofulvum* MSR1 (Abigail. M et al., 2015), *Penicillium janthinellum* (R. Kumar et al., 2008) and *Penicillium chrysogenum* (Park et al., 2005) were investigated for the removal of hexavalent chromium and *Penicillium griseofulvum* MSR1 (Abigail. M et al., 2015) was found to have high biosorption capacity of 75.1 mg/g.

1.5.1.3 Bacterial biomass

Various bacterial species have been investigated for the biosorption of hexavalent chromium from effluent. Gram positive bacteria viz. *Bacillus megaterium* (Srinath et al., 2002), *Bacillus coagulans* (Srinath et al., 2002), *Bacillus* sp. strain YB-1 (Liu et al., 2008, p. 1), *Bacillus salmalaya* Strain 139SI (Dadrasnia et al., 2015), *Bacillus cereus* (Yang et al., 2016) and *Bacillus thurnigiensis* (Şahin and Öztürk, 2005) were studied for the biosorption of hexavalent chromium from wastewater and found them to be highly productive with biosorption capacity of 30.7 mg/g, 39.9 mg/g, 17.8 mg/g, 20.3 mg/g, 30.9 mg/g and 35.2 mg/g, respectively. Also, Gram negative bacteria have been investigated for the abatement of hexavalent chromium from wastewater viz. *Aeromonas caviae* (Loukidou et al., 2004), *Aeromonas hydrophila* (Ranjan et al., 2009) and were found to have biosorption capacity of 124.4 mg/g and 184.9 mg/g, respectively. *Pseudomonas aeruginosa* (Kang et al., 2007) was also studied and found to be efficient. *Arthrobacter viscosus* was found to have 20.37 mg/g biosorption capacity for the abatement of hexavalent chromium from wastewater (Hlihor et al., 2017). Zakaria and coworkers isolated various bacteria from metal-containing industrial effluents viz. *Acinetobacter haemolyticus*, *Staphylococcus aureus*, *Bacillus cereus*, *Staphylococcus epidermidis*, *Bacillus* sp. and found that heat-acid treatment for *Staphylococcus epidermidis* and *Bacillus cereus* increased the biosorption capacity to 78.2 and 77.6 mg/g, respectively (Zakaria et al., 2007). Latha and group isolated actinobacterial probiont *Streptomyces werraensis* LD22 and observed that this bacterium was able to remove 82.3% hexavalent chromium at 100 mg/L concentration (Latha et al., 2015). Xie and coworkers isolated root nodule bacteria *Mesorhizobium amorphae* strain CCNWGS0123 and observed the biosorption capacity to be 53.5 mg/g and 47.6 mg/g for trivalent and hexavalent chromium, respectively (Xie et al., 2013). Srivastava and group isolate *Serratia* sp. isolated from tannery effluent and found the biosorption capacity to be 12.5 mg/g (Srivastava and Thakur, 2012). Masood and coworkers applied Artificial Neural Network (ANN) on a set of 360 data obtained in laboratory batch study and found that ANN predicted biosorption capacity to be 50.0 mg/g with good score (Masood et al., 2012).

1.5.2 Lignocellulosic materials

Lignocellulosic materials obtained from plants, trees and other living organisms are materials which are rich in cellulose, hemicellulose and lignin. These materials are

produced in huge quantities in nature and are very stable, non-degradable materials due to the presence of strong bonds among lignin, cellulose and hemicellulose. The content of lignin, cellulose and hemicellulose varies with the source, however, more or less, every plant contains all of these components. These materials are very cheap, easily available in huge quantities and environment friendly. Researchers have examined *Tamarindus indica* seeds (Agarwal et al., 2006), *Pinus sylvestris* cone biomass (Ucun et al., 2002), *Cupressus lusitanica* bark (Netzahuatl-Muñoz et al., 2015), Potato Peelings (Mutongo et al., 2014), *Araucaria angustifolia* seed (Brasil et al., 2006), *Nauclea diderrichii* seed biomass (Omorogie et al., 2012), *Pterospermum acerifolium* shells (Rangabhashiyam and Balasubramanian, 2018) and Tobacco-leaf residues (Chen et al., 2009) for abatement of hexavalent chromium and found their biosorption capacity as 90.0 mg/g, 201.8 mg/g, 305.4 mg/g, 3.2 mg/g, 125.0 mg/g, 483.0 mg/g, 76.9 mg/g and 113.2 mg/g, respectively. Park and group explored many agricultural biowastes namely banana skin, green tea waste, oak leaf, walnut shell, peanut shell and rice husk for the adsorption of hexavalent chromium from wastewater and found banana skin to have higher hexavalent chromium reduction capacity of 249.6 mg/g. Further, they immobilized banana skin powder in Ca-alginate beads and observed complete adsorption of reduced trivalent chromium from wastewater (Park et al., 2008). Sugarcane bagasse has been investigated for the eradication of hexavalent chromium from wastewater and was found to remove 80% chromium from wastewater (Ullah et al., 2013). Nag and coworkers examined jackfruit leaf, mango leaf, onion peel, garlic peel, bamboo leaf, acid treated rubber leaf and coconut shell powder and found mango leaf to have high biosorption capacity of 35.7 mg/g (Nag et al., 2017). Various shells have been investigated viz. walnut shell, hazelnut shell, almond shell (Pehlivan and Altun, 2008), Hass avocado shell (Aranda-García and Cristiani-Urbina, 2019), horse chesnut shell (Parlayıcı and Pehlivan, 2015), wallnut hull (Wang et al., 2009) and were found to have biosorption capacity 8.01 mg/g, 8.28 mg/g, 3.40 mg/g, 127.63 mg/g, 142.85 mg/g and 98.1 mg/g, respectively. Sillerova and group reported Pretreated Brewers draff as a good biosorbent of hexavalent chromium with biosorption capacity of 277.0 mg/g (Sillerová et al., 2013). Tea waste (Albadarin et al., 2013), Date pits (Albadarin et al., 2013) and garlic stem (Parlayıcı and Pehlivan, 2015) were also found to be useful for biosorption of hexavalent chromium with biosorption capacity of 107.8 mg/g, 96.02 mg/g and 103.09 mg/g. Wang and Lee have investigated the mechanism of hexavalent chromium biosorption on cellulose and found the involvement of hydroxyl functional groups which converted to carboxyl groups on

reduction of hexavalent chromium to trivalent chromium. Further, they found that trivalent chromium binds to the cellulosic carboxyl groups by forming bidentate-mononuclear complexes (Wang and Lee, 2011). Lin and Wang also found that the rate and capacity of biosorption of hexavalent chromium follows the order Hemicellulose >> Chitin >> Cellulose (Lin and Wang, 2012). Zheng and group also found the interactions of hydroxyl groups on the surface of Sargassum with hexavalent chromium in the process of biosorption (Zheng et al., 2011).

1.5.3 Activated carbon

Activated carbon is widely known for the removal of various pollutant from effluent on a large scale and is commercially available. Activated carbon has huge surface area and large pores and thus, the activated carbon is found to be highly porous. The commercial activated carbon is very expensive and obtained from few sources such as coal, peat, wood, coir and lignite etc. There is a good scope to produce activated carbon from other sources as well such as lignocellulosic biomasses and increase the adsorption capacity of activated carbon by exploring various methods of producing activated carbon.

There are two types of activated carbon; Physically activated carbon and Chemically activated carbon. Physically activated carbon also known as biochar is produced at low temperature in the absence of air/oxygen and chemicals. Chemically activated carbon commonly known as activated carbon is produced at high temperatures in the absence of air/oxygen and involves the impregnation of biomass with various chemicals such as sulphuric acid, phosphoric acid and zinc chloride.

Many investigators have made physically activated carbon or biochar by various lignocellulosic materials and applied them for the biosorption of hexavalent chromium from wastewater. Rajapaksha and group reported the preparation of biochar from soybean stover and burcucumber and the mechanism of biosorption by redox reactions (Rajapaksha et al., 2018). Biochar was produced from *Eucalyptus globulus* bark biochar (Choudhary and Paul, 2018), municipal sludge (Chen et al., 2015), oleaster seed, cherry stone (Kahraman and Pehlivan, 2017) and peanut shell (Xu et al., 2019) with the corresponding biosorption capacity as 21.3 mg/g, 7.0 mg/g, 0.474 mmoL/g, 0.308 mmoL/g and 30.9 mg/g, respectively. Tobacco petiole (Zhang et al., 2018), sugar beet tailing (Dong et al., 2011) and Corn straw (Zhao et al., 2018) were also used to prepare

biochar and adsorption capacity was found to be 195.2 mg/g, 123.0 mg/g and 33.3 mg/g, respectively.

Enniya produced phosphoric acid activated carbon from apple peels and found the biosorption capacity to be 36.0 mg/g which was higher than the apple peels (Enniya et al., 2018). Medler seed (*Mespilus germanica*) was used to produce activated carbon using KOH and were found to have adsorption capacity of 200.0 mg/g (Solgi et al., 2017). Sun and group investigated the influence of various agents such as $FeCl_3$, $AlCl_3$ and $MnCl_2$ in the preparation of H_3PO_4 activated carbon from *Arundo donax Linn* and found that the biosorption capacity followed the order AC-Fe > AC-Al > AC-Mn > AC (Sun et al., 2014).

1.5.4 Synthetic adsorbents

1.5.4.1 Metal organic frameworks

Metal organic frameworks are a new class of polymeric materials which are made up of transition metals and organic linkers such as benzene dicarboxylic acid, benzene tricarboxylic acid etc. (Evans et al., 2019). These materials are highly tunable and have been applied for various applications including environmental applications. Cu-BTC MOFs was synthesized by Maleki and group and applied for the adsorption of hexavalent chromium from effluent. The adsorption capacity of Cu-BTC MOF was found to be 48.0 mg/g (Maleki et al., 2015). Gao and coworkers prepared Fe-MOF and fine tuned the adsorption properties of Fe-MOF on the basis of TGA and found the optimum MOF to be $Fe_{0.72}^{(0)}Fe_{2.28}^{(II)}C$. The adsorption capacity of the prepared $Fe_{0.72}^{(0)}Fe_{2.28}^{(II)}C$ to be 354.6 mg/g (Gao et al., 2018).

1.5.4.2 Layered double hydroxides

Layered double hydroxides are materials which are made up of brucite ($Mg(OH)_2$) like layers comprising of divalent metal cations and few trivalent metal cations. In between the layers, there are negatively charged ions to compensate the charge and these negative ions are not orderly placed (Tran et al., 2019). OH^-, Cl^-, SO_4^{2-} are examples of anions that have been reported. These materials can be used for adsorption of negatively charged species such as chromion ions. Jaiswal and group have synthesized nano-Co/Bi-LDH by urea hydrolysis and found the adsorption capacity to be 277.7 mg/g (Jaiswal et al., 2015). de Oliveira and Wypych synthsized layered zinc hydroxide nitrate and zinc/nickel double hydroxide and evaluated them for the adsorption of hexavalent

chromium. The adsorption capacity of the prepared layered double hydroxides was 124.0 and 139.0 mg/g for Zn/NiHN-mag and Zn/NiHA-mag, respectively (de Oliveira and Wypych, 2016).

1.5.4.3 Amine based adsorbents

Having explored the potential of raw lignocellulosic biomass and activated carbon prepared from them as well, researchers tried exploring functionalizing these materials with various organic functional group which promote the adsorption of hexavalent chromium. One of the organic functional group which promotes the adsorption of hexavalent chromium is amine group. Primarily, all forms of amine: primary, secondary and tertiary promotes the adsorption of hexavalent chromium due to the electrostatic interaction between the positively charged amine group and the negatively charged chromium oxyanions at low pH. Polyethlyeneimine crosslinked graphene oxide material was synthesized and found to have adsorption capacity of 463.2 mg/g. Chitosan grafted graphene oxide nanocomposite was produced and investigated for the elimination of Cr(VI) from effluent. The maximum adsorption capacity was found to be 104.1 mg/g (Samuel et al., 2019). Yu and coworkers synthesized poly(m-phenylenediamine) with different oxidation states and observed the adsorption capacity to increase with decrease in oxidation state. The maximum adsorption capacity was found to be 500.0 mg/g (Yu et al., 2013). Liu and coworkers synthesized two chelating adsorbents (PCEA1) and (PCEA2) by using catechol, diethylenetriamine with two different chemicals viz. m-phenylenediamine and melamine, respectively. The maximum adsorption capacity was found to be 200.0 mg/g and 175.4 mg/g for PCEA1 and PCEA2, respectively (Liu et al., 2016).

1.5.4.4 Magnetic adsorbents

Magnetic materials have the property of getting separated easily. Researchers have incorporated this property in various adsorbents and investigated them for the elimination of hexavalent chromium from wastewater. Graphene coated iron oxide nanoparticles were synthesized and investigated for the removal of chromium from drain water. The maximum adsorption capacity was found to be 352.1 mg/g (Khare et al., 2018). Nitrogen doped magnetic carbon tubes were synthesized for investigation of hexavalent chromium from wastewater and were found to have high adsorption capacity of 970.87 mg/g (Huang et al., 2019). Functionalized magnetic iron oxide/polyacrylonitrile

composite (Zhao et al., 2017) was produced and applied for the removal of hexavalent chromium. Maximum adsorption capacity was found to be 684.93 mg/g.

1.6 Objectives

From the above literature survey done, we concluded that hexavalent chromium is highly toxic pollutant released in huge quanitites as a result of human activities. We also concluded that there is a dire need to explore low cost environment friendly materials for the removal of toxic hexavalent chromium using the adsorption technique. Therefore, we planned to work on lignocellulosic biomasses and the activated carbon prepared from them to find the best among them using batch and column studies. With these facts under consideration, we framed the objectives for this work as follows.

We explored three lignocellulosic plant materials viz. *Pinus kesiya* cone biomass, *Senna siamea* seed pod and *Phanera vahlii* fruit biomass in raw form and their activated carbon form as well for their application in adsorption of hexavalent chromium from synthetic wastewater. For each adsorbent explored, we performed these experiments which have been clubbed under the heading Batch biosorption.

Batch biosorption

a) Preparation of biosorbent.
b) Characterization of biosorbent by various techniques such as DSC/TGA, BET, FESEM, EDX, FTIR and XRD.
c) Quantitative studies of effect of various parameters such as pH, temperature, agitation, initial metal concentration, biosorbent dose and contact time on the biosorption and their optimization.
d) Modelling of various Adsorption isotherms and Kinetic models.
e) Regeneration and Recovery studies.

Having found out the best adsorbent with the highest adsorption capacity among the explored adsorbents, we constructed and used packed bed column and carried out experiments in continuous mode for examining the potential of the prepared adsorbent under continuous mode. The experiments have been clubbed under the heading Column studies.

Column studies

a) Packed bed construction

b) Optimization of bed height, flow rate and initial metal concentration

c) Dynamic models studies

References

Abigail. M, E.A., Samuel, M.S., Chidambaram, R., 2015. Hexavalent chromium biosorption studies using *Penicillium griseofulvum* MSR1 a novel isolate from tannery effluent site: Box–Behnken optimization, equilibrium, kinetics and thermodynamic studies. Journal of the Taiwan Institute of Chemical Engineers 49, 156–164. https://doi.org/10.1016/j.jtice.2014.11.026

Agarwal, G.S., Bhuptawat, H.K., Chaudhari, S., 2006. Biosorption of aqueous chromium(VI) by *Tamarindus indica* seeds. Bioresour. Technol. 97, 949–956. https://doi.org/10.1016/j.biortech.2005.04.030

Aksu, Z., Balibek, E., 2007. Chromium(VI) biosorption by dried *Rhizopus arrhizus*: Effect of salt (NaCl) concentration on equilibrium and kinetic parameters. Journal of Hazardous Materials 145, 210–220. https://doi.org/10.1016/j.jhazmat.2006.11.011

Aksu, Z., Özer, D., Ekiz, H.I., Kutsal, T., Çaglar, A., 1996. Investigation of Biosorption of Chromium(VI) on *Cladophora crispata* in Two-Staged Batch Reactor. Environmental Technology 17, 215–220. https://doi.org/10.1080/09593331708616379

Albadarin, A.B., Al-Muhtaseb, A.H., Al-laqtah, N.A., Walker, G.M., Allen, S.J., Ahmad, M.N.M., 2011. Biosorption of toxic chromium from aqueous phase by lignin: mechanism, effect of other metal ions and salts. Chemical Engineering Journal 169, 20–30. https://doi.org/10.1016/j.cej.2011.02.044

Albadarin, A.B., Mangwandi, C., Walker, G.M., Allen, S.J., Ahmad, M.N.M., Khraisheh, M., 2013. Influence of solution chemistry on Cr(VI) reduction and complexation onto date-pits/tea-waste biomaterials. J. Environ. Manage. 114, 190–201. https://doi.org/10.1016/j.jenvman.2012.09.017

Al-Homaidan, A.A., Al-Qahtani, H.S., Al-Ghanayem, A.A., Ameen, F., Ibraheem, I.B.M., 2018. Potential use of green algae as a biosorbent for hexavalent chromium removal from aqueous solutions. Saudi Journal of Biological Sciences 25, 1733–1738. https://doi.org/10.1016/j.sjbs.2018.07.011

Aranda-García, E., Cristiani-Urbina, E., 2019. Effect of pH on hexavalent and total chromium removal from aqueous solutions by avocado shell using batch and continuous systems. Environ Sci Pollut Res Int 26, 3157–3173. https://doi.org/10.1007/s11356-017-0248-z

Artioli, Y., 2008. Adsorption, in: Jørgensen, S.E., Fath, B.D. (Eds.), Encyclopedia of Ecology. Academic Press, Oxford, pp. 60–65. https://doi.org/10.1016/B978-008045405-4.00252-4

Bai R, S., Abraham, T.E., 2001. Biosorption of Cr (VI) from aqueous solution by *Rhizopus nigricans*. Bioresource Technology 79, 73–81. https://doi.org/10.1016/S0960-8524(00)00107-3

Bai, R.S., Abraham, T.E., 2003. Studies on chromium(VI) adsorption-desorption using immobilized fungal biomass. Bioresour. Technol. 87, 17–26.

Bai, R.S., Abraham, T.E., 2002. Studies on enhancement of Cr(VI) biosorption by chemically modified biomass of *Rhizopus nigricans*. Water Research 36, 1224–1236. https://doi.org/10.1016/S0043-1354(01)00330-X

Benila Smily, J.R.M., Sumithra, P.A., 2017. Optimization of Chromium Biosorption by Fungal Adsorbent, Trichoderma sp. BSCR02 and its Desorption Studies. HAYATI Journal of Biosciences 24, 65–71. https://doi.org/10.1016/j.hjb.2017.08.005

Bertagnolli, C., Uhart, A., Dupin, J.-C., da Silva, M.G.C., Guibal, E., Desbrieres, J., 2014. Biosorption of chromium by alginate extraction products from *Sargassum filipendula*: Investigation of adsorption mechanisms using X-ray photoelectron spectroscopy analysis. Bioresource Technology 164, 264–269. https://doi.org/10.1016/j.biortech.2014.04.103

Bhattacharyya, D., Carlton, J.A., Grieves, R.B., 1971. Precipitate flotation of chromium. AIChE Journal 17, 419–424. https://doi.org/10.1002/aic.690170233

Bhatti, M.S., Reddy, A.S., Thukral, A.K., 2009. Electrocoagulation removal of Cr(VI) from simulated wastewater using response surface methodology. J. Hazard. Mater. 172, 839–846. https://doi.org/10.1016/j.jhazmat.2009.07.072

Bishnoi, N.R., Kumar, R., Bishnoi, K., 2007. Biosorption of Cr (VI) with *Trichoderma viride* immobilized fungal biomass and cell free Ca-alginate beads. IJEB Vol.45(07) [July 2007].

Boast, D.A., 1988. Large scale chrome recovery from chrome wash liquors.

Brasil, J.L., Ev, R.R., Milcharek, C.D., Martins, L.C., Pavan, F.A., dos Santos, A.A., Dias, S.L.P., Dupont, J., Zapata Noreña, C.P., Lima, E.C., 2006. Statistical design of experiments as a tool for optimizing the batch conditions to Cr(VI) biosorption on *Araucaria angustifolia* wastes. J. Hazard. Mater. 133, 143–153. https://doi.org/10.1016/j.jhazmat.2005.10.002

Cazón, J.P.H., Benítez, L., Donati, E., Viera, M., 2012. Biosorption of chromium(III) by two brown algae *Macrocystis pyrifera* and *Undaria pinnatifida*: Equilibrium and kinetic study. Engineering in Life Sciences 12, 95–103. https://doi.org/10.1002/elsc.201100098

Cetin, G., Kocaoba, S., Akcin, G., 2013. Removal and Recovery of Chromium from Solutions Simulating Tannery Wastewater by Strong Acid Cation Exchanger [WWW Document]. Journal of Chemistry. https://doi.org/10.1155/2013/158167

Chen, T., Zhou, Z., Xu, S., Wang, H., Lu, W., 2015. Adsorption behavior comparison of trivalent and hexavalent chromium on biochar derived from municipal sludge. Bioresource Technology 190, 388–394. https://doi.org/10.1016/j.biortech.2015.04.115

Chen, Yuru, Tang, G., Yu, Q.J., Zhang, T., Chen, Yan, Gu, T., 2009. Biosorption properties of hexavalent chromium on to biomass of tobacco-leaf residues. Environ Technol 30, 1003–1010. https://doi.org/10.1080/09593330903019268

Choudhary, B., Paul, D., 2018. Isotherms, kinetics and thermodynamics of hexavalent chromium removal using biochar. Journal of Environmental Chemical Engineering 6, 2335–2343. https://doi.org/10.1016/j.jece.2018.03.028

Dadrasnia, A., Chuan Wei, K.S., Shahsavari, N., Azirun, M.S., Ismail, S., 2015. Biosorption Potential of *Bacillus salmalaya* Strain 139SI for Removal of Cr(VI) from Aqueous Solution. Int J Environ Res Public Health 12, 15321–15338. https://doi.org/10.3390/ijerph121214985

de Oliveira, H.B., Wypych, F., 2016. Evaluation of layered zinc hydroxide nitrate and zinc/nickel double hydroxide salts in the removal of chromate ions from solutions. Journal of Solid State Chemistry 243, 136–145. https://doi.org/10.1016/j.jssc.2016.08.019

Deng, L., Zhang, Y., Qin, J., Wang, X., Zhu, X., 2009. Biosorption of Cr(VI) from aqueous solutions by nonliving green algae *Cladophora albida*. Minerals Engineering 22, 372–377. https://doi.org/10.1016/j.mineng.2008.10.006

Dhal, B., Thatoi, H.N., Das, N.N., Pandey, B.D., 2013. Chemical and microbial remediation of hexavalent chromium from contaminated soil and mining/metallurgical solid waste: A review. Journal of Hazardous Materials 250–251, 272–291. https://doi.org/10.1016/j.jhazmat.2013.01.048

Dong, X., Ma, L.Q., Li, Y., 2011. Characteristics and mechanisms of hexavalent chromium removal by biochar from sugar beet tailing. Journal of Hazardous Materials 190, 909–915. https://doi.org/10.1016/j.jhazmat.2011.04.008

Dönmez, G., Aksu, Z., 2002. Removal of chromium(VI) from saline wastewaters by Dunaliella species. Process Biochemistry 38, 751–762. https://doi.org/10.1016/S0032-9592(02)00204-2

El-Hussaini, O.M., Lasheen, T.A., Helmy, E.M., Hady, M.A., Manaa, A.-S.A., 2012. Liquid-Liquid Extraction/Recovery of Chromium(VI) From Some Industrial Waste Solutions Using Alamine 336 in Kerosene. Journal of Dispersion Science and Technology 33, 1179–1187. https://doi.org/10.1080/01932691.2011.605338

El-Sikaily, A., Nemr, A.E., Khaled, A., Abdelwehab, O., 2007. Removal of toxic chromium from wastewater using green alga *Ulva lactuca* and its activated carbon. Journal of Hazardous Materials 148, 216–228. https://doi.org/10.1016/j.jhazmat.2007.01.146

El-Taweel, Y.A., Nassef, E.M., Elkheriany, I., Sayed, D., 2015. Removal of Cr(VI) ions from waste water by electrocoagulation using iron electrode. Egyptian Journal of Petroleum 24, 183–192. https://doi.org/10.1016/j.ejpe.2015.05.011

Enniya, I., Rghioui, L., Jourani, A., 2018. Adsorption of hexavalent chromium in aqueous solution on activated carbon prepared from apple peels. Sustainable Chemistry and Pharmacy 7, 9–16. https://doi.org/10.1016/j.scp.2017.11.003

Ertugay, N., Bayhan, Y.K., 2008. Biosorption of Cr (VI) from aqueous solutions by biomass of *Agaricus bisporus*. Journal of Hazardous Materials 154, 432–439. https://doi.org/10.1016/j.jhazmat.2007.10.070

Evans, J.D., Garai, B., Reinsch, H., Li, W., Dissegna, S., Bon, V., Senkovska, I., Fischer, R.A., Kaskel, S., Janiak, C., Stock, N., Volkmer, D., 2019. Metal–organic frameworks in Germany: From synthesis to function. Coordination Chemistry Reviews 380, 378–418. https://doi.org/10.1016/j.ccr.2018.10.002

Figueiredo, H., Quintelas, C., 2014. Tailored zeolites for the removal of metal oxyanions: overcoming intrinsic limitations of zeolites. J. Hazard. Mater. 274, 287–299. https://doi.org/10.1016/j.jhazmat.2014.04.012

Franco, D.V., Silva, L.M.D., Jardim, W.F., 2009. Chemical Reduction of Hexavalent Chromium Present in Contaminated Soil using a Packed- bed Column Reactor. CLEAN – Soil, Air, Water 37, 858–865. https://doi.org/10.1002/clen.200900180

Gao, G., Nie, L., Yang, S., Jin, P., Chen, R., Ding, D., Wang, X.C., Wang, W., Wu, K., Zhang, Q., 2018. Well-defined strategy for development of adsorbent using metal organic frameworks (MOF) template for high performance removal of hexavalent chromium. Applied Surface Science 457, 1208–1217. https://doi.org/10.1016/j.apsusc.2018.06.278

Gokhale, S.V., Jyoti, K.K., Lele, S.S., 2009. Modeling of chromium (VI) biosorption by immobilized *Spirulina platensis* in packed column. Journal of Hazardous Materials 170, 735–743. https://doi.org/10.1016/j.jhazmat.2009.05.005

Gokhale, S.V., Jyoti, K.K., Lele, S.S., 2008. Kinetic and equilibrium modeling of chromium (VI) biosorption on fresh and spent *Spirulina platensis*/*Chlorella vulgaris* biomass. Bioresource Technology 99, 3600–3608. https://doi.org/10.1016/j.biortech.2007.07.039

González Bermúdez, Y., Rodríguez Rico, I.L., Guibal, E., Calero de Hoces, M., Martín-Lara, M.Á., 2012. Biosorption of hexavalent chromium from aqueous solution by *Sargassum muticum* brown alga. Application of statistical design for process optimization. Chemical Engineering Journal 183, 68–76. https://doi.org/10.1016/j.cej.2011.12.022

Guidelines for Drinking-water Quality, 4th ed, 2011. . World Health Organization (WHO), Geneva.

Gupta, V.K., Rastogi, A., 2009. Biosorption of hexavalent chromium by raw and acid-treated green alga *Oedogonium hatei* from aqueous solutions. Journal of Hazardous Materials 163, 396–402. https://doi.org/10.1016/j.jhazmat.2008.06.104

Gupta, V.K., Shrivastava, A.K., Jain, N., 2001. Biosorption of Chromium(VI) From Aqueous solutions by green algae spirogyra species. Water Research 35, 4079–4085. https://doi.org/10.1016/S0043-1354(01)00138-5

Hlihor, R.M., Figueiredo, H., Tavares, T., Gavrilescu, M., 2017. Biosorption potential of dead and living *Arthrobacter viscosus* biomass in the removal of Cr(VI): Batch and column studies. Process Safety and Environmental Protection, Environmental Engineering and Management, Progresses and Challenges for Sustainability: An Introduction to ICEEM08 108, 44–56. https://doi.org/10.1016/j.psep.2016.06.016

Hou, Y., Liu, H., Zhao, X., Qu, J., Chen, J.P., 2012. Combination of electroreduction with biosorption for enhancement for removal of hexavalent chromium. Journal of Colloid and Interface Science 385, 147–153. https://doi.org/10.1016/j.jcis.2012.05.056

Huang, J., Cao, Y., Qin, B., Zhong, G., Zhang, J., Yu, H., Wang, H., Peng, F., 2019. Highly efficient and acid-corrosion resistant nitrogen doped magnetic carbon nanotubes for the hexavalent chromium removal with subsequent reutilization. Chemical Engineering Journal 361, 547–558. https://doi.org/10.1016/j.cej.2018.12.081

Jaiswal, A., Mani, R., Banerjee, S., Gautam, R.K., Chattopadhyaya, M.C., 2015. Synthesis of novel nano-layered double hydroxide by urea hydrolysis method and their application in removal of chromium(VI) from aqueous solution: Kinetic, thermodynamic and equilibrium studies. Journal of Molecular Liquids 202, 52–61. https://doi.org/10.1016/j.molliq.2014.12.004

Kahraman, H.T., Pehlivan, E., 2017. Cr^{6+} removal using oleaster (Elaeagnus) seed and cherry (*Prunus avium*) stone biochar. Powder Technology 306, 61–67. https://doi.org/10.1016/j.powtec.2016.10.050

Kalidhasan, S., Sricharan, S., Ganesh, M., Rajesh, N., 2010. Liquid−Liquid Extraction of Chromium(VI) with Tricaprylmethylammonium Chloride Using Isoamylalcohol as the Diluent and Its Application to Industrial Effluents. J. Chem. Eng. Data 55, 5627–5633. https://doi.org/10.1021/je100518w

Kang, S., Wang, G., Zhao, H., Cai, W., 2017. Highly efficient removal of hexavalent chromium in aqueous solutions via chemical reduction of plate-like micro/nanostructured zero valent iron. RSC Advances 7, 55905–55911. https://doi.org/10.1039/C7RA10846J

Kang, S.-Y., Lee, J.-U., Kim, K.-W., 2007. Biosorption of Cr(III) and Cr(VI) onto the cell surface of *Pseudomonas aeruginosa*. Biochemical Engineering Journal, A Special Issue for the APBioChEC '05 36, 54–58. https://doi.org/10.1016/j.bej.2006.06.005

Kayalvizhi, K., Vijayaraghavan, K., Velan, M., 2015. Biosorption of Cr(VI) using a novel microalga *Rhizoclonium hookeri*: equilibrium, kinetics and thermodynamic studies. Desalination and Water Treatment 56, 194–203. https://doi.org/10.1080/19443994.2014.932711

Khambhaty, Y., Mody, K., Basha, S., Jha, B., 2009. Kinetics, equilibrium and thermodynamic studies on biosorption of hexavalent chromium by dead fungal biomass of marine *Aspergillus niger*. Chemical Engineering Journal 145, 489–495. https://doi.org/10.1016/j.cej.2008.05.002

Khare, N., Bajpai, J., Bajpai, A.K., 2018. Graphene coated iron oxide (GCIO) nanoparticles as efficient adsorbent for removal of chromium ions: Preparation, characterization and batch adsorption studies. Environmental Nanotechnology, Monitoring & Management 10, 148–162. https://doi.org/10.1016/j.enmm.2018.06.002

Kumar, P.S., Kirthika, K., Kumar, K.S., 2008. Removal of Hexavalent Chromium Ions from Aqueous Solutions by an Anion-Exchange Resin. Adsorption Science & Technology 26, 693–703. https://doi.org/10.1260/026361708788251402

Kumar, R., Bishnoi, N.R., Garima, Bishnoi, K., 2008. Biosorption of chromium(VI) from aqueous solution and electroplating wastewater using fungal biomass. Chemical Engineering Journal 135, 202–208. https://doi.org/10.1016/j.cej.2007.03.004

Latha, S., Vinothini, G., Dhanasekaran, D., 2015. Chromium [Cr(VI)] biosorption property of the newly isolated actinobacterial probiont *Streptomyces werraensis* LD22. 3 Biotech 5, 423–432. https://doi.org/10.1007/s13205-014-0237-6

Lee, D.-C., Park, C.-J., Yang, J.-E., Jeong, Y.-H., Rhee, H.-I., 2000. Screening of hexavalent chromium biosorbent from marine algae. Appl Microbiol Biotechnol 54, 445–448. https://doi.org/10.1007/s002530000387

Lin, Y.-C., Wang, S.-L., 2012. Chromium(VI) reactions of polysaccharide biopolymers. Chemical Engineering Journal 181–182, 479–485. https://doi.org/10.1016/j.cej.2011.12.005

Liu, Qiang, Liu, Qinze, Ma, W., Liu, W., Cai, X., Yao, J., 2016. Comparisons of two chelating adsorbents prepared by different ways for chromium(VI) adsorption from aqueous solution. Colloids and Surfaces A: Physicochemical and Engineering Aspects 511, 8–16. https://doi.org/10.1016/j.colsurfa.2016.09.022

Liu, Y., Feng, B., Fan, T., Zhou, H., Li, X., 2008. Tolerance and removal of chromium(VI) by Bacillus sp. strain YB-1 isolated from electroplating sludge. Transactions of Nonferrous Metals Society of China 18, 480–487. https://doi.org/10.1016/S1003-6326(08)60085-0

Loukidou, M.X., Zouboulis, A.I., Karapantsios, T.D., Matis, K.A., 2004. Equilibrium and kinetic modeling of chromium(VI) biosorption by *Aeromonas caviae*. Colloids and Surfaces A: Physicochemical and Engineering Aspects 242, 93–104. https://doi.org/10.1016/j.colsurfa.2004.03.030

Lukman, S., Bukhari, A., Al-Malack, M.H., Mu'azu, N.D., Essa, M.H., 2014. Geochemical Modeling of Trivalent Chromium Migration in Saline-Sodic Soil

during Lasagna Process: Impact on Soil Physicochemical Properties [WWW Document]. The Scientific World Journal. https://doi.org/10.1155/2014/272794

M. Tobin, J., C. Roux, J., 1998. Mucor biosorbent for chromium removal from tanning effluent. Water Research 32, 1407–1416. https://doi.org/10.1016/S0043-1354(97)00343-6

Majumder, R., Sheikh, L., Naskar, A., Vineeta, Mukherjee, M., Tripathy, S., 2017. Depletion of Cr(VI) from aqueous solution by heat dried biomass of a newly isolated fungus *Arthrinium malaysianum*: A mechanistic approach. Scientific Reports 7, 11254. https://doi.org/10.1038/s41598-017-10160-0

Maleki, A., Hayati, B., Naghizadeh, M., Joo, S.W., 2015. Adsorption of hexavalent chromium by metal organic frameworks from aqueous solution. Journal of Industrial and Engineering Chemistry 28, 211–216. https://doi.org/10.1016/j.jiec.2015.02.016

Mane, C.P., Mahamuni, S.V., Kolekar, S.S., Han, S.H., Anuse, M.A., 2016. Hexavalent chromium recovery by liquid–liquid extraction with 2-octylaminopyridine from acidic chloride media and its sequential separation from other heavy toxic metal ions. Arabian Journal of Chemistry 9, S1420–S1427. https://doi.org/10.1016/j.arabjc.2012.03.021

Masood, F., Ahmad, M., Ansari, M.A., Malik, A., 2012. Prediction of Biosorption of Total Chromium by Bacillus sp. Using Artificial Neural Network. Bull Environ Contam Toxicol 88, 563–570. https://doi.org/10.1007/s00128-011-0517-3

Medina, B.Y., Torem, M.L., de Mesquita, L.M.S., 2005. On the kinetics of precipitate flotation of Cr III using sodium dodecylsulfate and ethanol. Minerals Engineering, Reagents '04 18, 225–231. https://doi.org/10.1016/j.mineng.2004.08.018

Mishra, S., Doble, M., 2008. Novel chromium tolerant microorganisms: Isolation, characterization and their biosorption capacity. Ecotoxicology and Environmental Safety 71, 874–879. https://doi.org/10.1016/j.ecoenv.2007.12.017

Mona, S., Kaushik, A., Kaushik, C.P., 2011. Biosorption of chromium(VI) by spent cyanobacterial biomass from a hydrogen fermentor using Box-Behnken model. International Biodeterioration & Biodegradation 65, 656–663. https://doi.org/10.1016/j.ibiod.2011.04.002

Mondal, N.K., Samanta, A., Dutta, S., Chattoraj, S., 2017. Optimization of Cr(VI) biosorption onto *Aspergillus niger* using 3-level Box-Behnken design: Equilibrium, kinetic, thermodynamic and regeneration studies. Journal of Genetic

Engineering and Biotechnology 15, 151–160. https://doi.org/10.1016/j.jgeb.2017.01.006

Moore, J.W., Stanitski, C.L., 2014. Chemistry: The Molecular Science. Cengage Learning.

Moussavi, G., Barikbin, B., 2010. Biosorption of chromium(VI) from industrial wastewater onto pistachio hull waste biomass. Chemical Engineering Journal 162, 893–900. https://doi.org/10.1016/j.cej.2010.06.032

Mungasavalli, D.P., Viraraghavan, T., Jin, Y.-C., 2007. Biosorption of chromium from aqueous solutions by pretreated *Aspergillus niger*: Batch and column studies. Colloids and Surfaces A: Physicochemical and Engineering Aspects 301, 214–223. https://doi.org/10.1016/j.colsurfa.2006.12.060

Mutongo, F., Kuipa, O., Kuipa, P.K., 2014. Removal of Cr(VI) from Aqueous Solutions Using Powder of Potato Peelings as a Low Cost Sorbent [WWW Document]. Bioinorganic Chemistry and Applications. https://doi.org/10.1155/2014/973153

Nag, S., Mondal, A., Bar, N., Das, S.K., 2017. Biosorption of chromium (VI) from aqueous solutions and ANN modelling. Environ Sci Pollut Res Int 24, 18817–18835. https://doi.org/10.1007/s11356-017-9325-6

Neagu, V., 2009. Removal of Cr(VI) onto functionalized pyridine copolymer with amide groups. Journal of Hazardous Materials 171, 410–416. https://doi.org/10.1016/j.jhazmat.2009.06.016

Netzahuatl-Muñoz, A.R., Cristiani-Urbina, M. del C., Cristiani-Urbina, E., 2015. Chromium Biosorption from Cr(VI) Aqueous Solutions by *Cupressus lusitanica* Bark: Kinetics, Equilibrium and Thermodynamic Studies. PLoS One 10. https://doi.org/10.1371/journal.pone.0137086

Omorogie, M.O., Babalola, J.O., Unuabonah, E.I., Gong, J.R., 2012. Kinetics and thermodynamics of heavy metal ions sequestration onto novel *Nauclea diderrichii* seed biomass. Bioresource Technology 118, 576–579. https://doi.org/10.1016/j.biortech.2012.04.053

Onyancha, D., Mavura, W., Ngila, J.C., Ongoma, P., Chacha, J., 2008. Studies of chromium removal from tannery wastewaters by algae biosorbents, *Spirogyra condensata* and *Rhizoclonium hieroglyphicum*. Journal of Hazardous Materials 158, 605–614. https://doi.org/10.1016/j.jhazmat.2008.02.043

Ouejhani, A., Dachraoui, M., Lalleve, G., Fauvarque, J.F., 2003. Hexavalent chromium recovery by liquid-liquid extraction with tributylphosphate from acidic chloride media. Anal Sci 19, 1499–1504.

Pandi, M., Shashirekha, V., Swamy, M., 2009. Bioabsorption of chromium from retan chrome liquor by cyanobacteria. Microbiological Research 164, 420–428. https://doi.org/10.1016/j.micres.2007.02.009

Parga, J.R., Cocke, D.L., Valverde, V., Gomes, J. a. G., Kesmez, M., Moreno, H., Weir, M., Mencer, D., 2005. Characterization of Electrocoagulation for Removal of Chromium and Arsenic. Chemical Engineering & Technology 28, 605–612. https://doi.org/10.1002/ceat.200407035

Park, D., Lim, S.-R., Yun, Y.-S., Park, J.M., 2008. Development of a new Cr(VI)-biosorbent from agricultural biowaste. Bioresour. Technol. 99, 8810–8818. https://doi.org/10.1016/j.biortech.2008.04.042

Park, D., Yun, Y.-S., Park, J.M., 2005. Use of dead fungal biomass for the detoxification of hexavalent chromium: screening and kinetics. Process Biochemistry 40, 2559–2565. https://doi.org/10.1016/j.procbio.2004.12.002

Parlayıcı, Ş., Pehlivan, E., 2015. Natural biosorbents (garlic stem and horse chesnut shell) for removal of chromium(VI) from aqueous solutions. Environ Monit Assess 187, 763. https://doi.org/10.1007/s10661-015-4984-6

Pehlivan, E., Altun, T., 2008. Biosorption of chromium(VI) ion from aqueous solutions using walnut, hazelnut and almond shell. J. Hazard. Mater. 155, 378–384. https://doi.org/10.1016/j.jhazmat.2007.11.071

Petruzzelli, D., Passino, R., Tiravanti, G., 1995. Ion Exchange Process for Chromium Removal and Recovery from Tannery Wastes. Ind. Eng. Chem. Res. 34, 2612–2617. https://doi.org/10.1021/ie00047a009

Pourkarim, S., Ostovar, F., Mahdavianpour, M., Moslemzadeh, M., 2017. Adsorption of chromium(VI) from aqueous solution by Artist's Bracket fungi. Separation Science and Technology 52, 1733–1741. https://doi.org/10.1080/01496395.2017.1299179

Prasad, P.V.V.V., Das, C., Golder, A.K., 2011. Reduction of Cr(VI) to Cr(III) and removal of total chromium from wastewater using scrap iron in the form of zerovalent iron(ZVI): Batch and column studies. The Canadian Journal of Chemical Engineering 89, 1575–1582. https://doi.org/10.1002/cjce.20590

Prasetyaningrum, A., Jos, B., Dharmawan, Y., Prabowo, B.T., Fathurrazan, M., Fyrouzabadi, 2018. The influence of electrode type on electrocoagulation process for removal of chromium (VI) metal in plating industrial wastewater. J. Phys.: Conf. Ser. 1025, 012126. https://doi.org/10.1088/1742-6596/1025/1/012126

Qin, G., McGuire, M.J., Blute, N.K., Seidel, C., Fong, L., 2005. Hexavalent Chromium Removal by Reduction with Ferrous Sulfate, Coagulation, and Filtration: A Pilot-Scale Study. Environ. Sci. Technol. 39, 6321–6327. https://doi.org/10.1021/es050486p

Rafati, L., Mahvi, A.H., Asgari, A.R., Hosseini, S.S., 2010. Removal of chromium (VI) from aqueous solutions using Lewatit FO36 nano ion exchange resin. Int. J. Environ. Sci. Technol. 7, 147–156. https://doi.org/10.1007/BF03326126

Rai, D., Eary, L.E., Zachara, J.M., 1989. Environmental chemistry of chromium. Science of The Total Environment, The Chromium Paradox in Modern Life 86, 15–23. https://doi.org/10.1016/0048-9697(89)90189-7

Rai, M.K., Shahi, G., Meena, V., Meena, R., Chakraborty, S., Singh, R.S., Rai, B.N., 2016. Removal of hexavalent chromium Cr (VI) using activated carbon prepared from mango kernel activated with H_3PO_4. Resource-Efficient Technologies, Special Issue on Technoscape-2016 2, S63–S70. https://doi.org/10.1016/j.reffit.2016.11.011

Rajapaksha, A.U., Alam, Md.S., Chen, N., Alessi, D.S., Igalavithana, A.D., Tsang, D.C.W., Ok, Y.S., 2018. Removal of hexavalent chromium in aqueous solutions using biochar: Chemical and spectroscopic investigations. Science of The Total Environment 625, 1567–1573. https://doi.org/10.1016/j.scitotenv.2017.12.195

Ramrakhiani, L., Majumder, R., Khowala, S., 2011. Removal of hexavalent chromium by heat inactivated fungal biomass of *Termitomyces clypeatus*: Surface characterization and mechanism of biosorption. Chemical Engineering Journal, Special Section: Symposium on Post-Combustion Carbon Dioxide Capture 171, 1060–1068. https://doi.org/10.1016/j.cej.2011.05.002

Rangabhashiyam, S., Balasubramanian, P., 2018. Adsorption behaviors of hazardous methylene blue and hexavalent chromium on novel materials derived from *Pterospermum acerifolium* shells. Journal of Molecular Liquids 254, 433–445. https://doi.org/10.1016/j.molliq.2018.01.131

Ranjan, D., Srivastava, P., Talat, M., Hasan, S.H., 2009. Biosorption of Cr(VI) from Water Using Biomass of *Aeromonas hydrophila*: Central Composite Design for

Optimization of Process Variables. Appl Biochem Biotechnol 158, 524–539. https://doi.org/10.1007/s12010-008-8404-z

Rapti, S., Pournara, A., Sarma, D., T. Papadas, I., S. Armatas, G., C. Tsipis, A., Lazarides, T., G. Kanatzidis, M., J. Manos, M., 2016. Selective capture of hexavalent chromium from an anion-exchange column of metal organic resin–alginic acid composite. Chemical Science 7, 2427–2436. https://doi.org/10.1039/C5SC03732H

Rengaraj, S., Yeon, K.-H., Moon, S.-H., 2001. Removal of chromium from water and wastewater by ion exchange resins. Journal of Hazardous Materials 87, 273–287. https://doi.org/10.1016/S0304-3894(01)00291-6

Rezaei, H., 2016. Biosorption of chromium by using Spirulina sp. Arabian Journal of Chemistry 9, 846–853. https://doi.org/10.1016/j.arabjc.2013.11.008

Saha, R., Nandi, R., Saha, B., 2011. Sources and toxicity of hexavalent chromium. Journal of Coordination Chemistry 64, 1782–1806. https://doi.org/10.1080/00958972.2011.583646

Şahin, Y., Öztürk, A., 2005. Biosorption of chromium(VI) ions from aqueous solution by the bacterium *Bacillus thuringiensis*. Process Biochemistry 40, 1895–1901. https://doi.org/10.1016/j.procbio.2004.07.002

Salmani Abyaneh, A., Fazaelipoor, M.H., 2016. Evaluation of rhamnolipid (RL) as a biosurfactant for the removal of chromium from aqueous solutions by precipitate flotation. Journal of Environmental Management 165, 184–187. https://doi.org/10.1016/j.jenvman.2015.09.034

Samuel, M.S., Bhattacharya, J., Raj, S., Santhanam, N., Singh, H., Pradeep Singh, N.D., 2019. Efficient removal of Chromium(VI) from aqueous solution using chitosan grafted graphene oxide (CS-GO) nanocomposite. International Journal of Biological Macromolecules 121, 285–292. https://doi.org/10.1016/j.ijbiomac.2018.09.170

Sari, A., Tuzen, M., 2009. Removal of mercury(II) from aqueous solution using moss (*Drepanocladus revolvens*) biomass: Equilibrium, thermodynamic and kinetic studies. Journal of Hazardous Materials 171, 500–507. https://doi.org/10.1016/j.jhazmat.2009.06.023

Sari, A., Tuzen, M., 2008. Biosorption of total chromium from aqueous solution by red algae (*Ceramium virgatum*): equilibrium, kinetic and thermodynamic studies. J Hazard Mater 160, 349–355. https://doi.org/10.1016/j.jhazmat.2008.03.005

Senol, A., 2004. Amine extraction of chromium(VI) from aqueous acidic solutions. Separation and Purification Technology 36, 63–75. https://doi.org/10.1016/S1383-5866(03)00153-9

Sharma, D., Chaudhari, P.K., Prajapati, A.K., 2019. Removal of chromium (VI) and lead from electroplating effluent using electrocoagulation. Separation Science and Technology 0, 1–11. https://doi.org/10.1080/01496395.2018.1563157

Sibi, G., 2016. Biosorption of chromium from electroplating and galvanizing industrial effluents under extreme conditions using *Chlorella vulgaris*. Green Energy & Environment 1, 172–177. https://doi.org/10.1016/j.gee.2016.08.002

Sillerová, H., Komárek, M., Chrastný, V., Novák, M., Vaněk, A., Drábek, O., 2013. Brewers draff as a new low-cost sorbent for chromium (VI): comparison with other biosorbents. J Colloid Interface Sci 396, 227–233. https://doi.org/10.1016/j.jcis.2013.01.029

Solgi, M., Najib, T., Ahmadnejad, S., Nasernejad, B., 2017. Synthesis and characterization of novel activated carbon from Medlar seed for chromium removal: Experimental analysis and modeling with artificial neural network and support vector regression. Resource-Efficient Technologies 3, 236–248. https://doi.org/10.1016/j.reffit.2017.08.003

Someda, H.H., El-Shazly, E.A., Sheha, R.R., 2005. The role of some compounds on extraction of chromium(VI) by amine extractants. J. Hazard. Mater. 117, 213–219. https://doi.org/10.1016/j.jhazmat.2004.09.024

Song, Z., Williams, C.J., Edyvean, R.G.J., 2004. Treatment of tannery wastewater by chemical coagulation. Desalination 164, 249–259. https://doi.org/10.1016/S0011-9164(04)00193-6

Srinath, T., Verma, T., Ramteke, P.W., Garg, S.K., 2002. Chromium (VI) biosorption and bioaccumulation by chromate resistant bacteria. Chemosphere 48, 427–435.

Srivastava, S., Thakur, I.S., 2012. Biosorption and biotransformation of chromium by Serratia sp. isolated from tannery effluent. Environmental Technology 33, 113–122. https://doi.org/10.1080/09593330.2011.551842

Sun, Y., Yue, Q., Mao, Y., Gao, B., Gao, Y., Huang, L., 2014. Enhanced adsorption of chromium onto activated carbon by microwave-assisted H_3PO_4 mixed with Fe/Al/Mn activation. Journal of Hazardous Materials 265, 191–200. https://doi.org/10.1016/j.jhazmat.2013.11.057

Tran, H.N., Nguyen, D.T., Le, G.T., Tomul, F., Lima, E.C., Woo, S.H., Sarmah, A.K., Nguyen, H.Q., Nguyen, P.T., Nguyen, D.D., Nguyen, T.V., Vigneswaran, S., Vo, D.-V.N., Chao, H.-P., 2019. Adsorption mechanism of hexavalent chromium onto layered double hydroxides-based adsorbents: A systematic in-depth review. Journal of Hazardous Materials 373, 258–270. https://doi.org/10.1016/j.jhazmat.2019.03.018

Tunali, S., Kiran, I., Akar, T., 2005. Chromium(VI) biosorption characteristics of Neurospora crassa fungal biomass. Minerals Engineering 18, 681–689. https://doi.org/10.1016/j.mineng.2004.11.002

Ucun, H., Bayhan, Y.K., Kaya, Y., Cakici, A., Algur, O.F., 2002. Biosorption of chromium(VI) from aqueous solution by cone biomass of *Pinus sylvestris*. Bioresour. Technol. 85, 155–158.

Ullah, I., Nadeem, R., Iqbal, M., Manzoor, Q., 2013. Biosorption of chromium onto native and immobilized sugarcane bagasse waste biomass. Ecological Engineering 60, 99–107. https://doi.org/10.1016/j.ecoleng.2013.07.028

Wang, S.-L., Lee, J.-F., 2011. Reaction mechanism of hexavalent chromium with cellulose. Chemical Engineering Journal 174, 289–295. https://doi.org/10.1016/j.cej.2011.09.031

Wang, X.S., Li, Z.Z., Tao, S.R., 2009. Removal of chromium (VI) from aqueous solution using walnut hull. Journal of Environmental Management 90, 721–729. https://doi.org/10.1016/j.jenvman.2008.01.011

Xie, P., Hao, X., Mohamad, O.A., Liang, J., Wei, G., 2013. Comparative study of chromium biosorption by *Mesorhizobium amorphae* strain CCNWGS0123 in single and binary mixtures. Appl. Biochem. Biotechnol. 169, 570–587. https://doi.org/10.1007/s12010-012-9976-1

Xu, X., Huang, H., Zhang, Y., Xu, Z., Cao, X., 2019. Biochar as both electron donor and electron shuttle for the reduction transformation of Cr(VI) during its sorption. Environmental Pollution 244, 423–430. https://doi.org/10.1016/j.envpol.2018.10.068

Xu, X.-R., Li, H.-B., Li, X.-Y., Gu, J.-D., 2004. Reduction of hexavalent chromium by ascorbic acid in aqueous solutions. Chemosphere 57, 609–613. https://doi.org/10.1016/j.chemosphere.2004.07.031

Yang, K., Zhang, J., Yang, T., Wang, H., 2016. Investigation of equilibrium and kinetics of Cr(VI) adsorption by dried *Bacillus cereus* using response surface

methodology. Water Sci. Technol. 73, 617–627. https://doi.org/10.2166/wst.2015.522

Yang, L., Chen, J.P., 2008. Biosorption of hexavalent chromium onto raw and chemically modified Sargassum sp. Bioresource Technology 99, 297–307. https://doi.org/10.1016/j.biortech.2006.12.021

Yu, W., Zhang, L., Wang, H., Chai, L., 2013. Adsorption of Cr(VI) using synthetic poly(m-phenylenediamine). J. Hazard. Mater. 260, 789–795. https://doi.org/10.1016/j.jhazmat.2013.06.045

Zakaria, Z.A., Aruleswaran, N., Kaur, S., Ahmad, W.A., 2007. Biosorption and bioreduction of Cr(VI) by locally isolated Cr-resistant bacteria. Water Sci Technol 56, 117–123. https://doi.org/10.2166/wst.2007.674

Zhang, X., Fu, W., Yin, Y., Chen, Z., Qiu, R., Simonnot, M.-O., Wang, X., 2018. Adsorption-reduction removal of Cr(VI) by tobacco petiole pyrolytic biochar: Batch experiment, kinetic and mechanism studies. Bioresource Technology 268, 149–157. https://doi.org/10.1016/j.biortech.2018.07.125

Zhao, N., Yin, Z., Liu, F., Zhang, M., Lv, Y., Hao, Z., Pan, G., Zhang, J., 2018. Environmentally persistent free radicals mediated removal of Cr(VI) from highly saline water by corn straw biochars. Bioresource Technology 260, 294–301. https://doi.org/10.1016/j.biortech.2018.03.116

Zhao, R., Li, X., Li, Yumei, Li, Yanzi, Sun, B., Zhang, N., Chao, S., Wang, C., 2017. Functionalized magnetic iron oxide/polyacrylonitrile composite electrospun fibers as effective chromium (VI) adsorbents for water purification. Journal of Colloid and Interface Science 505, 1018–1030. https://doi.org/10.1016/j.jcis.2017.06.094

Zheng, Y.-M., Liu, T., Jiang, J., Yang, L., Fan, Y., Wee, A.T.S., Chen, J.P., 2011. Characterization of hexavalent chromium interaction with Sargassum by X-ray absorption fine structure spectroscopy, X-ray photoelectron spectroscopy, and quantum chemistry calculation. Journal of Colloid and Interface Science 356, 741–748. https://doi.org/10.1016/j.jcis.2010.12.070

Chapter 2
Theoretical Aspects

2.1 Adsorption Isotherms

Adsorption isotherms are theoretical graphs through which the adsorption process is studied as a function of increase in concentration of adsorbate at a constant termperature, hence, the name adsorption isotherms. Adsorption isotherm have been studied in great detail during the course of adsorption studies by many researchers. Adsorption isotherms are used for determining various important parameters such as maximum adsorption capacity, physisorption or chemisorption etc. and are very important part of any adsorption study. Various adsorption isotherms, their mathematical expression and the underlying assumptions have been described below.

2.1.1 Langmuir adsorption isotherm

Langmuir adsorption considers the following assumptions

a. There are fixed number of adsorption sites on the material surface ("Langmuir Adsorption Isotherm | Chemistry Learning," n.d.)
b. All adsorbption sites are alike
c. Only one molecule can be adsorbed on one adsorption site
d. The adsorbed molecules do not have any interaction among them
e. The adsorption take place in a monolayer fasion
f. There is a dynamic equilibrium between the adsorbed and the unadsorbed molecules

Derivation of Langmuir adsorption isotherm

Suppose the number of total sites available for biosorption at time 0 is N_o or the maximum biosorption capacity is Q_o

Suppose the number of sites available for biosorption is (N_o-N_t), where, N_t is number of sites occupied at time t or the biosorption capacity at time t is q_t and at equilibrium is q_e

Suppose the concentration of the adsorbate at time 0 is C_o, at time t is C_t and at equilibrium is C_e

We know that the rate of forward reaction or adsorption at time t is directly proportional to the number of sites available for adsorption i.e. Q_o- q_t and concentration of the adsorbate at time t i.e. C_t

Rate of forward reaction $\propto C_t(Q_o - q_t)$ or

Rate of adsorption = $K_a C_t(Q_o - q_t)$, where, K_a is the constant for backward reaction

We also know that rate of backward reaction or desorption at time t is directly proportional to the number of sites occupied i.e. q_t

Rate of backward reaction $\propto C_t(q_t)$ or

Rate of desorption = $K_d C_t(q_t)$, where, K_d is the constant for backward reaction

At equilibrium, Rate of forward reaction = Rate of backward reaction

$K_a C_e(Q_o - q_e) = K_d C_e(q_e)$

Now, we can put $K_a/K_d = K_L$, where, K_L is the Langmuir adsorption isotherm constant.

So, $K_L C_e Q_o - K_L C_e q_e = q_e$

$K_L C_e Q_o = K_L C_e q_e + q_e$

$$\frac{C_e}{q_e} = \frac{1 + C_e K_L}{Q_o K_L}$$

The mathematical representation of Langmuir model is as follows (Langmuir, 1918)

$$\frac{C_e}{q_e} = \frac{1}{Q_o K_L} + \frac{C_e}{Q_o} \quad (1)$$

where, q_e represents the biosorption capacity when equilibrium is reached (mg/g), C_e symbolizes the amount of metal at equilibrium (mg/L), K_L denotes the Langmuir isotherm constant (L/mg) and Q_0 denotes the adsorption potential (mg/g).

The following expression gives an idea of the feasibility of the adsorption phenomenon in Langmuir manner. The biosorption process based on R_L values is unconducive when $R_L > 1$, conducive when $0 < R_L < 1$, linear when $R_L = 1$, and irreversible if $R_L = 0$.

$$R_L = \frac{1}{1 + C_o K_L} \quad (2)$$

Drawbacks of Langmuir adsorption isotherm

a. Langmuir isotherm model is relevant only for low concentrations of adsorbate

b. The real surface of solid material is heterogeneous rather homogeneous

c. van der Waal interactions exist among the adsorbed molecules

2.1.2 Freundlich adsorption isotherm

Freundlich model of adsorption considers that there occurs association among the adsorbed molecules. The model also assumes that adsorption occurs in a heterogeneous multilayer fashion**.**

Derivation of Freundlich adsorption isotherm

From the Langmuir adsorption isotherm, we know that

$$\frac{q_e}{Q_o} = \frac{K_L C_e}{1 + K_L C_e}$$

At very low concentrations of adsorbate, $K_L C_e$ beomes negligible or very low i.e. $K_L C_e$ <<< 1

Therefore, the equation becomes

$$\frac{q_e}{Q_o} = K_L C_e$$

The adsorption capacity is directly proportional to the concentration of the adsorbate

At very high concentration of adsorbate, $K_L C_e$ beomes very high i.e. $K_L C_e$ >>> 1

Therefore, the equation becomes

$$\frac{q_e}{Q_o} = \frac{K_L C_e}{K_L C_e}$$

The adsorption capacity becomes independent of the concentration of the adsorbate

From the above two expressions, we can write

$$\frac{q_e}{Q_o} = K_L C_e^{\frac{1}{n_F}}$$

The mathematical representation of the Freundlich model is (Freundlich, 1907)

$$q_e = K_f C_e^{\frac{1}{n_F}} \qquad (3)$$

where, K_f represents a constant corresponding to the biosorption capacity and $1/n_F$, an empirical parameter affiliated to the biosorption intensity. The value of term $1/n_F$ range from 0 to 1. At higher concentration of adsorbate, the value of $1/n_F$ is approximately zero. Hence, at high adsorbate concentration, the adsorption potential of the adsorbent becomes independent of the concentration of the adsorbent. On the contrary, when the concentration of the adsorbate is low, the value of $1/n_F$ is more than zero and less than 1. Therefore, at low adsorbate concentration, Freundlich adsorption isotherm assumes that the biosorption capacity of adsorbent is in accordance with the adsorbate concentration. Freundlich model in linearized form is represented as below.

$$\log_{10} q_e = \log_{10}(K_f) + \left(\frac{1}{n_F}\right)\log_{10} C_e \tag{4}$$

2.1.3 Redlich Peterson adsorption isotherm

Redlich Peterson model lies on the assumptions of both Langmuir and Freundlich adsorption model taken together. Redlich Peterson model is described by the following equation (Redlich and Peterson, 1959)

$$q_e = \frac{K_{RP} C_e}{1 + a_{RP} C_e^{\beta}} \tag{5}$$

where, K_{RP} denotes the Redlich Peterson model constant (L/g), a_{RP} denotes the Redlich Peterson constant (L/mg). The exponential term β, varies in the range 0 and 1. If β = 1, the Redlich–Peterson model assumes the Langmuir model form and when β = 0, the Redlich-Peterson model takes the form of Henry's law.

2.1.4 Dubninin Radushkevich adsorption isotherm

The Dubinin Radushkevich isotherm model in mathematical form is expressed as (Sing, 1985)

$$\ln q_e = \ln Q_m - K\,\varepsilon^2 \tag{6}$$

where, Q_m denotes highest adsorption potential (mg/g), K denotes the activity coefficient (mol^2/J^2). ε is the Polanyi potential, estimated from the mathematical expression

$$\varepsilon = RT(\ln(1 + C_e^{-1})) \tag{7}$$

where, T is the absolute temperature (K) and R denotes universal gas constant (J/mol K).

The Apparent adsorption energy, E (kJ/mol) is expressed as

$$E = \frac{1}{\sqrt{2K}} \quad (8)$$

On the basis of Apparent adsorption energy, the biosorption process is categorized as physical biosorption if $1<E<16$ kJ/mol and chemisorption if $E>16$ kJ/mol. The mechanism primarily relates to ion exchange if $8<E<16$kJ/mol (Aytas et al., 2011).

2.1.5 Brunauer Emmett Teller (BET) isotherm

Brunauer Emmett Teller (BET) isotherm lies on the following assumptions

a. The adsorption process is primarily multilayer
b. Adsorbed molecules do not interact with themselves alike the Langmuir adsorption process
c. The surface is homogeneous

BET adsorption theory is based on the following principles

a. There exists an equilibrium between the adsorption process and the desorption procss
b. The desorption rate is equal to the adsorption rate as the equilibrium is achieved
c. The magnitude of adsorption in the n^{th} layer is in accordance with the sum total of sites present in the adsorbent in the $(n-1)^{th}$ layer and the concentration of the adsorbate molecules
d. The amount of desorption in the n^{th} layer is proportional to the number of site occupied by single adsorbate molecules in these sites.

Derivation of BET adsorption isotherm

We assume that there is certain number of sites or fixed surface area viz. A_0, A_1, A_2,….A_n on the layers viz. 0, 1, 2,……..N, respectively on the adsorbent available for the adsorption. We also assume that adsorption takes place in a multilayer fashion so that the rate of desorption from the $(n-1)^{th}$ layer is equal to the rate of adsorption for the n^{th} layer at equilibrium.

At equilibrium,

Rate of formation of i^{th} layer = Rate of destruction of i^{th} layer

Ways in which i^{th} layer can be formed

If adsorption takes place on $(i-1)^{th}$ layer, Rate = $(k_a)_i n_{i-1} p$

If desorption takes place on $(i+1)^{th}$ layer, Rate = $(k_d)_{i+1} n_{i+1}$

Ways in which i^{th} layer can be destroyed

If adsorption takes place on i^{th} layer, Rate = $(k_a)_{i+1} n_{i+1}$

If desorption takes place on i^{th} layer, Rate = $(k_d)_i n_i$

Therefore, we can write

$$(k_a)_i n_{i-1} p + (k_d)_{i+1} n_{i+1} = (k_a)_{i+1} n_{i+1} + (k_d)_i n_i$$

Writing this equation for various layers and on addition

$$(k_a)_1 n_0 p + (k_d)_2 n_2 = (k_a)_2 n_2 + (k_d)_1 n_1$$

$$(k_a)_2 n_1 p + (k_d)_3 n_3 = (k_a)_3 n_3 + (k_d)_2 n_2$$

$$(k_a)_3 n_2 p + (k_d)_4 n_4 = (k_a)_4 n_4 + (k_d)_3 n_3$$

.

.

We have

$$(k_d)_{i+1} n_{i+1} = (k_a)_{i+1} n_i p$$

$n_{i+1} = x.\, n_i$ where, $x = ((k_a)_{i+1})/ ((k_d)_{i+1})*p$

We know that the forces of attraction between the bare surface and the first layer are higher than the forces between the adsorbate particles in the higher layers. So, we have to compensate for this effect. For this, we multiply by extra constant c for the i=0 equation

$$n_1 = c.x.\, n_0$$

Also, we know that the adsorption and desorption constant almost remains constant for layer higher than 1, so

$$((k_a)_{i+1})/((k_d)_{i+1}) = k_a/ k_d$$

Further, as in case of gas molecules, adsorption and desorption constant are dependent on partial pressures, therefore we have

$x = p/p_o$

Now, we will count the total number of molecules adsorbed at a given time and the total number of sites so as to come to the simple form of BET adsorption isotherm

We have from above,

$n_i = c.x.\ n_{i-1} = x^2.\ n_{i-2} = x^3.n_{i-3} = \ldots\ldots = x^{i-1}.n_1 = c.x^i.n_0$

Therefore, $n_i = c.x^i.n_0$

The total number of molecules adsorbed N is given by

$$N = \sum_{i=0}^{\infty} i.n_i = c.n_o.x\frac{d}{dx}\sum_{i=1}^{\infty} x^i$$

The total number of sites, N_T is given by

$$N_T = \sum_{i=0}^{\infty} n_i = n_0 + \sum_{i=1}^{\infty} n_i$$

We have,

$$\sum_{i=1}^{\infty} x_i = \frac{x}{1-x}$$

Substituting this in equation for total number of sites and total number of molecules adsorbed

$$N = \frac{c.n_o.x}{(1-x)^2}$$

$$N_T = n_o\left(1 + \frac{c.x}{1-x}\right)$$

The total number of sites N_T is proportional to the monolayer volume v_m which is the volume of gas adsorbed when the entire surface is covered with a complete monolayer.

The total number of molecules adsorbed, *N* is proportional to the volume v, which is the volume of adsorbed molecules.

$$\frac{N}{N_T} = \frac{v}{v_m} = \frac{c.x}{(1-x)(1-x+c.x)}$$

The mathematical expression of BET adsorption isotherm is (Naderi, 2015)

$$\frac{v}{v_m} = \frac{c.x}{(1-x).(1-x+c.x)} \quad (9)$$

where, v denotes the volume of molecules or gas adsorbed at random. v_m is the volume of molecules or gas adsorbed on occupying the whole surface by a monolayer and is a constant. c is the ratio of heat of adsorption of the first layer and second layer. x is the relative pressure expressed as p/p_o.

BET adsorption isotherm in linearized form is given as

$$\frac{1}{v(1-x)} = \frac{1}{v_m} + \left(\frac{1}{v_m.c}\right)\left(\frac{1-x}{x}\right) \quad (10)$$

Using this equation, v_m and c is estimated from the plot between $1/v(1-x)$ and $(1-x)/x$.

Limitations of BET adsorption isotherm

a. The BET adsorption isotherm assumes uniform surface which may not be the case.
b. There may be interaction between the adsorbed molecules which is not considered.
c. Heat of adsorption from 2nd layer and subsequent layers is assumed equal which is not always true.

2.2 Kinetic models

The determination of mechanism is an important aspect of any study and it applies to adsorption as well. Various kinetic models have been proposed by researchers for determining the mechanism of the adsorption process such as Pseudo first order and Pseudo second order. Kinetic studies are an integral part of adsorption studies. Different important kinetic models used in adsorption studies, their mathematical representation and the underlying assumptions have been described in detail below.

2.2.1 Pseudo first order

Pseudo first order kinetic model considers that the practical order of a reaction should be one. The term pseudo comes into existence when the concentration of one or more reactant is excess and/or is a catalyst so that the change in concentration of these reactant/catalyst is negligible as compared to a single reactant whose concentration changes significantly during the reaction. These type of reaction are known as Pseudo-first order reactions and follow Pseudo first order kinetic model.

The mathematical form of pseudo first order Lagergren model (Lagergren, 1898) is $\log(q_e - q_t) = \log q_e - \frac{k_1}{2.303} t$ (11)

where, q_e and q_t are the magnitude of Cr(VI) adsorbed (mg/g) at equilibrium and at time t. k_1 (min) represents the pseudo-first-order rate constant. Further, the pseudo first order model assumes the rate of engaging biosorption sites to be in accordance with the number of vacant sites.

2.2.2 Pseudo second order

Pseudo second order is alike pseudo first order in that its order is pseudo and it is also a pseudo-model. The Pseudo second order model has true order more than two. However, when the other chemicals/catalysts are provided in excess, except one or two chemicals which gets depleted considerably during the reaction, the order of the reaction becomes two and hence, is known as Pseudo second order model.

The Pseudo second order model expression is expressed as follows (Ho and McKay, 1999)

$$\frac{t}{q_t} = \frac{1}{k_2 q_e^{\,2}} + \frac{t}{q_e} \quad (12)$$

where, k_2 (g/mg/min) denotes the pseudo-second-order constant.

2.2.3 Intraparticle diffusion

Intraparticle diffusion kinetic model assumes that there is mass transfer to the internal part of the adsorbent and it occurs through diffusion of the adsorbate inside the pores of the adsorbent. Weber and Morris proposed the mathematical form of the intraparticle diffusion model follows (Morris and Weber, 1964)

$$q_t = k_{id} t^{1/2} + C \quad (13)$$

where, k_{id} represents the intraparticle diffusion rate constant (mg/g/min$^{1/2}$), C is the constant.

2.3 Thermodynamic parameters

Thermodynamic variables viz. enthalpy ΔH^0, free energy change ΔG^0 and entropy ΔS^0 are indicators of spontaneity and heat change. The relation between enthalpy ΔH^0, free energy change ΔG^0 and entropy ΔS^0 is given by (Khosravi et al., 2018)

$$\Delta G^o = \Delta H^o - T\Delta S^o \quad (14)$$

The mathematical relation between free energy change and equilibrium constant is

$$\Delta G^o = -RT \ln K_C \quad (15)$$

$$\ln K_C = -\frac{\Delta H^o}{RT} + \frac{\Delta S^o}{R} \quad (16)$$

$$K_C = \frac{q_e}{C_e} \quad (17)$$

The activation energy (E_a) is estimated by the following expression

$$\ln K_C = \ln A - \frac{E_a}{RT} \quad (18)$$

where, A is pre-exponential factor.

2.4 Continuous column models

Theoretical models underlying continuous mode have been proposed by many investigators. These continuous column models provide important information hidden beneath the experimental data and are highly useful for the determination of maximum adsorption capacity. Further, these models play important role in designing the column reactor at a large scale. Various important continuous column models, the fundamental assumptions and mathematical denotations have been discussed in detail below.

2.4.1 Thomas model

Thomas model considers the following theory (Thomas, 1944)

a. Adsorption follows Langmuir model

b. The adsorption process kinetics obey reversible 2nd order reaction kinetics

c. External and internal diffusion limitations do not occur

d. The column behaves as plug flow reactor

The linear representation of the Thomas model is

$$\ln\left(\frac{C_o}{C_t}-1\right)=\frac{k_{TH}Q_oW}{F}-k_{TH}C_ot \quad (19)$$

where, k_{TH} is a symbol for the adsorption rate constant (mg/L/min) and Q_o depicts the maximum adsorption potential (mg/g). W denotes the quantity of adsorbent used in column experiment (g). F represent the flow rate (mL/min). C_o/C_t is the ratio of the effluent to the inlet initial metal concentration. k_{TH} and Q_o were calculated from the linear plot between $\ln(C_o/C_t - 1)$ and t. Thomas model is used to estimate the highest adsorption potential of the biosorbent in column studies.

2.4.2 Adams Bohart model

The theoretical basis of Adams Bohart model is that the adsorption capacity (P) is

corresponding to the residual capacity as well as the initial metal concentration (Bohart and Adams, 1920). The mathematical representation of the model is

$$\ln\left(\frac{C_t}{C_o}\right)=k_{AB}C_ot-k_{AB}N_{AB}\left(\frac{Z}{u}\right) \quad (20)$$

where, N_{AB} represents the saturation concentration (mg/L), k_{AB} depicts the kinetic constant (L/mg min) and u denotes the linear velocity (cm/min). Z represents the bed height. N_{AB} and k_{AB} were determined from the linear plot between $\ln(C_t/C_o)$ and t.

2.4.3 Yoon Nelson model

The Yoon Nelson model is derived from the notion that the probability of a molecule getting adsorbed on adsorbent (P) is directly proportional to the probability of a molecule not getting adsorbed (escape) (1-P) (YOON and NELSON, 1984). The assumption is expressed as

$$\frac{dP}{dt}=kP(1-P) \quad (21)$$

where, k is a constant.

The mathematical representation of the Yoon Nelson model is expressed as

$$\ln\left(\frac{C_t}{C_o - C_t}\right) = k_{YN}t - k_{YN}\tau \quad (22)$$

where, k_{YN} represents the Yoon Nelson rate constant (L/min) and τ depicts the time duration for 50% adsorbate breakthrough (min).

2.4.4 Bed Depth Service time model

Bed Depth Service time model (BDST) was suggested by Hutchins to anticipate the association between bed height (Z) and service time (t). BDST model considers that bed height (Z) is directly proportional to the service time (t). BDST model is the modification of Adams Bohart model (Bohart and Adams, 1920) proposed by Hutchins (Hutchins, 1973). The mathematical form of the BDST model is given as

$$t = \left(\frac{N_o Z}{C_o u}\right) - \left(\frac{1}{C_o K_a}\right)\ln\left(\frac{C_o}{C_t} - 1\right) \quad (23)$$

where, t is the service time (min) at breakthrough time, u represents the linear flow velocity (cm/min), N_o depicts the adsorption capacity of the bed (mg/L). The bed height is represented by Z and the rate constant is represented by K_a (L/mg min).

References

Aytas, S., Turkozu, D.A., Gok, C., 2011. Biosorption of uranium(VI) by bi-functionalized low cost biocomposite adsorbent. Desalination 280, 354–362. https://doi.org/10.1016/j.desal.2011.07.023

Bohart, G.S., Adams, E.Q., 1920. Some aspects of the behvior of charcoal with respect to chlorine. J. Am. Chem. Soc. 42, 523–544. https://doi.org/10.1021/ja01448a018

Freundlich, H., 1907. Über die Adsorption in Lösungen. Zeitschrift für Physikalische Chemie 57U, 385–470. https://doi.org/10.1515/zpch-1907-5723

Ho, Y.S., McKay, G., 1999. Pseudo-second order model for sorption processes. Process Biochemistry 34, 451–465. https://doi.org/10.1016/S0032-9592(98)00112-5

Hutchins, R.A., 1973. New method simplifies design of activated carbon systems. Chemical Engineering 133–138.

Khosravi, R., Moussavi, G., Ghaneian, M.T., Ehrampoush, M.H., Barikbin, B., Ebrahimi, A.A., Sharifzadeh, G., 2018. Chromium adsorption from aqueous solution using novel green nanocomposite: Adsorbent characterization, isotherm, kinetic and thermodynamic investigation. Journal of Molecular Liquids 256, 163–174. https://doi.org/10.1016/j.molliq.2018.02.033

Lagergren, S.Y., 1898. Zur Theorie der sogenannten Adsorption gelöster Stoffe. Bihang till Kungliga Svenska Vetenskapsakademiens, Handlingar 24, 1–39.

Langmuir Adsorption Isotherm | Chemistry Learning [WWW Document], n.d. URL http://www.chemistrylearning.com/langmuir-adsorption-isotherm/ (accessed 6.16.19).

Langmuir, I., 1918. The Adsorption of Gases on Plane Surfaces of Glass, Mica and Platinum. J. Am. Chem. Soc. 40, 1361–1403. https://doi.org/10.1021/ja02242a004

Morris, J.C., Weber, W.J., 1964. Removal of biologically-resistant pollutants from waste waters by adsorption, in: Southgate, B.A. (Ed.), Advances in Water Pollution Research. Pergamon, pp. 231–266. https://doi.org/10.1016/B978-1-4832-8391-3.50032-4

Naderi, M., 2015. Chapter Fourteen - Surface Area: Brunauer–Emmett–Teller (BET), in: Tarleton, S. (Ed.), Progress in Filtration and Separation. Academic Press, Oxford, pp. 585–608. https://doi.org/10.1016/B978-0-12-384746-1.00014-8

Redlich, O., Peterson, D.L., 1959. A Useful Adsorption Isotherm. J. Phys. Chem. 63, 1024–1024. https://doi.org/10.1021/j150576a611

Sing, K.S.W., 1985. Reporting physisorption data for gas/solid systems with special reference to the determination of surface area and porosity (Recommendations 1984). Pure Appl. Chem., PAC 57, 603–619. https://doi.org/10.1351/pac198557040603

Thomas, H.C., 1944. Heterogeneous Ion Exchange in a Flowing System. J. Am. Chem. Soc. 66, 1664–1666. https://doi.org/10.1021/ja01238a017

YOON, Y.H., NELSON, J.H., 1984. Application of Gas Adsorption Kinetics I. A Theoretical Model for Respirator Cartridge Service Life. American Industrial Hygiene Association Journal 45, 509–516. https://doi.org/10.1080/15298668491400197

Chapter 3
Biosorption of chromium (VI) by *Pinus kesiya* cone biomass

3.1 Materials and methods

3.1.1 Preparation of chromium solution

2.828 g of potassium dichromate was dissolved in 1000 mL deionized water to prepare 1000 ppm stock solution. Working standards of 100 to 500 mg/L solutions were made by appropriate dilutions in deionized water.

3.1.2 Preparation of biosorbent

P. kesiya cone biomass (PKB) was collected from Nehru Park, Shillong, Meghalaya, India. The collected cones were washed thrice with deionized water before keeping in hot air oven at 353 K for drying. Pine cones were ground in a mixer-grinder before separating them into three different particle size range (<300 μm, 300-425 μm, 425-600 μm). Sieved pine cone biomass was kept in sealed bags for further use.

3.1.3 Characterization of biosorbent

Point of Zero charge (PZC) analysis of PKB was carried out by agitating 0.5 g of biosorbent in 0.1 M KNO_3 of different pH (pH 2.0 to 9.0) for 24 h at 313 K. pH of the solutions was adjusted using 0.1 N HCl and 0.1 N NaOH measured by a digital pH meter (PB-11, Sartorius, Germany). The variation in the pH between initial and final state was measured and plotted vs. the initial pH. The point of intersection at which ΔpH is zero was considered as PZC.

Surface characteristics of the biosorbent were determined using Field emission scanning electron microscopy (FESEM) (Zeiss, Sigma, Germany). Energy dispersive X-ray spectrometry (EDX) (Zeiss, Sigma, Germany) was done for PKB before and after Cr(VI) adsorption. Functional groups involved in the Cr(VI) adsorption were identified using Fourier transform infrared spectrometry (FTIR) (Spectrum Two, PerkinElmer, USA). Surface area and pore size of PKB were measured by Surface area and Pore Size analyzer (Autosorb-IQ MP, Quantachrome, USA). Thermal stability of the biosorbent was analyzed by subjecting the biosorbent to temperatures in the range of 25°C to 800°C by increasing temperature at a rate of 10°C min^{-1} in N_2 atmosphere using High temperature DSC/TG system (TG) (STA449F3A00, Netzsch, Bavaria, Germany).

Biosorption parameter optimization experiments were performed in 250 mL screw capped conical flasks with 50 mL working volume. Agitation of the PKB and Cr(VI) solution was carried out using incubator shaker (Orbitek, Scigenics Biotech, India) at 303 K. Various parameters such as biosorbent dose (0.5 - 5 g/L), Biosorbent size

(< 300 - 600 µm), pH (2.0 - 5.0), Temperature (303 - 323 K) and initial chromium concentration (100 - 500 mg/L) were optimized for maximum Cr(VI) removal. Residual Cr(VI) concentration in the filtrate from samples after contacting with the biosorbent was measured using a UV-Visible spectrophotometer (GeneQuant 1300, GE, USA) after addition of 1, 5-Diphenyl Carbazide in acidic conditions at 540 nm. The percentage removal of Cr(VI) was calculated by using the equation:

$$\%\text{Removal} = \left(\frac{C_o - C_e}{C_o}\right) \times 100 \quad (1)$$

where, C_o is the initial Cr(VI) concentration (mg/L), C_e is the equilibrium Cr(VI) concentration at time 't' (mg/L).

The adsorption capacity q_t of PKB was calculated using the equation

$$q_t = \frac{(C_o - C_e) \times V}{m} \quad (2)$$

where, C_t is the Cr(VI) concentration at any time 't' (mg/L), 'm' is the mass of PKB (g) and 'V' is the volume of Cr(VI) solution (mL). A general schematic diagram of the work flow for batch studies is shown below in Fig. 3.1.

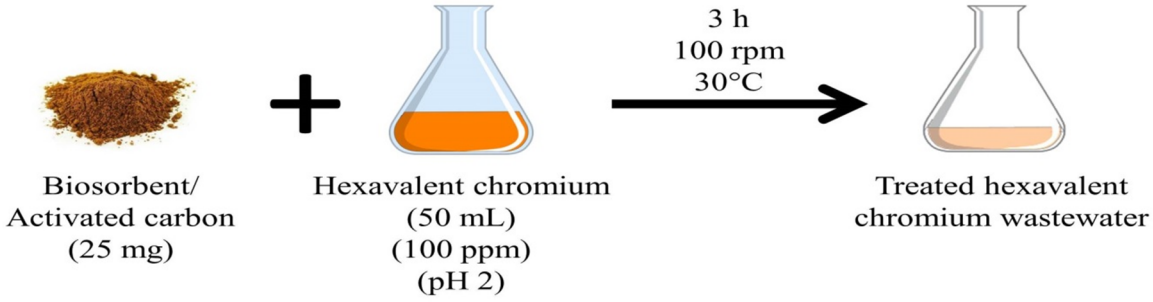

Figure 3.1. Schematic diagram representing work flow of batch studies

3.1.4 Desorption and regeneration studies

Desorption studies were carried out using 0.1 N NaOH as desorbing agent. The biosorbent after adsorption of Cr(VI) was filtered using Whatmann filter paper No. 1 and added in 50 mL of 0.1 N NaOH solution and measured for Cr(VI) at regular intervals till maximum desorption occurred. The regenerated biosorbent was subjected to Cr(VI) adsorption studies to check the efficacy of used PKB. Desorption percentages were calculated using the following equation:

$$\%\text{Desorption} = \frac{C_{des}}{C_{ads}} \times 100 \quad (3)$$

where, C_{des} is the concentration of chromium desorbed at time 't' (mg/L), C_{ads} is the concentration of chromium adsorbed at the same time 't' (mg/L).

3.1.5 Column studies

Continuous mode of Cr(VI) biosorption was performed with PKB packed as bed in glass column with dimensions of internal diameter 1 cm and length 15 cm. The packed column was washed several times with deionized water, loaded with glass wool at the bottom of the column to a height of 1 cm approximately. 3 mm diameter glass beads were loaded next to the glass wool to a height of 1.5 cm. Approximately 4.5 g of PKB was packed to 5 cm height in the column. 100 mg/L of Cr(VI) solution was passed through the packed bed column by a peristaltic pump (PP-20-EX, Miclins, India) at the flow rate of 5 mL/min. Up flow movement of Cr(VI) solution was chosen in order to attain even distribution throughout the packed bed of PKB. 20 mL of sample from the outlet was collected at fixed time duration, filtered and estimated for Cr(VI) until equilibrium attained. Effective volume of Cr(VI) solution that can be treated using PKB was determined by plotting a breakthrough curve between C_t/C_o and volume treated.

3.2 Results and discussion

3.2.1 Biosorbent characterization

Point of Zero charge of the biosorbent was calculated to be pH 4.0 (Fig. 3.2) which showed that the biosorbent surface is prone to anionic Cr(VI) binding below this critical pH. BET analysis presented in the Table 3.1 showed that the biosorbent has considerable surface area with pores in it which is suitable for metal binding. Further, the biosorbent was found to be microporous in nature.

Table 3.1.BET analysis of PKB

Parameters	Values
Total pore volume	1.084×10^{-2} cc/g
Surface area	3.938 m²/g
Pore diameter	3.312 nm
Average pore diameter	1.10092 nm

The TG curve (Fig. 3.3) showed that two weight loss stages occurred in the process: when the temperature is below 150°C, the reduction in weight is primarily due to moisture loss. From 240°C to 375°C, the weight loss was owing to pyrolysis of PKB. From 375°C to 465°C, there was a relatively less sharp decrease; however, a weight loss of 10% occurred in this span of temperature change. From this temperature profile, the

carbonation temperature may be chosen as 465°C to produce stable activated carbon for further studies. In a previous report, Li et. al. also reported that TG curve for pine cone showed two weight loss stages: from 200°C to 400°C, the weight loss was mainly due to the pyrolysis of pine cone shells: from 400°C to 500°C, the weight loss rate became slow (Li et al., 2016).

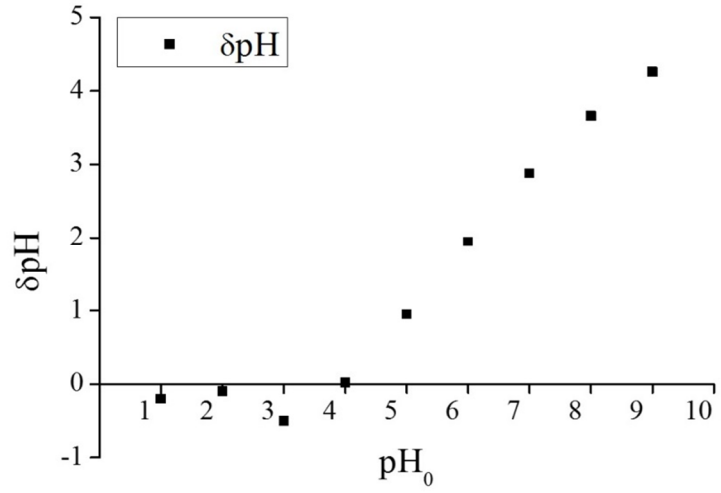

Figure 3.2. Determination of PZC (PKB dose 0.5 g in 40 mL of 0.1 N KNO_3 agitated for 24 h)

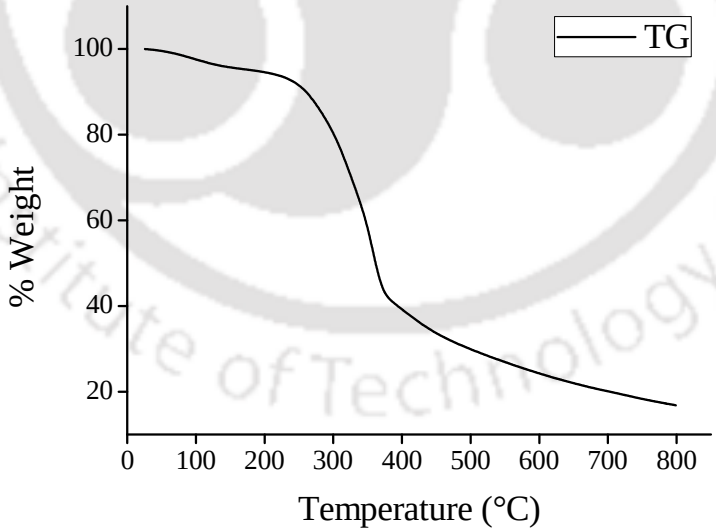

Figure 3.3. Determination of stability of the raw biosorbent (PKB) using TG in the temperature range of 25°C to 800°C

FESEM micrographs of PKB before Cr(VI) treatment (Fig. 3.4a) showed that the surface of the biosorbent is rough, striated with ridges and pores upon them. Similar observation has been noticed in several plant based biosorbents like *Caryota urens*

(Rangabhashiyam and Selvaraju, 2015a), *Annona reticulata* Linn. (Saranya et al., 2017) and *Colocasia esculenta* (Nakkeeran et al., 2016) exhibiting surface properties conducive for hexavalent chromium removal. FESEM micrograph of the PKB after Cr(VI) adsorption is showed in Fig. 3.4b. The surface of the biosorbent was observed to contain smaller particles adhering and occupying the pores.

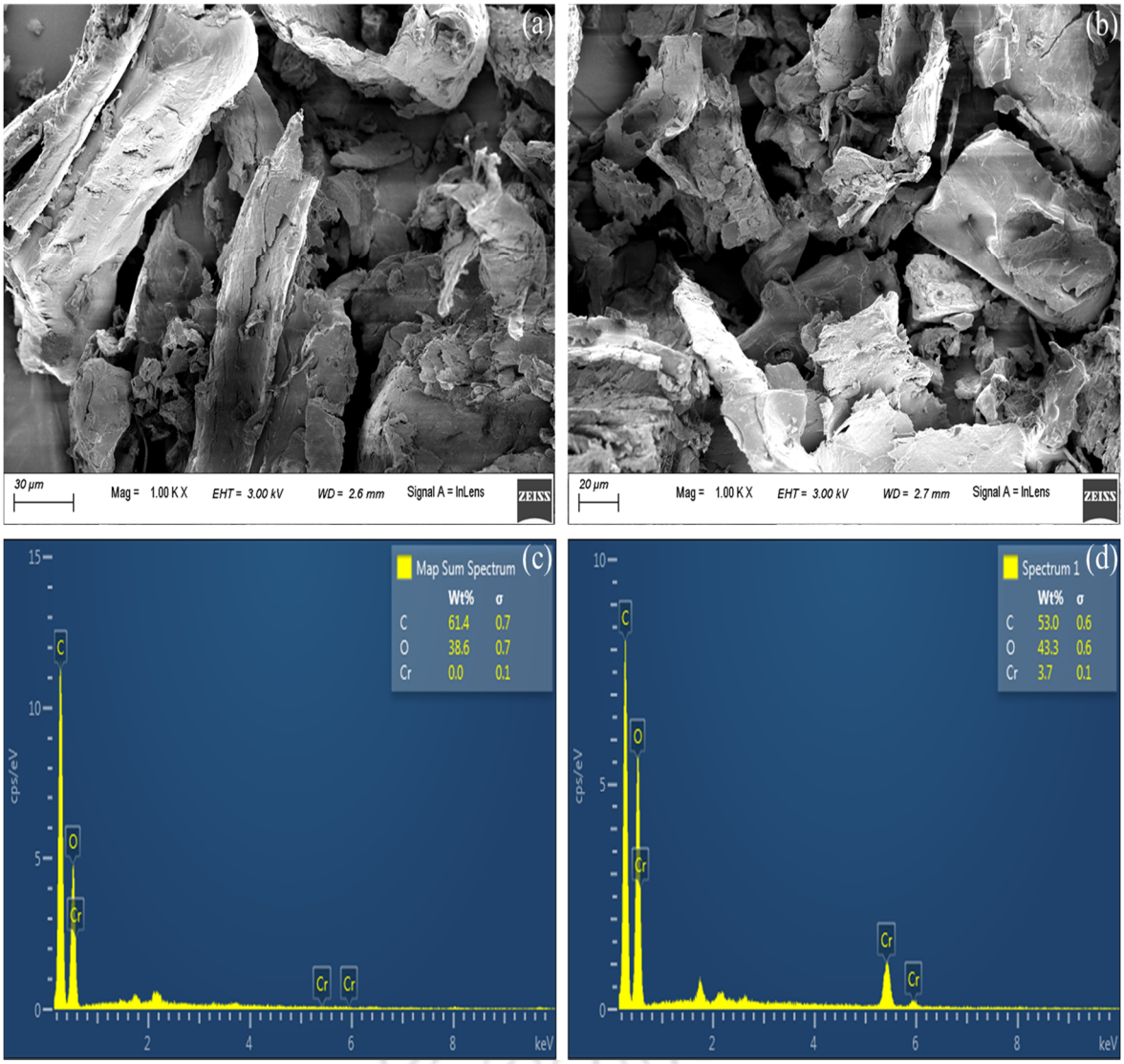

Figure 3.4. SEM image of (a) Pine Cone particles size < 300 µm (x 1000) and (b) Chromium loaded Pine Cone particles size < 300 µm (x 1000). EDX image of (c) Pine Cone particles size < 300 µm (x 1000) and (d) Chromium loaded Pine Cone particles size < 300 µm (x 1000)

EDX analyses (Fig. 3.4c and 3.4d) revealed that these particulates were indeed the adsorbed Cr(VI) attesting its applicability as a suitable biosorbent. There were no peaks found (Fig. 3.4c) for chromium ions from any spectral lines of X-ray energies

before adsorption. However, after Cr(VI) adsorption, there are distinct peaks for Chromium at energy levels 0.57 KeV, 5.4 KeV and 5.9 KeV which clearly reveals that Chromium has been adsorbed over the surface of the PKB.

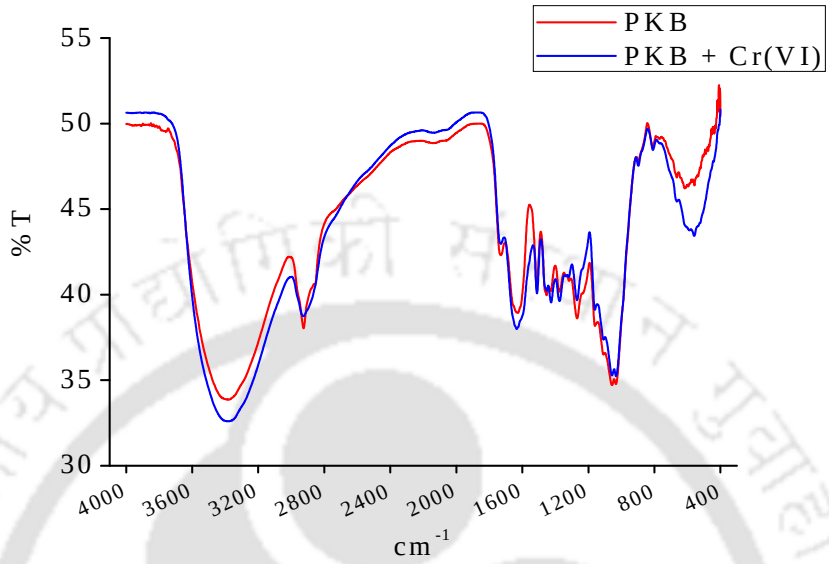

Figure 3.5. FTIR spectral analysis of PKB before and after Cr(VI) adsorption

Surface functional groups of the biosorbent have been found to play a role in adsorption of Cr(VI) by analyzing the FTIR spectrum before and after adsorption. The shift in the wavenumber from 3396.53 cm^{-1} to 3385.53 cm^{-1} indicated the association of surface –OH group in Cr(VI) adsorption on PKB (Fig. 3.5). The wavenumber shift from 2925.14 cm^{-1} to 2916.62 cm^{-1} indicated the involvement of C–H (stretching). Wavenumber shift from 1632.96 cm^{-1} to 1620.84 cm^{-1} represented the C=C (stretching). Involvement of alkenes is often represented by several researchers in the use of plant based lignocellulosic wastes for removal of heavy metals (Gebrehawaria et al., 2015). The minor shift in wavenumber at 1057.65 cm^{-1}, 1268.24 cm^{-1} and 1730.33 cm^{-1} indicates the non-involvement of C-O (stretching), CN (stretching) and C=O in Cr(VI) adsorption. From the FTIR analysis done, the functional moieties interacting in the biosorption of chromium onto the surface of the PKB were determined as hydroxyl, alkenes and alkyl groups.

3.2.2 Influence of biosorbent size

The influence of biosorbent size on Cr(VI) removal was studied using three different size ranges <300µm, 300 to 450 µm, 456 to 600 µm at pH 2.0, temperature 303 K, biosorbent dose of 0.25 g in 50 mL of 100 mg/L chromium solution. Fig. 3.6 shows

that smaller sized particles of <300 µm presented higher Cr(VI) removal percentage of 99.10 than that of other larger sized particles utilized. This may be attributed to the larger surface area contribution by the smaller sized particles with the exposure of more number of functional groups prone to Cr(VI) binding (Kuppusamy et al., 2016). The chromium removal percentage gradually declined with the increase in the particle size owing to the decreased surface area and surface characteristics.

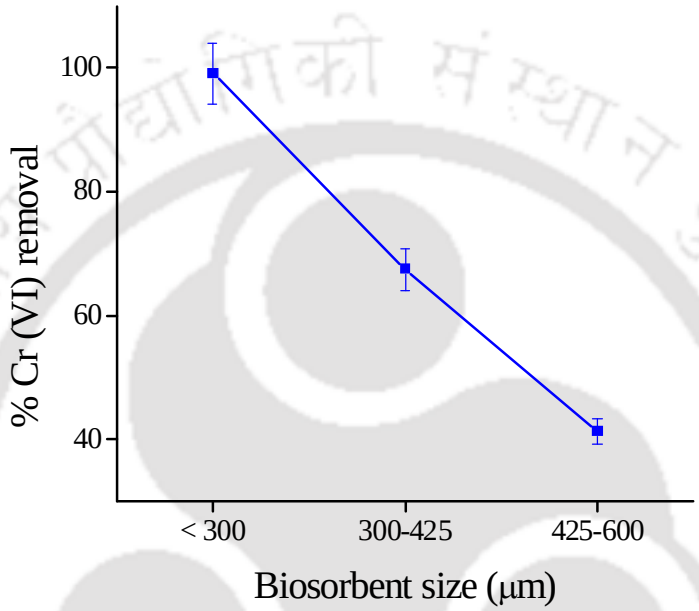

Figure 3.6. Influence of biosorbent size on Cr(VI) removal

3.2.3 Influence of biosorbent dose

Influence of PKB dose was analyzed by using 0.5 g to 5.0 g of biosorbent of size less than 300 µm with 50 mL solution of 100 mg/L initial chromium concentration maintained at pH 2.0, temperature 303 K and agitation speed 100 rpm. Fig. 3.7 shows that the chromium removal percentage sharply increased with increase in the dose of PKB from 0.5 to 3.0 g. This may be due to more surface area and reactive functional groups available with the increase in the biosorbent dose (Nair et al., 2014). However, increase in chromium removal percentage was less with 3.5 g of PKB. Further, there was no considerable change in chromium removal percentage on increasing the PKB dose from 3.5 to 5.0 g. The maximum chromium removal was 99.33% with 5.0 g of PKB. On increasing the PKB dose beyond 3.5 g, due to the less availability of surface area per unit weight of PKB, there was relatively less increase in the removal percentage which resulted in equilibrium.

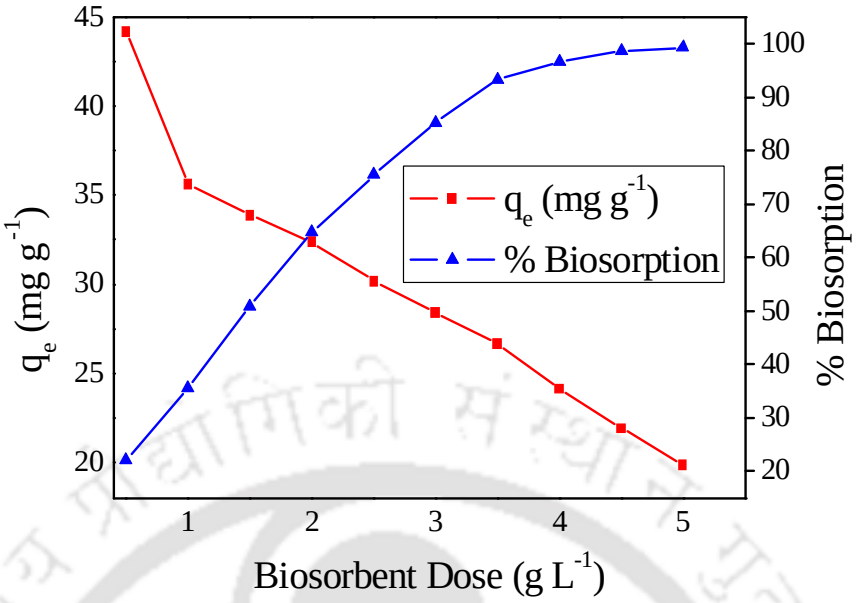

Figure 3.7. Plot showing influence of biosorbent dose upon removal percentage and adsorption capacity (C_o 100 mg/L, contact time 3 h, agitation speed 100 rpm, pH 2.0, temperature 303 K)

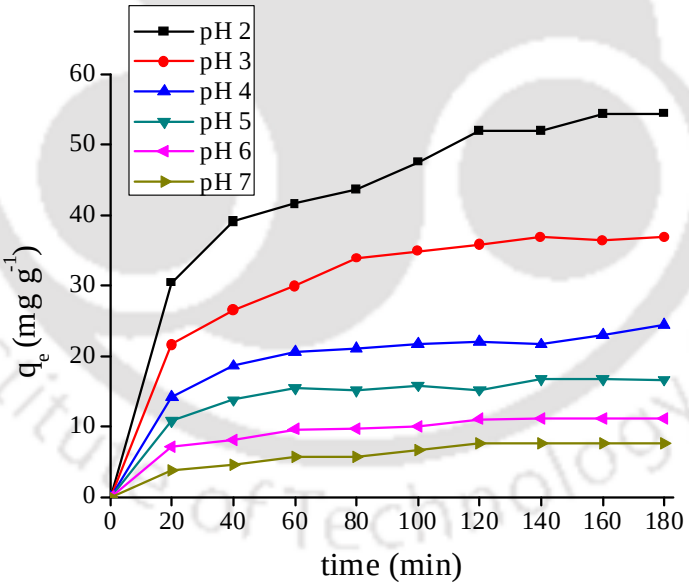

Figure 3.8. Influence of pH on Cr(VI) adsorption using PKB

3.2.4 Effect of pH

Influence of pH upon Cr(VI) adsorption was examined in the pH range of 2.0 through 7.0 at 303 K with 100 mg/L of Cr(VI) solution, optimum dose and size of biosorbent. It was found that at lower pH 2.0, maximum chromium adsorption occurred with magnitude of 53.88 mg/g. As the pH increased to 3.0, 4.0 and 5.0, adsorption

capacity got decreased to 35.6, 27.4 and 16.6 mg/g, respectively shown in the Fig. 3.8. With further increase in pH, the adsorption capacity got further decreased. The obvious fact behind this is that hydrogen chromate ($HCrO_4^-$), chromate (CrO_4^{2-}) and dichromate ($Cr_2O_7^{2-}$) ions being anionic tend to attract positively charged ions in solution. At lower pH solutions, the biosorbent surface becomes more protonated and hence, there is an electrostatic interaction between chromium ions and positively charged ions of the biosorbent resulted in increased adsorption capacity. The surface of the biosorbent become less protonated with the increase in pH and repels off the anionic chromium ions (Saha and Saha, 2014).

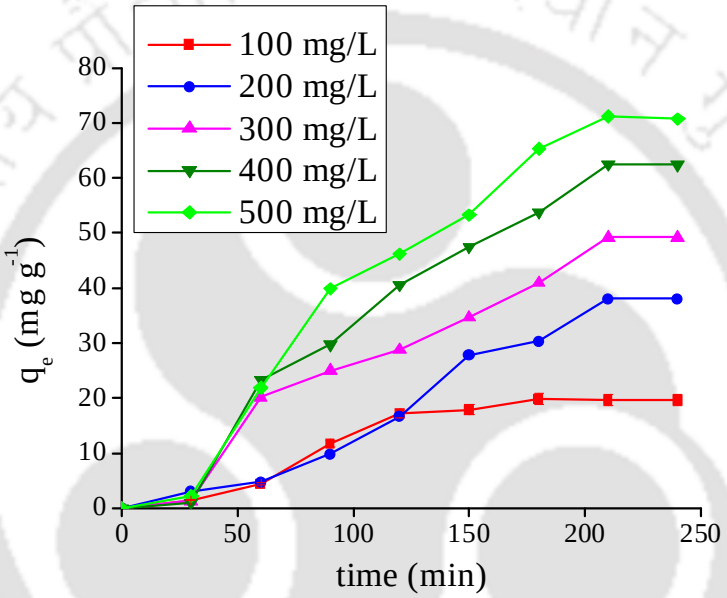

Figure 3.9. Influence of contact time and Cr(VI) concentration

3.2.5 Influence of contact time and initial Cr(VI) concentration

The time at which equilibrium adsorption capacity attained was analyzed for different Cr(VI) concentrations (100 mg/L to 500 mg/L) at optimized sorbent size, dose, pH 2.0 at 100 rpm and 303 K. The maximum adsorption capacity of 71.24 mg/g of the biosorbent was attained for 500 mg/L Cr(VI) solution at 210 min. The equilibrium adsorption capacity gradually decreased with decrease in Cr(VI) concentration and attained minimum of 19.60 mg/g for 100 mg/L Cr(VI) solution. This may be due to the increased driving force between Cr(VI) and functional groups of biosorbent owing to the development of concentration gradient (Moussavi and Barikbin, 2010). The optimum time for biosorbent to attain equilibrium was 210 min, after which there was no considerable increase in adsorption capacity for all the Cr(VI) concentrations (Fig. 3.9).

This might be due to the exhaustion of active sites for the adsorption of Cr(VI) ions to attach with the biosorbent surface (Ullah et al., 2013).

3.2.6 Adsorption Isotherm studies

Isotherm studies informed about the nature of interaction amid the biosorbent and Cr(VI) ions. Isotherm studies were done using two parameter isotherm models viz. Langmuir, Freundlich, Redlich Peterson and Dubinin-Raduschkevich models with the experimental equilibrium adsorption capacity data at different initial concentration of Cr(VI) solution.

3.2.6.1 Langmuir adsorption isotherm model

Langmuir isotherm model assumes monolayer attachment of ions over the surface of the biosorbent with no interaction between the adjacent ions. Further, the model assumes that all the ions covering the monolayer of the biosorbent surface have same affinity (Langmuir, 1918) (Sivarajasekar et al., 2017). The linear form of the Langmuir model is written as

$$\frac{C_e}{q_e} = \frac{1}{Q_0 K_L} + \frac{1}{Q_0} C_e \tag{4}$$

where, 'q_e' represents the equilibrium adsorption capacity in mg/g, 'C_e' represents the equilibrium concentration of metal ion (mg/L), 'Q_0' is the monolayer adsorption capacity (mg/g) and 'K_L' denotes the Langmuir isotherm constant (L/mg). From the K_L values, separation factor 'R_L' can be determined as

$$R_L = \frac{1}{1 + K_L C_o} \tag{5}$$

The separation factor value is significant in determining the nature of the adsorption process. If R_L lies between 0 and 1, the adsorption may be favorable, it is unfavorable if it is 1 and the process is irreversible if the value is 0. Fig. 3.10a. shows the linear isotherm plot of the ratio of equilibrium Cr(VI) concentration and equilibrium adsorption capacity of PKB vs. equilibrium Cr(VI) concentration constructed using OriginPro 8.5 (OriginLab, USA). From the Table 3.2, it is apparent that the regression value is 0.968 which is comparatively higher than the other isotherm models. The monolayer adsorption capacity of PKB was found to be 73.96 mg/g. Lower value of K_L, 0.0789 L/mg showed that there was a higher affinity between Chromium ions and the

biosorbent. R_L value of 0.112 to 0.024 for initial metal concentrations of 100-500 mg/L Cr(VI) showed that the adsorption process was favorable.

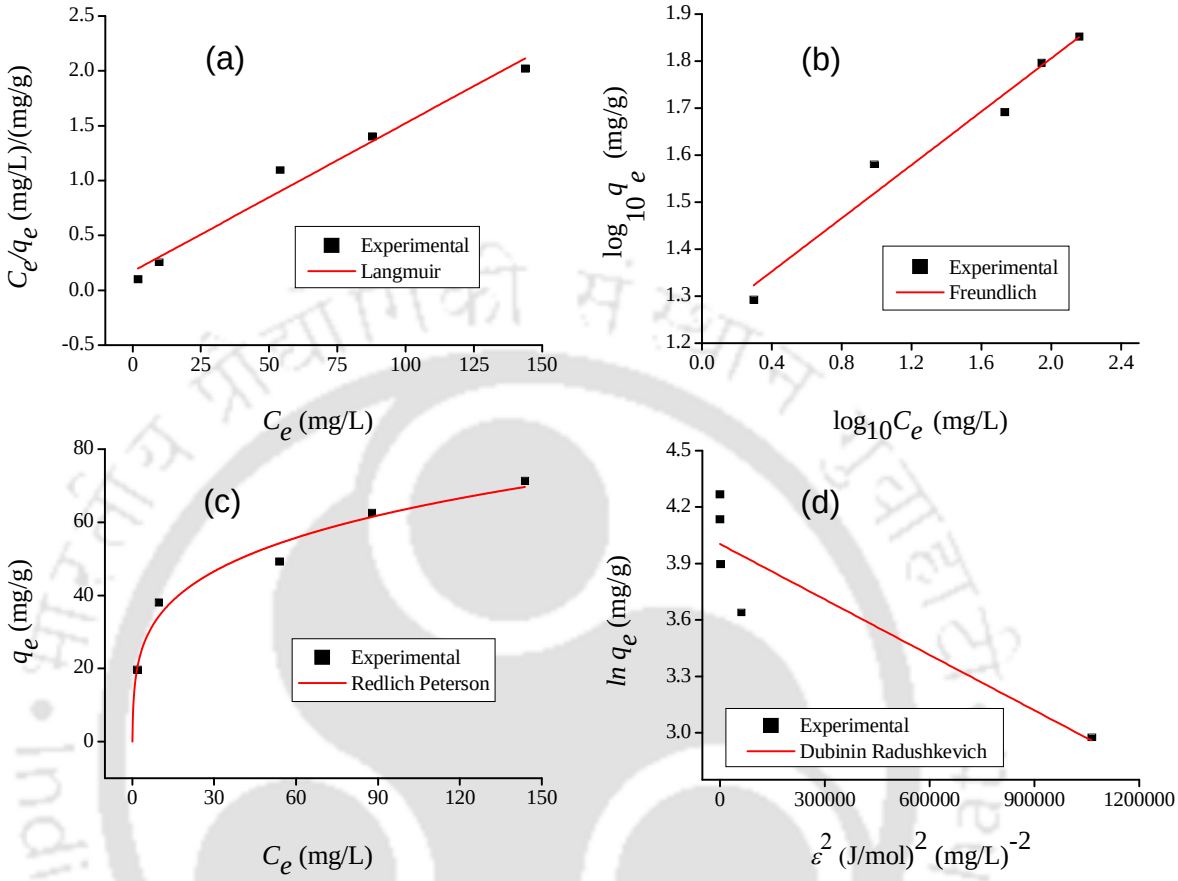

Figure 3.10. Isotherm plot of PKB for the adsorption of Cr(VI) solution at equilibrium Cr(VI) concentrations (a) Langmuir isotherm, (b) Freundlich isotherm, (c) Redlich Peterson isotherm and (d) Dubinin-Radushkevich isotherm

3.2.6.2 Freundlich adsorption isotherm model

Multilayer adsorption is explained by Freundlich isotherm which assumes that the surface of the adsorbing material is heterogeneous with varying affinity towards the adsorbing ligands (Freundlich, 1907). The linear form of Freundlich isotherm model is expressed as

$$\log_{10} q_e = \log_{10} K_F + \frac{1}{n_F} \log_{10} C_e \qquad (6)$$

where, K_F and n_F represents the Freundlich isotherm constant (mg/g)(L/mg)$^{1/n}{}_F$ and Freundlich exponent (dimensionless) respectively. Freundlich constant (n_F) represents the degree to which adsorption deviates from linearity. From the linear isotherm plotted (Fig.

3.10b), the value of K_F was found to be 17.33. Lower value of $1/n_F$ depicted that the Cr(VI) over surface of PKB is favorable. Regression value of 0.957 (Table 3.2) represented a fit of Freundlich isotherm comparable to Langmuir isotherm depicted that the adsorption process may be multilayer as well.

Table 3.2. Isotherm parameters of PKB for adsorption of Cr(VI)

Isotherm Analysis	Parameters	PK biomass
Langmuir	Q_o (mg/g)	73.96
	K_L (L/mg)	0.0789
	R_L (100 – 500 mg/L)	0.112 – 0.024
	Goodness of fit	
	R^2	0.96809
	Number of points	5
	Degrees of freedom	3
	Residual sum of squares	0.06145
Freundlich	K_F (mg/g)(L/mg)$^{1/n}{}_F$	17.33
	n_F	3.525
	Goodness of fit	
	R^2	0.95794
	Number of points	5
	Degrees of freedom	3
	Residual sum of squares	0.0062
Redlich Peterson	α_{RP} (L/mg)	75.23
	B	0.7525
	K_{RP} (L/g)	3.67
	Goodness of fit	
	R^2	0.98750
	Number of points	5
	Degrees of freedom	2
	Residual sum of squares	1.24E-2
Dubinin-Radushkevich	Q_m (mg/g)	54.830
	K (mol^2/J^2)	9.834E-7
	E (kJ/mol)	0.713
	Goodness of fit	
	R^2	0.75624
	Number of points	5
	Degrees of freedom	3
	Residual sum of squares	0.19053

3.2.6.3 Redlich Peterson isotherm

Redlich Peterson model consider the postulates of both Langmuir and Freundlich adsorption models taken together. The mathematical form of Redlich-Peterson model is

$$q_e = \frac{K_{RP} C_e}{1 + a_{RP} C_e^{\beta}} \qquad (7)$$

where, K_{RP} is the Redlich Peterson model isotherm constant (L/g), a_{RP} is the Redlich Peterson model constant (L/mg). The exponent, β, lies between 0 and 1. The experimental data was fitted to the Redlich Peterson model (Fig. 3.10c). It was found that the experimental data fitted well to the Redlich Peterson model (R^2 value 0.9875). The Redlich Peterson constant α_{RP} and K_{RP} were found to be 75.23 L/mg and 3.67 L/g, respectively. The exponent β was found to be 0.7525 which suggested that the adsorption followed Langmuir as well as Freundlich adsorption isotherm.

3.2.6.4 Dubinin–Radushkevich (D–R) isotherm

The linear D-R isotherm model equation is given by (Sing, 1985)

$$\ln q_e = \ln Q_m - K\varepsilon^2 \tag{8}$$

where, Q_m symbolizes the maximum adsorption capacity (mg/g), K symbolizes the activity coefficient (mol^2/J^2), ε denotes the Polanyi potential which is obtained by the equation

$$\varepsilon = RT(\ln(1+C_e^{-1})) \tag{9}$$

where, R represents the universal gas constant in (J/mol K) and T represents the absolute temperature (K). Q_m and K values estimated by plot (Fig. 3.10d) of log (q_e) vs. ε^2 were found to be 54.830 mg/g and 9.834E-7 mol^2/J^2, respectively. An important parameter obtained from D-R model is apparent adsorption energy, E (kJ/mol) which is calculated by the expression

$$E = \frac{1}{\sqrt{2K}} \tag{10}$$

If $1<E<16$ kJ/mol, the adsorption process occurs by physical adsorption and if $E>16$ kJ/mol, the adsorption process occurs by chemisorption. If $8<E<16$ kJ/mol, the mechanism predominantly involves ion exchange (Aytas et al., 2011). The Dubinin-Radushkevich constants were determined and are depicted in Table 1.2. However, the value of E for PKB was 0.713 kJ/mol which indicated that the biosorption process occurs by physisorption.

3.2.7 Kinetic studies

3.2.7.1 Pseudo-first order model

The linear form of pseudo-first order kinetic model is given by

$$\log(q_e - q_t) = \log q_e - \frac{k_1}{2.303}t \tag{11}$$

where, k_1 is the pseudo-first order rate constant (min^{-1}), q_e is the equilibrium adsorption capacity (mg/g) and q_t is the adsorption capacity (mg/g) (Lagergren, 1898). Table 3.3 depicts various kinetic model parameters and regression values of the model. q_e values calculated from the plot of $\log(q_e-q_t)$ vs. t did not correlated well with the experimental values. The R^2 values obtained for Pseudo-first order model were found to be less than the R^2 values for other kinetic models, which reveal that the adsorption of Cr(VI) upon PKB does not obey pseudo-first order reaction.

3.2.7.2 Pseudo-second order model

The pseudo-second order kinetic model is represented by equation

$$\frac{t}{q_t} = \frac{1}{k_2 q_e^{\,2}} + \frac{t}{q_e} \qquad (12)$$

where, k_2 (g/mg/min) denotes the Pseudo-second order rate constant (Ho and McKay, 1999). The linear form of the pseudo-second order kinetic model is shown in Fig. 3.11a. at different initial Cr(VI) concentrations. There was a good correlation in the experimental and calculated q_e values with the increase in the concentration of Cr(VI) (Table 3.3.). The R^2 values obtained for pseudo-second order model were comparatively higher than the other kinetic models analyzed. Hence, the adsorption process of Cr(VI) by PKB involved pseudo-second order reaction with sharing of electrons between sorbent and sorbate.

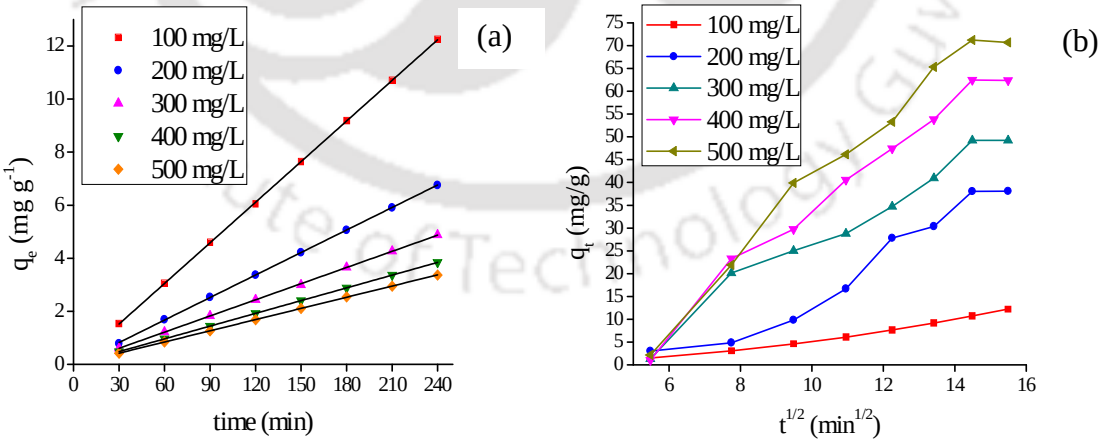

Figure 3.11. (a) Pseudo-second order plot (b) Intraparticle diffusion plot

3.2.7.3 Intraparticle diffusion model

Intraparticle diffusion model that represents the rate limiting steps is represented by equation

$$q_t = k_{id} t^{1/2} + C \quad (13)$$

where, k_{id} is the intra-particle diffusion rate constant (mg/g/min$^{1/2}$), C is the intercept (Morris and Weber, 1964). The q_e values calculated from the model plot were not close to experimental values. R^2 values are lower than pseudo-second order and pseudo-first order kinetic models (Table 3.3). Also, the plot between $t^{1/2}$ and q_t did not passed through the origin and multilinearity resulted which is clearly shown in the Fig. 3.11b. It was inferred that the process of Cr(VI) adsorption upon the PKB surface may not be solely controlled by intraparticle diffusion (Morris and Weber, 1964).

Table 3.3. Kinetic parameters of PKB for Cr(VI) removal

C_o (mg/g)	Pseudo-first order			Pseudo-second Order			Intraparticle diffusion	
	k_1 (min^{-1})	q_e (mg/g)	R^2	k_2 (g/mg/min)	q_e (mg/g)	R^2	k_{id} (mg/g/min$^{1/2}$)	R^2
100	0.013	1.476	0.662	0.216	19.60	0.999	1.07888	0.976
200	0.017	1.2918	0.882	0.039	35.71	0.999	4.05558	0.934
300	0.0207	1.5980	0.751	0.137	49.26	0.999	4.61159	0.965
400	0.0237	1.6865	0.762	2.77×10^{-5}	62.50	0.999	6.11128	0.977
500	0.0207	1.5427	0.780	2.84×10^{-5}	71.42	0.999	7.04445	0.973

3.2.8 Thermodynamic studies

Influence of temperature for various Cr(VI) concentrations was studied in the temperature range 303 K to 323 K and shown in the Fig. 3.12a. The study was carried out by using different initial metal concentrations keeping the temperature constant. It was determined that the adsorption capacity gradually increased with the simultaneous increase in the temperature and initial Cr(VI) concentration. The rise in biosorption capacity may be due to the increased mobility of the ions and modification that would have taken place in the functional groups of the biosorbent which makes them more available for contacting ions with the increase in temperature (Rangabhashiyam and Selvaraju, 2015b).

Gibbs free energy (ΔG^o), enthalpy (ΔH^o) and entropy (ΔS^o) were calculated using the following equations (Safa Özcan et al., 2009)

$$\Delta G^o = -RT\ln K_C \quad (14)$$

where, 'T' denotes absolute temperature (K) and 'R' represents universal gas constant (8.314 J/mol/K) and K_C symbolizes the distribution coefficient given by

$$ln\ K_C = -\frac{\Delta H^o}{RT} + \frac{\Delta S^o}{R} \quad (15)$$

$$K_C = \frac{q_e}{C_e} \quad (16)$$

ΔH° and ΔS° were estimated by calculating the slope and intercept from the linear plot of R*lnK*$_c$ vs. -1/T. Table 3.4 shows the thermodynamic parameters estimated from the temperature studies at various metal concentrations. The negative ΔG° values indicated the spontaneous nature of the biosorption process (Tran et al., 2016). The ΔH° values were negative which indicated exothermic nature of process. Further, the ΔS° values were negative which revealed the stable bonding of Cr(VI) on PKB surface (Kumar and Jena, 2017). This may be due to the decrease in the randomness and movement of molecules at the sorbent-sorbate interface.

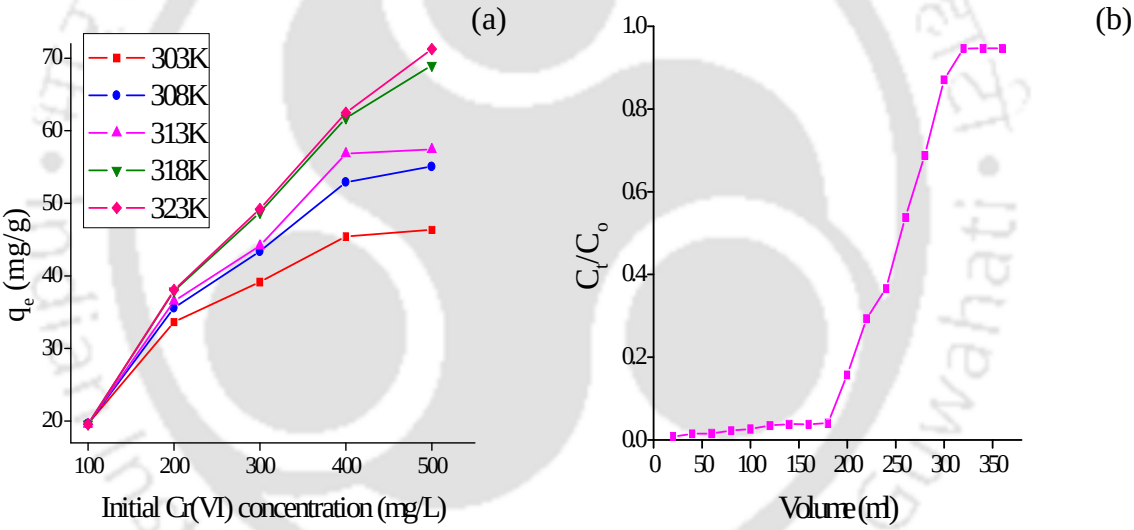

Figure 3.12. (a) Influence of temperature at various concentrations of Cr(VI) (b) Break through curve of PKB in column studies

Table 3.4. Thermodynamic parameters of PKB for Cr(VI) removal

Temperature (K)	ΔG° (kJ/mol) Initial metal concentration (mg/L)					ΔH° (kJ/mol)	ΔS° (kJ/mol K)
	100	200	300	400	500		
303	-24.98	-8.73	-1.83	-1.30	-0.81	-59.07	-0.106
308	-29.33	-8.75	-1.97	-1.48	-0.90	-101.28	-0.303
313	-24.66	-5.51	-1.44	-1.27	-0.70	-11.22	-0.030
318	-25.05	-4.57	-1.55	-1.20	-0.81	-5.7	-0.014
323	-24.36	-3.21	-1.27	-1.08	-0.71	-2.6	-0.006

3.2.9 Desorption and regeneration studies

Desorption experiments were carried out after adsorption studies for a period of 6 h using 0.1 N NaOH as desorption agent at 100 rpm, 303 K. Maximum desorption was achieved in 300 min and no further increase in desorption was found. The regenerated sorbent was filtered and adsorption experiments were performed with optimized conditions of 100 mg/L initial metal concentration, 2.0 pH, 303 K and 100 rpm. These steps were repeated until considerable adsorption of Cr(VI) was attained. The maximum desorption percentage in the 1st run was 47.61 and it was reduced to 32.46 in the 2nd run (Table 3.5). The regenerated PKB at the 1st run showed a maximum of 82.30% Cr(VI) removal and in the 2nd run of regeneration, it showed only 31.80% Cr(VI) removal. The decrease in the desorption percentage might be due to the change of functional groups or Cr binding groups after continuous exposure of desorbing agent and Cr(VI) solution. Tremendous decrease in the removal percentage post desorption was due to the unavailability of binding sites for chromium ions.

Table 3.5. Desorption and regeneration data of PKB using 100 ppm initial Cr(VI) concentration

Time (min)	Cycle 1		Cycle 2	
	Chromium desorption (%)	Chromium adsorption (%)	Chromium desorption (%)	Chromium adsorption (%)
30	11.85	1.79	15.91	0.35
60	12.39	15.63	14.16	2.15
90	21.31	20.12	11.02	6.64
120	42.04	39.89	14.58	12.93
150	45.29	50.67	15.77	14.73
180	42.42	70.88	26.04	24.61
210	45.45	81.22	36.12	28.12
240	45.45	82.12	33.41	30.90
300	47.61	82.30	32.69	31.80
360	47.61	82.30	32.69	30.90

3.2.10 Continuous Column studies

Continuous column studies of Cr(VI) removal was performed using a packed bed column of PKB at 5 cm height. Fig. 3.12b. shows breakthrough curve of the PKB obtained after the passage of 100 mg/L of Cr(VI) solution through the column. Breakthrough curve was constructed from a plot between volumes of outlet collected vs. C_t/C_o. It was found that a packed bed made of 4.5 g of PKB was capable of remediating

180 mL of Cr(VI) solution under given conditions. Hence, PKB can be used an ecofriendly sorbent for treating real Cr(VI) containing aqueous effluents.

3.3 Conclusion

Removal of Cr(VI) from simulated solutions has been investigated using a novel biosorbent *P. kesiya* cone biomass. The physicochemical characteristic studies of the biosorbent showed that it has a considerable surface area and pore volume with several functional groups embedded over their surface which are prone to metal binding. The biosorption of Cr(VI) onto PKB has been confirmed by FTIR, FESEM-EDX, XRD and ESR studies. It was depicted that the Cr(VI) removal was highest at an optimum initial solution pH 2.0, temperature 303 K, PKB particle size of < 300 µm, PKB dose of 0.5 g/L, contact time 210 min, initial chromium concentration of 500 mg/L at a constant agitation speed of 100 rpm. Isotherm studies obeyed Langmuir model which imply that the biosorption is predominantly monolayer over a homogenous sorbent surface. Maximum adsorption capacity of the biosorbent was 73.96 mg/g which is comparatively higher than reported in the literature. Kinetic parameters fitted well with pseudo-second order kinetics. Thermodynamic parameters revealed that the biosorption process is spontaneous, stable and exothermic. Desorption studies with NaOH revealed that the biosorbent is reusable. Continuous packed bed column studies showed that the *P. kesiya* cone biosorbent is an environmental friendly option to abate Cr(VI) from synthetic Cr(VI) solutions.

References

Aytas, S., Turkozu, D.A., Gok, C., 2011. Biosorption of uranium(VI) by bi-functionalized low cost biocomposite adsorbent. Desalination 280, 354–362. https://doi.org/10.1016/j.desal.2011.07.023

Freundlich, H., 1907. Über die Adsorption in Lösungen. Zeitschrift für Physikalische Chemie 57U, 385–470. https://doi.org/10.1515/zpch-1907-5723

Gebrehawaria, G., Hussen, A., Rao, V.M., 2015. Removal of hexavalent chromium from aqueous solutions using barks of *Acacia albida* and leaves of *Euclea schimperi*. Int. J. Environ. Sci. Technol. 12, 1569–1580. https://doi.org/10.1007/s13762-014-0530-2

Ho, Y.S., McKay, G., 1999. Pseudo-second order model for sorption processes. Process Biochemistry 34, 451–465. https://doi.org/10.1016/S0032-9592(98)00112-5

Jin, R., Liu, Y., Liu, G., Tian, T., Qiao, S., Zhou, J., 2017. Characterization of Product and Potential Mechanism of Cr(VI) Reduction by Anaerobic Activated Sludge in a Sequencing Batch Reactor. Sci Rep 7, 1681. https://doi.org/10.1038/s41598-017-01885-z

Kumar, A., Jena, H.M., 2017. Adsorption of Cr(VI) from aqueous solution by prepared high surface area activated carbon from Fox nutshell by chemical activation with H_3PO_4. Journal of Environmental Chemical Engineering 5, 2032–2041. https://doi.org/10.1016/j.jece.2017.03.035

Kuppusamy, S., Thavamani, P., Megharaj, M., Venkateswarlu, K., Lee, Y.B., Naidu, R., 2016. Potential of *Melaleuca diosmifolia* leaf as a low-cost adsorbent for hexavalent chromium removal from contaminated water bodies. Process Safety and Environmental Protection 100, 173–182. https://doi.org/10.1016/j.psep.2016.01.009

Lagergren, S.Y., 1898. Zur Theorie der sogenannten Adsorption gelöster Stoffe. Bihang till Kungliga Svenska Vetenskapsakademiens, Handlingar 24, 1–39.

Langmuir, I., 1918. The Adsorption of Gases on Plane Surfaces of Glass, Mica and Platinum. J. Am. Chem. Soc. 40, 1361–1403. https://doi.org/10.1021/ja02242a004

Li, K., Tian, S., Jiang, J., Wang, J., Chen, X., Yan, F., 2016. Pine cone shell-based activated carbon used for CO_2 adsorption. J. Mater. Chem. A 4, 5223–5234. https://doi.org/10.1039/C5TA09908K

Morris, J.C., Weber, W.J., 1964. Removal of biologically-resistant pollutants from waste waters by adsorption, in: Southgate, B.A. (Ed.), Advances in Water Pollution

Research. Pergamon, pp. 231–266. https://doi.org/10.1016/B978-1-4832-8391-3.50032-4

Moussavi, G., Barikbin, B., 2010. Biosorption of chromium(VI) from industrial wastewater onto pistachio hull waste biomass. Chemical Engineering Journal 162, 893–900. https://doi.org/10.1016/j.cej.2010.06.032

Nair, V., Panigrahy, A., Vinu, R., 2014. Development of novel chitosan–lignin composites for adsorption of dyes and metal ions from wastewater. Chemical Engineering Journal 254, 491–502. https://doi.org/10.1016/j.cej.2014.05.045

Nakkeeran, E., Saranya, N., Nandagopal, M.S.G., Santhiagu, A., Selvaraju, N., 2016. Hexavalent chromium removal from aqueous solutions by a novel powder prepared from *Colocasia esculenta* leaves. International Journal of Phytoremediation 18, 812–821. https://doi.org/10.1080/15226514.2016.1146229

Rangabhashiyam, S., Selvaraju, N., 2015a. Evaluation of the biosorption potential of a novel *Caryota urens* inflorescence waste biomass for the removal of hexavalent chromium from aqueous solutions. Journal of the Taiwan Institute of Chemical Engineers 47, 59–70. https://doi.org/10.1016/j.jtice.2014.09.034

Rangabhashiyam, S., Selvaraju, N., 2015b. Adsorptive remediation of hexavalent chromium from synthetic wastewater by a natural and $ZnCl_2$ activated *Sterculia guttata* shell. Journal of Molecular Liquids 207, 39–49. https://doi.org/10.1016/j.molliq.2015.03.018

Safa Özcan, A., Tunali, S., Akar, T., Özcan, A., 2009. Biosorption of lead(II) ions onto waste biomass of *Phaseolus vulgaris* L.: estimation of the equilibrium, kinetic and thermodynamic parameters. Desalination 244, 188–198. https://doi.org/10.1016/j.desal.2008.05.023

Saha, R., Saha, B., 2014. Removal of hexavalent chromium from contaminated water by adsorption using mango leaves (*Mangifera indica*). Desalination and Water Treatment 52, 1928–1936. https://doi.org/10.1080/19443994.2013.804458

Saranya, N., Nakeeran, E., Giri Nandagopal, M.S., Selvaraju, N., 2017. Optimization of adsorption process parameters by response surface methodology for hexavalent chromium removal from aqueous solutions using *Annona reticulata* Linn peel microparticles. Water Sci. Technol. 75, 2094–2107. https://doi.org/10.2166/wst.2017.092

Sing, K.S.W., 1985. Reporting physisorption data for gas/solid systems with special reference to the determination of surface area and porosity (Recommendations

1984). Pure Appl. Chem., PAC 57, 603–619. https://doi.org/10.1351/pac198557040603

Sivarajasekar, N., Baskar, R., Ragu, T., Sarika, K., Preethi, N., Radhika, T., 2017. Biosorption studies on waste cotton seed for cationic dyes sequestration: equilibrium and thermodynamics. Appl Water Sci 7, 1987–1995. https://doi.org/10.1007/s13201-016-0379-2

Tran, H.N., You, S.-J., Chao, H.-P., 2016. Thermodynamic parameters of cadmium adsorption onto orange peel calculated from various methods: A comparison study. Journal of Environmental Chemical Engineering 4, 2671–2682. https://doi.org/10.1016/j.jece.2016.05.009

Ullah, I., Nadeem, R., Iqbal, M., Manzoor, Q., 2013. Biosorption of chromium onto native and immobilized sugarcane bagasse waste biomass. Ecological Engineering 60, 99–107. https://doi.org/10.1016/j.ecoleng.2013.07.028

Chapter 4
Biosorption of chromium (VI) by *Senna siamea* seed pods and carbon

4.1 Materials and methods

4.1.1 Preparation of stock solution

Stock solution of 1000 ppm potassium dichromate was prepared by dissolving 2.828 g $K_2Cr_2O_7$ in 1000 mL deionized water. Working solutions of concentration 100 to 500 mg/L were made by appropriately diluting stock solution in deionized water.

4.1.2 Preparation of biosorbent and activated carbon

S. siamea seedpod biomass (SSSP) was collected from Indian Institute of Technology Guwahati, Guwahati, Assam, India. The seedpods were washed with deionized water for removal of sand and dust and kept at 80°C for 24 h for drying. Seedpods were ground in a mixer-grinder and sieved into < 300 μm particle size range.

Senna siamea zinc chloride activated carbon (SSAC) was prepared by modifying the procedure given elsewhere (Viswanathan et al., 2008). Briefly, *Senna siamea* seedpod biomass was impregnated with zinc chloride in the ratio 1:1 (Wt %) followed by drying at 80°C for 24 h. The impregnated biomass was activated at 550°C for 1 h. The activated biomass was washed with distilled water until the pH changed to 7.0.

4.1.3 Characterization of biosorbent

The pristine biomass and activated carbon were characterized for surface morphology by using Field emission scanning electron microscopy (FESEM) (Zeiss, Sigma, Germany). Energy dispersive X-ray spectrometry (EDX) (Zeiss, Sigma, Germany) was carried out for SSSP and SSAC for elemental analysis. Functional groups involved in the Cr(VI) biosorption were identified using Fourier transform infrared spectrometry (FTIR) (Spectrum Two, PerkinElmer, USA). Surface area and pore size of SSSP and SSAC were estimated by surface area and pore size analyzer (Autosorb-IQ MP, Quantachrome, USA). Thermal stability of the pristine biosorbent was analyzed by subjecting the biosorbent to temperatures in the range of 25°C to 800°C by increasing temperature at a rate of 10°C min^{-1} in N_2 atmosphere using High temperature DSC/TG system (TG) (STA449F3A00, Netzsch, Bavaria, Germany).

Biosorption parameter optimization experiments were performed in 250 mL Erlenmeyer flasks with 50 mL working volume. All the experiments were carried out at 30°C using incubator shaker (Orbitek, Scigenics Biotech, India). The chromium biosorption process was optimized for various parameters which influences biosorption capacity such as biosorbent dose (0.5 - 5 g/L), pH (2.0 - 7.0), Temperature (30 - 50°C)

and initial chromium concentration (100 - 500 mg/L). The range of parameters that were selected for our studies were mostly based on literature survey and feasibility. Residual Cr(VI) concentration in the filtrate from samples was measured using a UV-Visible spectrophotometer (GeneQuant 1300, GE, USA) after addition of 1, 5-Diphenyl Carbazide in acidic conditions at 540 nm. The percentage removal of Cr(VI) was calculated by using the equation

$$\%\text{Removal} = \left(\frac{C_o - C_t}{C_o}\right) \times 100 \quad (1)$$

where, C_o is the initial Cr(VI) concentration (mg/L), C_t is the equilibrium Cr(VI) concentration at time 't' (mg/L).

The biosorption capacity q_t of biosorbent was calculated using the equation

$$q_t = \frac{(C_o - C_t) \times \text{V}}{\text{m}} \quad (2)$$

where, C_t is the Cr(VI) concentration at time 't' (mg/L), 'm' is the mass of biosorbent (g) and 'V' is the volume of Cr(VI) solution (mL).

4.1.4 Desorption-Regeneration Studies

Desorption-Regeneration studies were carried out to determine the reuse of SSSP and SSAC up to 2 cycles. 0.1 M NaOH was used as desorption reagent and checked for chromium desorption up to 4 h. The desorption capacity was estimated using the following equation

$$\%Desorption = \frac{C_{des} \times 100}{C_{ads}} \quad (3)$$

where C_{des} and C_{ads} are the concentration of chromium ions during desorption and adsorption at time 't' (mg/L), respectively.

4.2 Results and discussion

4.2.1 Biosorbent characterization

Table 4.1. BET analysis of SSSP and SSAC

Parameters	SSSP	SSAC
Total pore volume	1.009×10^{-2} cc/g	3.491×10^{-1} cc/g
Surface area	3.615 m²/g	627.906 m^2/g
Pore diameter	3.059 nm	3.041 nm
Average pore diameter	1.11659 nm	2.22415 nm

BET analysis depicted in the Table 4.1 revealed that the biosorbent SSSP has surface area 3.615 m²/g which is relatively less. On activation of the biomass by zinc

chloride, the surface area increased significantly to a value of 627.906 m^2/g. The values of average pore diameter of SSSP and SSAC viz. 1.11659 nm and 2.22415 nm suggested that SSSP and SSAC are microporous and mesoporous in nature, respectively.

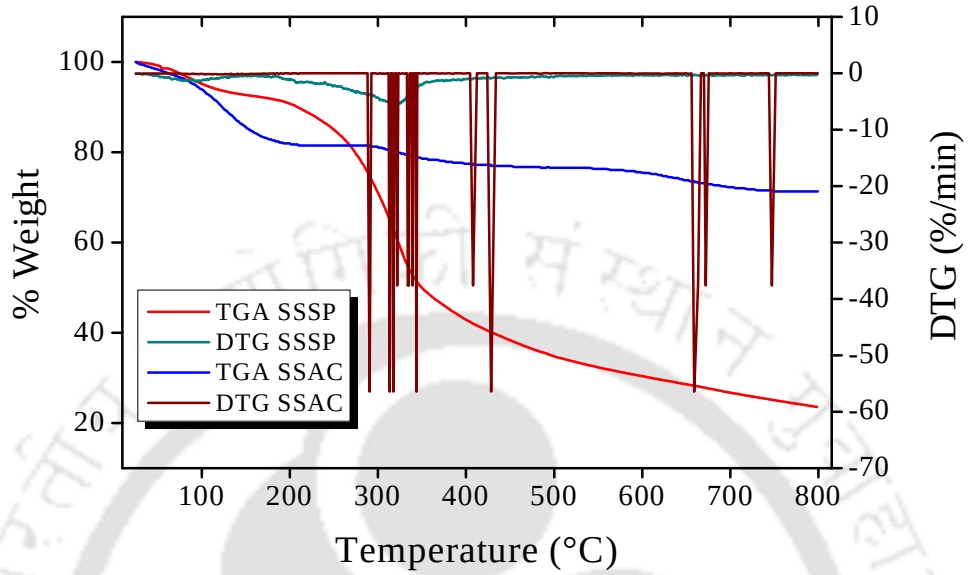

Figure 4.1. TGA and DTG plot of the raw biosorbent (SSSP) and activated carbon (SSAC) in the temperature range of 25 to 800°C

The TGA and DTG analysis of SSSP (Fig. 4.1.) showed that with increase in temperature up to 203°C, the mass of the biosorbent decreased mainly due to moisture reduction. On further increasing the temperature up to 343°C, the mass of the biosorbent decreased by pyrolysis. From 343°C to 550°C, there was a relatively less sharp decrease in mass of biomass; however, a weight reduction of 18% occurred in this temperature range. From this temperature profile, the carbonization temperature was chosen as 550°C to produce stable activated carbon for further studies. The TGA and DTG analysis of SSAC showed that it was very less affected by temperature change. Further, the relatively small decrease in weight (18%) was owing to moisture loss on increasing the temperature up to 194°C.

FESEM micrographs of SSSP (Fig. 4.2a) showed that the biosorbent surface is rough, irregular, striated with ridges and porous. Upon activation with zinc chloride (Fig. 4.2b), the porosity of biomass increased considerably leading to rise in surface area and pore volume. The FESEM images of activated carbon suggest that the active carbon promotes the removal of hexavalent chromium from wastewater. Similar observations have been made in several chemically activated plant based biosorbents like *Sterculia*

guttata shell (Rangabhashiyam and Selvaraju, 2015) and Strychnine tree fruit shell (Nakkeeran and Selvaraju, 2017).

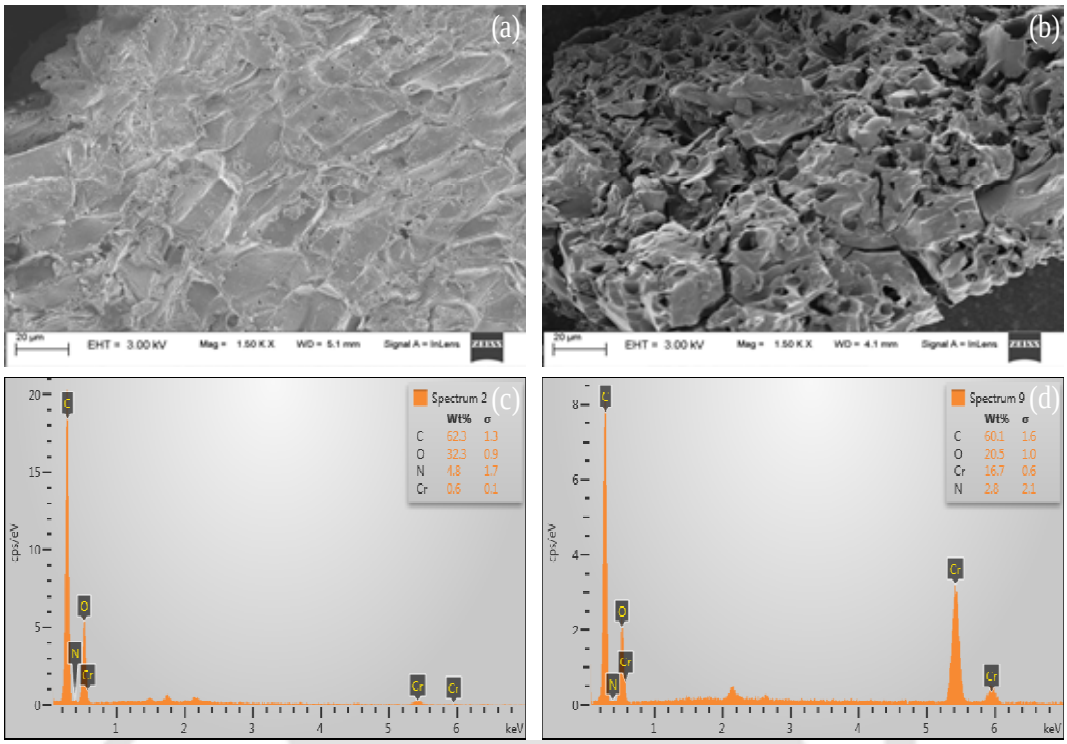

Figure 4.2. FESEM image of (a) *Senna siamea* seed pods (SSSP) particle size < 300 µm (x 1500) and (b) *Senna siamea* zinc chloride activated carbon (SSAC) particle size < 300 µm (x 1500). EDX image of (c) Chromium loaded *Senna siamea* seed pods (SSSP) particle size < 300 µm (x 1000) and (d) Chromium loaded *Senna siamea* zinc chloride activated carbon (SSAC) particle size < 300 µm (x 1000)

EDX analyses (Fig. 4.2c and 4.2d) of Cr(VI) loaded SSSP and SSAC revealed the presence of peculiar peaks for chromium at energy levels 0.57 KeV, 5.4 KeV and 5.9 KeV which confirmed that Cr(VI) was adsorbed on SSSP as well as SSAC attesting their applicability as a suitable biosorbent. Further, the Cr(VI) biosorption capacity of SSAC was higher than the SSSP as shown in the EDX spectra.

Surface functional groups of the biosorbent have been found to play a role in biosorption of Cr(VI) by analyzing the FTIR spectrum before and after biosorption. The shift in the wavenumber from 3394.20 cm^{-1} to 3386.18 cm^{-1} indicated the association of surface –OH group in Cr(VI) biosorption on SSSP (Fig. 4.3). Wavenumber shift from 1648.96 cm^{-1} to 1642.84 cm^{-1} represented the C=C (stretching). Involvement of alkenes is often represented by several researchers in the use of plant based lignocellulosic wastes for removal of heavy metals (Kuppusamy et al., 2016). The minor shift in wavenumber at

1055.65 cm^{-1}, 1268.24 cm^{-1} and 1730.33 cm^{-1} indicates the non-involvement of C-O (stretching), CN (stretching) and C=O in Cr(VI) biosorption. From the FTIR analysis done, the functional moieties interacting in the biosorption of chromium onto the surface of the SSSP were determined as hydroxyl and alkenes groups. The FTIR spectra of SSAC before and after chromium biosorption suggest that there was no functional group present on the SSAC and the biosorption occurred by the phenomenon of physisorption.

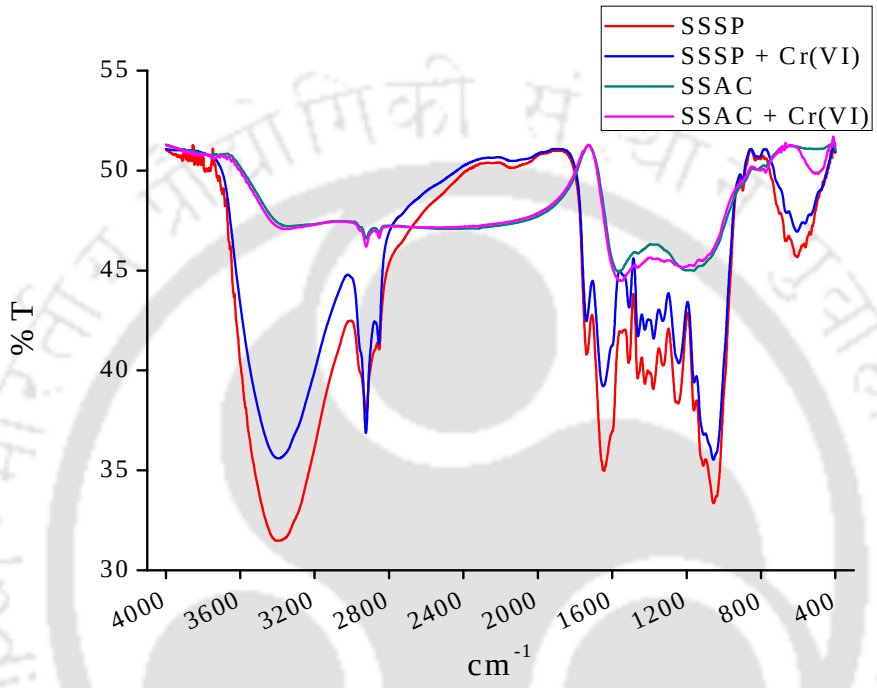

Figure 4.3. FTIR spectral analysis of SSSP and SSAC before and after Cr(VI) biosorption

4.2.2 Influence of biosorbent dose

Influence of biosorbent dose was investigated by using 0.5 g/L to 5.0 g/L of biosorbent of size less than 300 µm with 50 mL solution of 100 mg/L initial chromium concentration kept at pH 2.0, temperature 30°C and agitation speed 100 rpm. Fig. 4.4 shows that the chromium percentage removal increased sharply with increase in the dose of SSSP from 0.5 to 2.5 g/L and relatively less sharply increased from 2.5 to 5.0 g/L. On the contrary, the chromium removal percentage increased relatively less sharply with increase in dose of SSAC up to 2.5 g/L and increased more sharply beyond 2.5 g/L to 5.0 g/L. Further, it was found that biosorbent dose for removing 100% chromium for SSAC was 4.0 g/L while in case of SSSP biosorbent dose was 5.0 g/L. This may be due to increased surface area and reactive functional groups available with the increase in the biosorbent (Gupta et al., 2013). The biosorption capacity of both SSSP and SSAC

followed same pattern of decreasing with increase in biosorbent dose. This may be due to the less availability of surface area per unit weight.

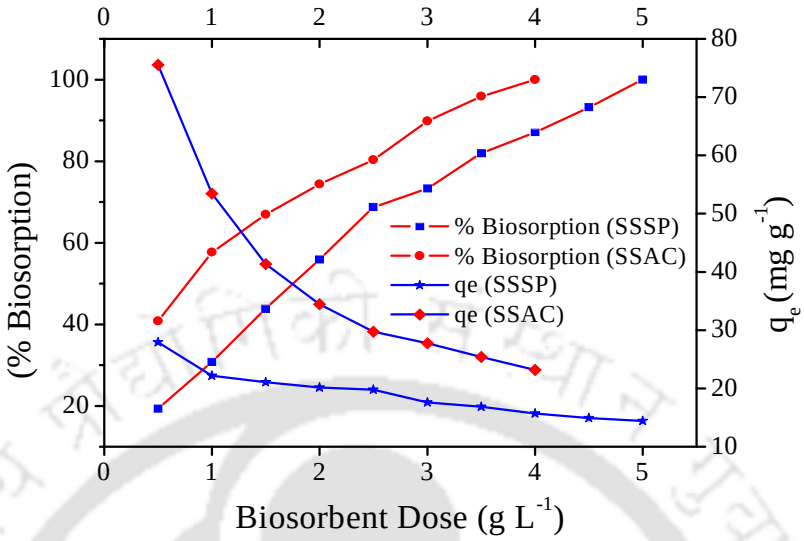

Figure 4.4. Plot showing influence of biosorbent dose on percentage removal and biosorption capacity (C_o 100 mg/L, contact time 3 h, agitation speed 100 rpm, pH 2.0, temperature 30°C)

4.2.3 Effect of pH

Influence of pH on Cr(VI) biosorption was examined in the pH range of 2.0 to 7.0 at 30°C with 100 mg/L of Cr(VI) solution, 0.5 g/L biosorbent dose. It was found that with SSSP and SSAC, maximum chromium biosorption occurred at pH 2.0 with magnitude of 24.74 and 88.19 mg/g, respectively. The biosorption capacity of SSAC got decreased to 48.01, 31.84 and 24.49 mg/g at pH 3.0, 4.0 and 5.0, respectively as shown in the Fig. 4.5. The biosorption capacity of SSAC declined further with increase in pH. The main reason behind this pattern is that at lower pH negatively charged hydrogen chromate ($HCrO_4^-$), chromate (CrO_4^{2-}) and dichromate ($Cr_2O_7^{2-}$) ions in solution bind the positively charged functional groups present on the biosorbent through electrostatic interaction. At higher pH, the biosorbent surface becomes less protonated and hence repels off the anionic chromium ions (Labied et al., 2018). We find that the biosorption capacity of SSSP became negligible as the pH was increased beyond 3.0 (data not shown). This may be due to the presence of less or negligible number of sites on the surface at pH beyond 3.0.

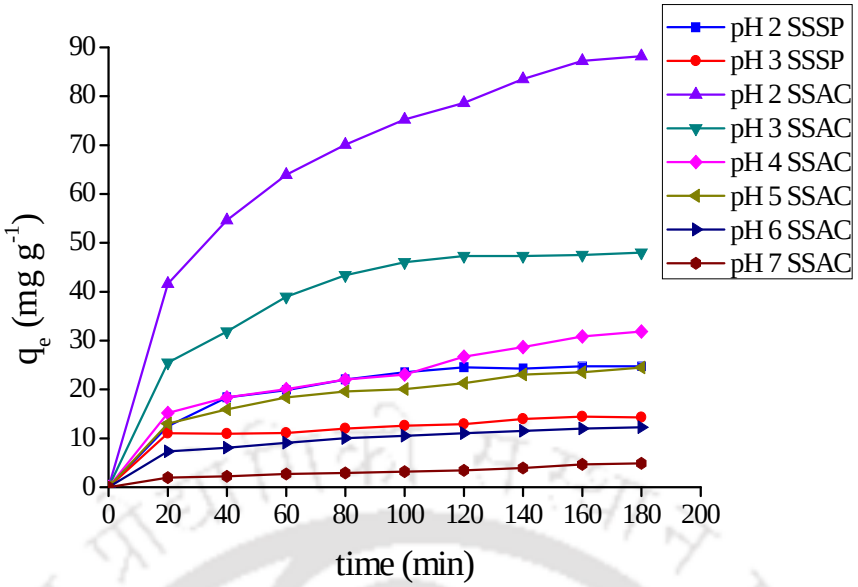

Figure 4.5. Influence of pH on Cr(VI) biosorption using SSSP and SSAC

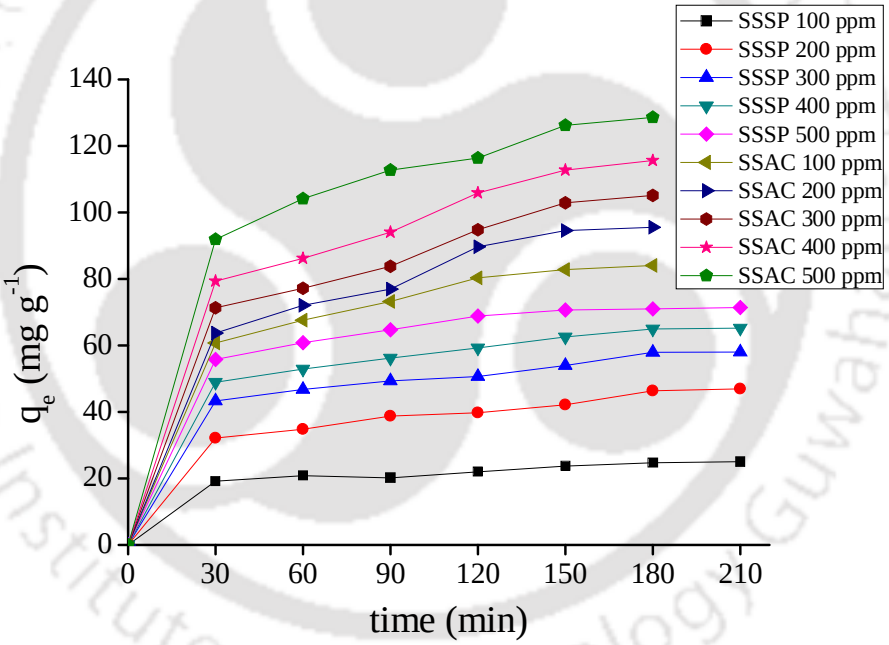

Figure 4.6. Influence of contact time and Cr(VI) concentration

4.2.4 Influence of contact time and initial Cr(VI) concentration

The equilibrium time was investigated for various initial metal concentrations (100 mg/L to 500 mg/L) at 0.5 g/L dose, pH 2.0 at 100 rpm and 30°C. The equilibrium time for SSSP and SSAC was found to be 210 and 180 minutes, respectively (Fig. 4.6). The maximum biosorption capacity of SSSP and SSAC was found to be 71.38 mg/g and 128.62 mg/g, respectively at 500 mg/L initial Cr(VI) concentration. The equilibrium biosorption capacity gradually declined with reduction in Cr(VI) concentration and

attained lowest of 25.05 mg/g and 84.03 mg/g for 100 mg/L Cr(VI) solution. This may be due to the increased driving force between Cr(VI) and functional groups of biosorbent due to the development of concentration gradient (Moussavi and Barikbin, 2010).

4.2.5 Isotherm studies

Isotherm models informed regarding the nature of interaction between the biosorbent and Cr(VI) ions. Two parameter isotherm models such as Langmuir, Freundlich and Dubinin-Radushkevich models were fitted to the experimental equilibrium biosorption capacity data at different initial Cr(VI) concentration.

4.2.5.1 Langmuir adsorption isotherm

Langmuir isotherm model considers attachment of ions over the surface of the biosorbent in a monolayer fashion with no interaction between the adjacent ions. Further, all ions have same affinity (Langmuir, 1918). The linear form of the Langmuir model is written as

$$\frac{C_e}{q_e} = \frac{1}{Q_0 K_L} + \frac{1}{Q_0} C_e \qquad (4)$$

where, 'q_e' denotes the equilibrium biosorption capacity (mg/g), 'C_e' denotes the equilibrium concentration of metal ion (mg/L), 'Q_0' represents the monolayer biosorption capacity (mg/g) and 'K_L' denotes the Langmuir isotherm constant (L/mg). The separation factor 'R_L' is estimated by the expression

$$R_L = \frac{1}{1 + K_L C_o} \qquad (5)$$

The nature of the biosorption process is concluded by the value of separation factor R_L. If R_L lies between 0 and 1, the biosorption may be favorable. If R_L is 1, biosorption is unfavorable and if R_L is 0, the biosorption is irreversible. Fig. 4.7a shows the isotherm plot of the ratio of equilibrium Cr(VI) concentration (C_e) and equilibrium biosorption capacity of SSSP and SSAC (q_e) vs. equilibrium Cr(VI) concentration (C_e). From the Table 4.2, it is apparent that the regression values are 0.971 and 0.975 for SSSP and SSAC, respectively which are comparatively higher regression values for other isotherm models. The monolayer biosorption potential of SSSP and SSAC was found to be 119.18 and 139.86 mg/g, respectively. Lower value of K_L, 0.0033 and 0.016 L/mg for SSSP and SSAC, respectively showed that there was good affinity between chromium ions and the biosorbent. R_L value of 0.750 - 0.375 and 0.375 - 0.107 for SSSP and SSAC,

respectively for initial Cr(VI) concentrations of 100-500 mg/L showed that the biosorption process was favorable.

4.2.5.2 Freundlich adsorption isotherm

Freundlich isotherm considers that biosorption occurs in a multilayer fashion with heterogeneous affinity towards the adsorbing ligands (Freundlich, 1907). The linear form of Freundlich isotherm model is expressed as

$$\log_{10} q_e = \log_{10} K_F + \frac{1}{n_F} \log_{10} C_e \quad (6)$$

where, K_F and n_F represents the Freundlich isotherm constant (mg/g)(L/mg)$^{1/n}{}_F$ and Freundlich exponent (dimensionless), respectively. Freundlich constant (n_F) represents the degree to which biosorption deviates from linearity. From the linear isotherm (Fig. 4.7b), the value of K_F was found to be 1.68 and 36.08 for SSSP and SSAC, respectively. Lower value of $1/n_F$ suggested that the Cr(VI) biosorption on the surface of both SSSP and SSAC is favorable. Regression value of 0.947 and 0.924 for SSSP and SSAC, respectively (Table 4.2) revealed Freundlich isotherm and Langmuir isotherm fitted to the experimental data equivalently which suggested that the biosorption process may be multilayer as well.

4.2.5.3 Redlich Peterson adsorption isotherm

Redlich Peterson model incorporates the principles of both Langmuir and Freundlich adsorption model taken together. Redlich Peterson model is expressed as

$$q_e = \frac{K_{RP} C_e}{1 + a_{RP} C_e^{\beta}} \quad (7)$$

where, K_{RP} represents the Redlich Peterson model isotherm constant (L/g), a_{RP} is the Redlich Peterson model constant (L/mg). The exponent, β, lies between 0 and 1. We fitted the experimental data to the Redlich Peterson isotherm model and found that the data fitted well to the model (R^2 value 0.9955 and 0.9886 for SSSP and SSAC, respectively). Further, we found that the Redlich Peterson constant α_{RP} and K_{RP} for SSSP and SSAC were found to be 0.4176 and 1.706E4 L/mg and 0.00364 and 506.8 L/g, respectively. The exponent β was found to be 1 and 0.7862 for SSSP and SSAC, respectively which suggested that the adsorption followed mostly Langmuir isotherm for SSSP while for SSAC, adsorption followed Langmuir and Freundlich isotherm.

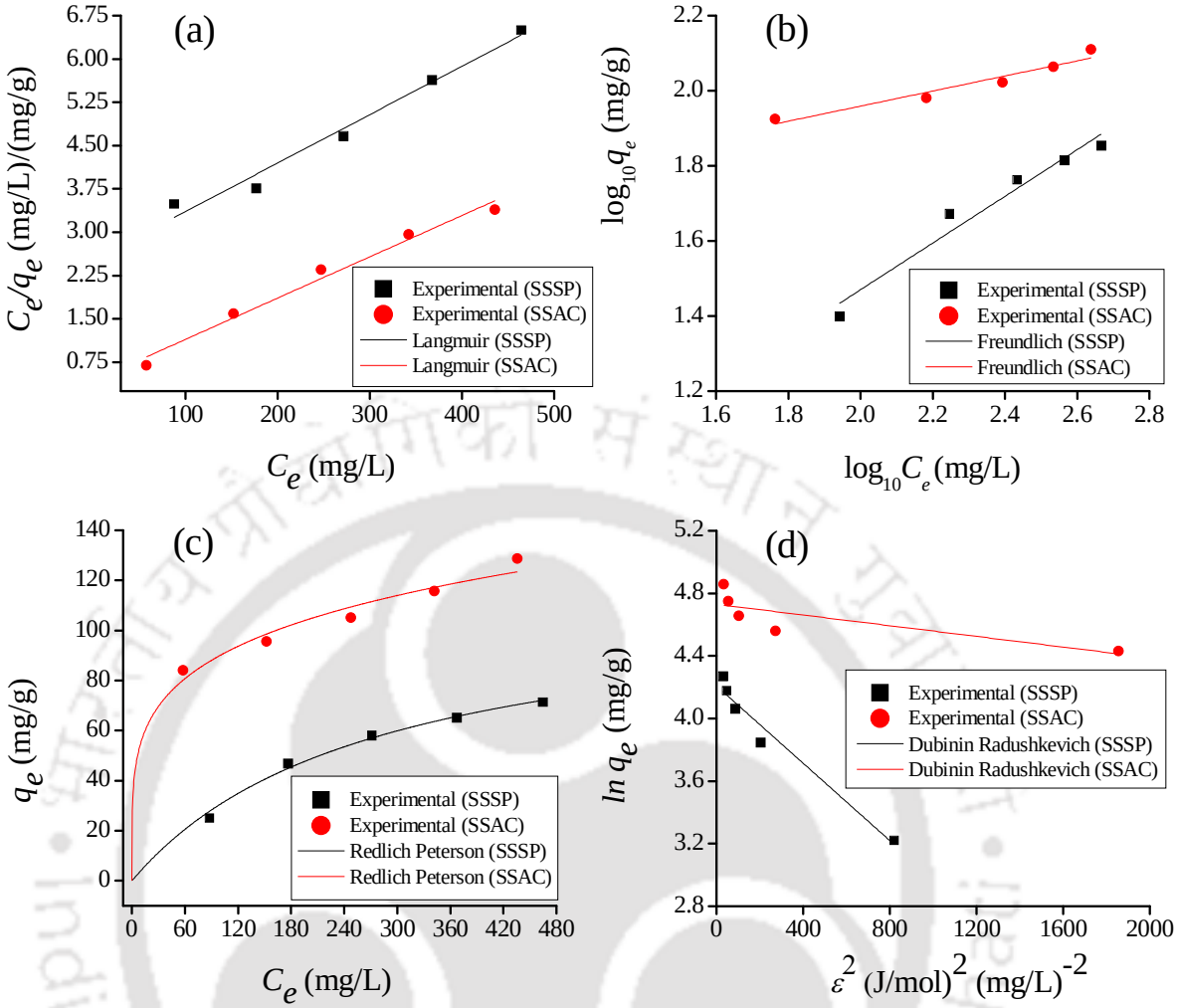

Figure 4.7. Langmuir isotherm (a), Freundlich isotherm (b), Redlich Peterson isotherm (c) and Dubinin-Radushkevich isotherm (d) plot of SSSP and SSAC for the biosorption of Cr(VI) solution at equilibrium Cr(VI) concentrations

4.2.5.4 Dubinin–Radushkevich adsorption (D–R) isotherm

The DR isotherm model equation is given by (Sing, 1985)

$$\ln q_e = \ln Q_m - K\varepsilon^2 \quad (8)$$

where Q_m symbolizes the maximum biosorption capacity (mg/g), K symbolizes the activity coefficient (mol^2/J^2), ε denotes the Polanyi potential which is obtained by the equation

$$\varepsilon = \mathrm{RT}(\ln(1+C_e^{-1})) \quad (9)$$

where R represents the universal gas constant (J/mol K) and T represents the absolute temperature (K). Q_m and K values estimated by graph of log (q_e) vs. ε^2 were found to be 67.233 mg/g and 0.00124 mol^2/J^2, respectively for SSSP, while Q_m and K values were

estimated at 113.264 mg/g and 1.71E-4 mol^2/J^2, respectively for SSAC (Fig. 4.7c). Apparent biosorption energy, *E* (kJ/mol) is calculated by the expression

$$E = \frac{1}{\sqrt{2K_{DR}}} \quad (10)$$

If 1<*E*<16 kJ/mol, physical biosorption occurs between the adsorbate and adsorbent. If *E*>16 kJ/mol, chemisorption occurs between the adsorbate and adsorbent. If 8<*E*<16 kJ/mol, the mechanism predominantly involves ion exchange (Aytas et al., 2011). The Dubinin-Radushkevich model was solved for various parameters and parameters are depicted in Table 4.2. The value of *E* for SSSP and SSAC was found as 0.02 and 0.05 kJ/mol, respectively which indicated that the physisorption occurred between the adsorbent and the adsorbate.

4.2.6. Kinetic studies

4.2.6.1 Pseudo-first order model

The Pseudo-first order kinetic model is given by

$$\log(q_e - q_t) = \log q_e - \frac{k_1}{2.303}t \quad (11)$$

where, k_1 is the Pseudo-first order rate constant (min^{-1}), q_e is the equilibrium biosorption capacity (mg/g) and q_t is the biosorption capacity (mg/g) (Lagergren, 1898). Table 4.3 depicts various parameters and regression values of the model. q_e values calculated from the plot of $\log(q_e-q_t)$ vs. *t* did not correlated well with the experimental values. The R^2 values of SSSP and SSAC obtained for Pseudo-first order model were found to be less than the R^2 values for other kinetic models which reveal that the biosorption of Cr(VI) upon SSSP and SSAC does not obey pseudo-first order reaction.

4.2.6.2 Pseudo-second order model

The Pseudo-second order kinetic model is represented by equation

$$\frac{t}{q_t} = \frac{1}{k_2 q_e^{\,2}} + \frac{t}{q_e} \quad (12)$$

where, k_2 (g/mg/min) denotes the Pseudo-second order rate constant (Ho and McKay, 1999). The pseudo-second order kinetic model is shown in Fig. 4.8a at different initial Cr(VI) concentrations. The experimental q_e values correlated well with calculated q_e values with increase in the initial concentration of Cr(VI) (Table 4.3). The R^2 values obtained for pseudo-second order model were better than the other kinetic models

analyzed. Hence, the biosorption process of Cr(VI) by SSSP and SSAC followed Pseudo-second order kinetics with sharing of electrons between sorbent and sorbate.

Table 4.2. Isotherm parameters of SSSP and SSAC for biosorption of Cr(VI)

Isotherm Analysis	Parameters	SSSP	SSAC
Langmuir	Q_o (mg/g)	119.18	139.86
	K_L (L/mg)	0.0033	0.016
	R_L (100 – 500 mg/L)	0.750 – 0.375	0.375-0.107
	Goodness of fit		
	R^2	0.97101	0.9756
	Number of points	5	5
	Degrees of freedom	3	3
	Residual sum of squares	0.13955	0.08525
Freundlich	K_F (mg/g)(L/mg)$^{1/n}{}_F$	1.68	36.08
	n_F	1.60	4.97
	Goodness of fit		
	R^2	0.94784	0.92422
	Number of points	5	5
	Degrees of freedom	3	3
	Residual sum of squares	0.00517	0.00117
Redlich Peterson	α_{RP} (L/mg)	0.4176	1.706E4
	β	1	0.7862
	K_{RP} (L/g)	0.00364	506.8
	Goodness of fit		
	R^2	0.9955	0.9886
	Number of points	5	5
	Degrees of freedom	2	2
	Residual sum of squares	3.57E-3	6.8E-3
Dubinin-Radushkevich	Q_m (mg/g)	67.233	113.264
	K (mol^2/J^2)	0.00124	1.71 x 10^{-4}
	E (kJ/mol)	0.02	0.05
	Goodness of fit		
	R^2	0.9541	0.5418
	Number of points	5	5
	Degrees of freedom	3	3
	Residual sum of squares	0.02412	0.03744

4.2.6.3 Intraparticle diffusion kinetic model

Intraparticle diffusion model is represented by equation

$$q_t = k_{id} t^{1/2} + C \quad (13)$$

where, k_{id} denotes the intra-particle diffusion rate constant (mg/g/min$^{1/2}$), C denotes the intercept (Morris and Weber jr., 1964). The calculated q_e values did not correlate well

Table 4.3. Kinetic parameters of SSSP and SSAC for Cr(VI) removal

Biomass	C_o (mg/g)	Pseudo-first order			Pseudo-second order			Intraparticle diffusion	
		k_1 (min^{-1})	q_e (mg/g)	R^2	k_2 (g/mg/min)	q_e (mg/g)	R^2	k_{id} ($mg/g/min^{1/2}$)	R^2
SSSP	100	0.038	14.059	0.764	0.055	26.97	0.988	0.686	0.895
	200	0.041	36.946	0.697	0.02	51.92	0.985	1.702	0.968
	300	0.062	70.237	0.559	0.01	62.81	0.990	1.712	0.965
	400	0.059	64.012	0.738	0.007	70.62	0.996	1.933	0.986
	500	0.059	46.343	0.956	0.004	76.04	0.999	1.82	0.938
SSAC	100	0.056	65.443	0.918	0.0046	93.10	0.996	3.121	0.974
	200	0.064	117.156	0.810	0.0047	110.61	0.985	4.376	0.956
	300	0.062	94.057	0.793	0.0041	120.77	0.982	4.643	0.958
	400	0.047	91.617	0.857	0.0032	131.57	0.987	4.939	0.970
	500	0.046	83.698	0.822	0.002	141.24	0.994	4.661	0.985

with the experimental q_e values. R^2 values obtained from intraparticle diffusion model were lower than pseudo-second order and pseudo-first order kinetic models (Table 4.3).

Further, the plot between $t^{1/2}$and q_t did not pass through the origin which suggested that multilinearity occurred which is clearly depicted in the Fig. 4.8b. It was inferred that the process of Cr(VI) biosorption on the SSSP and SSAC surface may not be controlled by intraparticle diffusion (Morris and Weber jr., 1964).

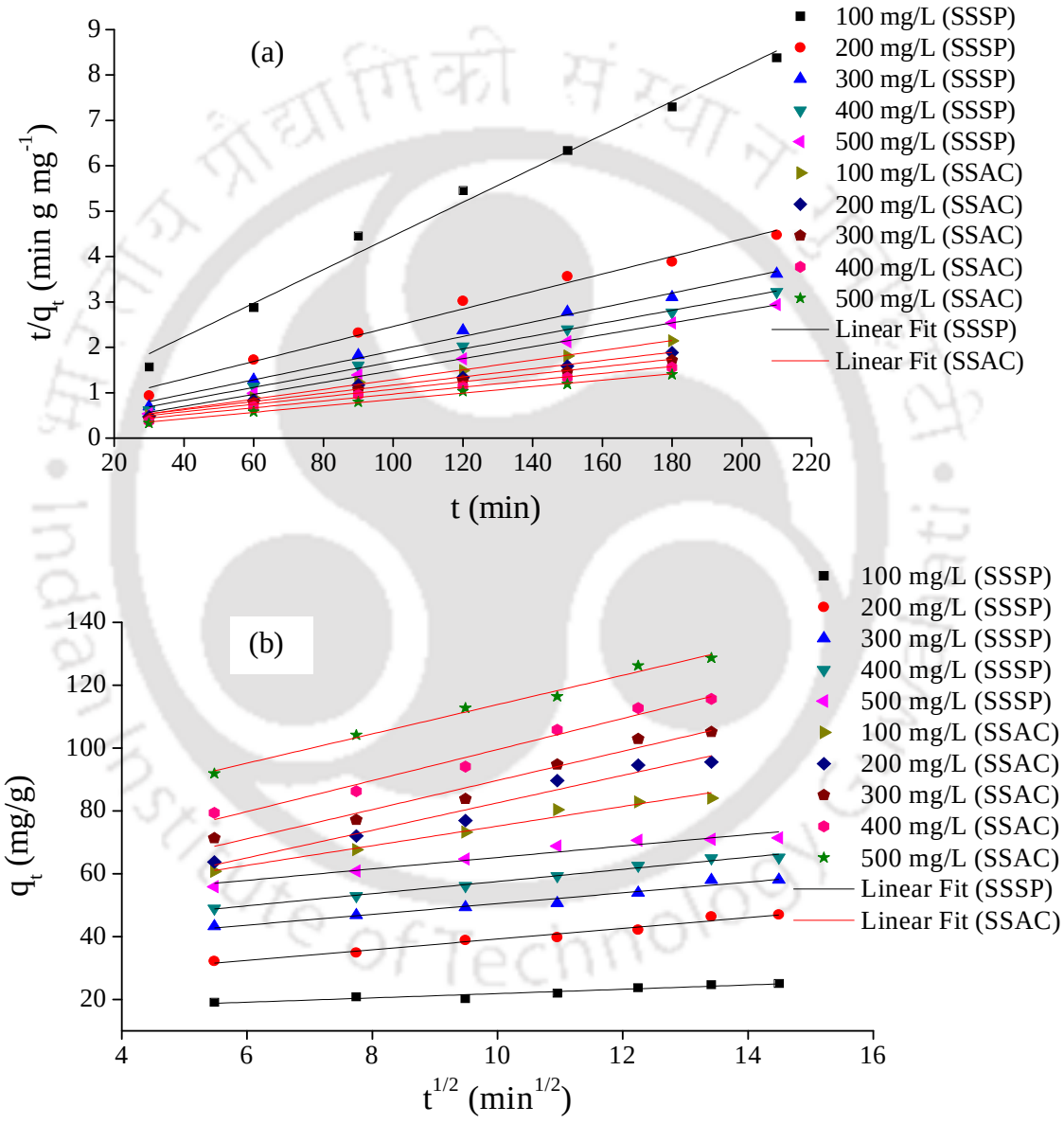

Figure 4.8. (a) Pseudo-second order plot and (b) Intraparticle diffusion plot

4.2.7 Thermodynamic studies

Influence of temperature for various Cr(VI) concentrations has been studied in the temperature range 303 K to 323 K and shown in the Fig. 4.9. The study was carried

out by using different initial metal concentrations keeping the temperature constant. It was found that the biosorption capacity moderately increased with increase in both the initial Cr(VI) concentration and temperature. The increase in biosorption capacity might be due to the higher ion mobility and modification of functional groups present on the biosorbent surface and the interaction between the functional groups and chromium ions increases with increase in temperature (Tran et al., 2016).

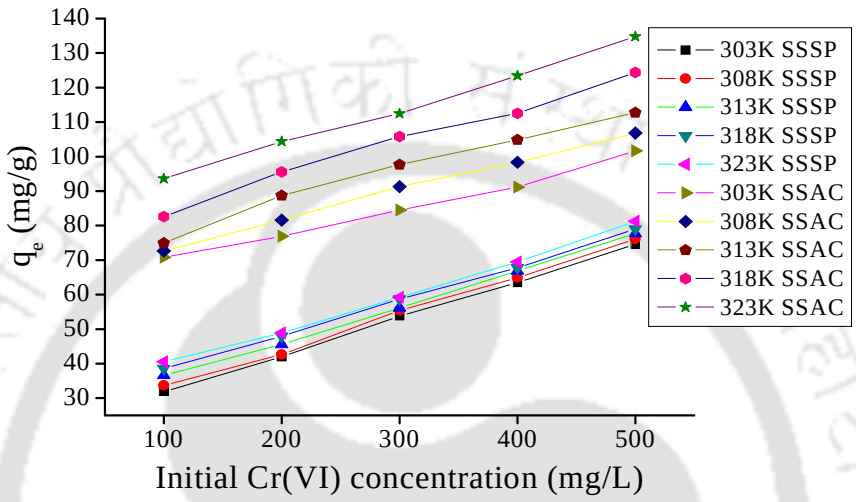

Figure 4.9. Influence of temperature at various concentrations of Cr(VI)

Gibbs free energy (ΔG°), enthalpy (ΔH°) and entropy (ΔS°) were determined by the following equations (Kumar and Jena, 2017)

$$\Delta G^o = -RT \ln K_C \quad (14)$$

where, 'T' denotes absolute temperature (K) and 'R' represents universal gas constant (8.314 J/mol/K) and K_C symbolizes the distribution coefficient as

$$\ln K_C = -\frac{\Delta H^o}{RT} + \frac{\Delta S^o}{R} \quad (15)$$

$$K_C = \frac{q_e}{C_e} \quad (16)$$

ΔH° and ΔS° were estimated by calculating the slope and intercept from the linear plot of RlnK_c vs. -1/T. Table 4.4 depicts the thermodynamic parameters estimated from the temperature studies at various metal concentrations. ΔG° was found to be positive and relatively less at various conditions which suggested that the biosorption process was non-spontaneous. Under very few conditions, the ΔG° values were negative which indicated the spontaneity of biosorption process (Gao et al., 2008). The ΔH° values were

positive which indicated endothermic nature of process. Further, the ΔS° values were approximately zero under many conditions which revealed the relatively stable bonding of Cr(VI) on SSSP and SSAC surface (Dakiky et al., 2002). The negative values of ΔS° suggested that the bonding of Cr(VI) on SSSP and SSAC surface was stable under these conditions. This may be due to the decline in the randomness of molecules at the sorbent-sorbate interface.

4.2.8 Regeneration studies

In the present study, repeated batch desorption studies were performed to examine the reusability of the SSSP and SSAC for commercial applications. The biosorption capacity of SSSP and SSAC was 38.7 and 36.5% (relative) after two cycles. The decline in biosorption capacity may be due to irreversible loss of sites on surface of SSAP and SSAC.

Table 4.4. Thermodynamic parameters of SSSP and SSAC for Cr(VI) removal

Biomass	Temperature (K)	*ΔG°* (kJ/mol) Initial metal concentration (mg/L)					*ΔH°* (kJ/mol)	*ΔS°* (kJ/mol K)
		100	200	300	400	500		
SSSP	303	4.18	5.40	5.84	6.17	6.90	12.28	0.026
	308	4.09	5.44	5.85	6.21	6.96	7.74	0.007
	313	3.89	5.33	5.90	6.23	7.01	4.52	-0.004
	318	3.78	5.27	5.87	6.29	7.08	3.95	-0.007
	323	3.67	5.29	5.93	6.31	7.11	3.69	-0.01
SSAC	303	0.47	2.85	3.92	4.63	5.62	22.37	0.072
	308	0.023	0	3.77	4.50	5.53	12.68	0.032
	313	-0.41	2.43	3.67	4.39	5.46	9.4	0.018
	318	-0.72	2.28	3.56	4.36	5.44	8.93	0.014
	323	-0.95	2.23	3.57	4.35	5.41	8.71	0.010

Table 4.5. Desorption and regeneration data of SSSP and SSAC using 100 ppm initial Cr(VI) concentration

Adsorbent	Cycle 1		Cycle 2	
	Chromium desorption (%)	Chromium adsorption (%)	Chromium desorption (%)	Chromium adsorption (%)
SSSP	42.8	82.0	27.7	38.7
SSAC	58.7	91.5	29.2	36.5

4.3 Conclusion

Removal of Cr(VI) from simulated solutions has been investigated using a novel biosorbent *Senna siamea* seedpod biomass (SSSP) and *Senna siamea* zinc chloride activated carbon (SSAC). Characterization of the pristine biomass and activated carbon

biosorbent suggested that it has large surface area and pore volume with numerous functional groups embedded over the surface which are susceptible to metal binding. The biosorption of Cr(VI) onto SSSP and SSAC was confirmed by FTIR, FESEM-EDX. The Cr(VI) removal was highest at an optimum initial solution pH 2.0, temperature 30°C, SSSP and SSAC dose of 0.5 g/L, contact time 210 min and 180 min, initial chromium concentration of 500 mg/L at a constant agitation speed of 100 rpm. Biosorption followed Langmuir isotherm model which imply that the biosorption occurs predominantly in a monolayer fashion. Maximum biosorption capacity of the biosorbent was 119.18 and 139.86 mg/g for SSSP and SSAC which is higher than reported in the literature. Biosorption followed Pseudo-second order kinetics model. Thermodynamics studies suggested that the biosorption process is non-spontaneous, stable and endothermic.

References

Aytas, S., Turkozu, D.A., Gok, C., 2011. Biosorption of uranium(VI) by bi-functionalized low cost biocomposite adsorbent. Desalination 280, 354–362. https://doi.org/10.1016/j.desal.2011.07.023

Dakiky, M., Khamis, M., Manassra, A., Mer'eb, M., 2002. Selective adsorption of chromium(VI) in industrial wastewater using low-cost abundantly available adsorbents. Advances in Environmental Research 6, 533–540. https://doi.org/10.1016/S1093-0191(01)00079-X

Freundlich, H., 1907. Über die Adsorption in Lösungen. Zeitschrift für Physikalische Chemie 57U, 385–470. https://doi.org/10.1515/zpch-1907-5723

Gao, H., Liu, Y., Zeng, G., Xu, W., Li, T., Xia, W., 2008. Characterization of Cr(VI) removal from aqueous solutions by a surplus agricultural waste—Rice straw. Journal of Hazardous Materials 150, 446–452. https://doi.org/10.1016/j.jhazmat.2007.04.126

Gupta, V.K., Pathania, D., Agarwal, S., Sharma, S., 2013. Removal of Cr(VI) onto *Ficus carica* biosorbent from water. Environ Sci Pollut Res Int 20, 2632–2644. https://doi.org/10.1007/s11356-012-1176-6

Ho, Y.S., McKay, G., 1999. Pseudo-second order model for sorption processes. Process Biochemistry 34, 451–465. https://doi.org/10.1016/S0032-9592(98)00112-5

Kumar, A., Jena, H.M., 2017. Adsorption of Cr(VI) from aqueous solution by prepared high surface area activated carbon from Fox nutshell by chemical activation with H_3PO_4. Journal of Environmental Chemical Engineering 5, 2032–2041. https://doi.org/10.1016/j.jece.2017.03.035

Kuppusamy, S., Thavamani, P., Megharaj, M., Venkateswarlu, K., Lee, Y.B., Naidu, R., 2016. Potential of *Melaleuca diosmifolia* leaf as a low-cost adsorbent for hexavalent chromium removal from contaminated water bodies. Process Safety and Environmental Protection 100, 173–182. https://doi.org/10.1016/j.psep.2016.01.009

Labied, R., Benturki, O., Eddine Hamitouche, A.Y., Donnot, A., 2018. Adsorption of hexavalent chromium by activated carbon obtained from a waste lignocellulosic material (*Ziziphus jujuba* cores): Kinetic, equilibrium, and thermodynamic study. Adsorption Science & Technology 36, 1066–1099. https://doi.org/10.1177/0263617417750739

Lagergren, S.Y., 1898. Zur Theorie der sogenannten Adsorption gelöster Stoffe. Bihang till Kungliga Svenska Vetenskapsakademiens, Handlingar 24, 1-39.

Langmuir, I., 1918. The Adsorption of Gases on Plane Surfaces of Glass, Mica and Platinum. J. Am. Chem. Soc. 40, 1361–1403. https://doi.org/10.1021/ja02242a004

Morris, J.C., Weber jr., W.J., 1964. Removal of biologically-resistant pollutants from waste waters by adsorption, in: Southgate, B.A. (Ed.), Advances in Water Pollution Research. Pergamon, pp. 231–266. https://doi.org/10.1016/B978-1-4832-8391-3.50032-4

Moussavi, G., Barikbin, B., 2010. Biosorption of chromium(VI) from industrial wastewater onto pistachio hull waste biomass. Chemical Engineering Journal 162, 893–900. https://doi.org/10.1016/j.cej.2010.06.032

Nakkeeran, E., Selvaraju, N., 2017. Biosorption of chromium(VI) in aqueous solutions by chemically modified Strychnine tree fruit shell. Int J Phytoremediation 19, 1065–1076. https://doi.org/10.1080/15226514.2017.1328386

Rangabhashiyam, S., Selvaraju, N., 2015. Adsorptive remediation of hexavalent chromium from synthetic wastewater by a natural and $ZnCl_2$ activated *Sterculia guttata* shell. Journal of Molecular Liquids 207, 39–49. https://doi.org/10.1016/j.molliq.2015.03.018

Sing, K.S.W., 1985. Reporting physisorption data for gas/solid systems with special reference to the determination of surface area and porosity (Recommendations 1984). Pure Appl. Chem., PAC 57, 603–619. https://doi.org/10.1351/pac198557040603

Tran, H.N., You, S.-J., Chao, H.-P., 2016. Thermodynamic parameters of cadmium adsorption onto orange peel calculated from various methods: A comparison study. Journal of Environmental Chemical Engineering 4, 2671–2682. https://doi.org/10.1016/j.jece.2016.05.009

Viswanathan, B., Varadarajan, T.K., Indra Neel, P., 2008. A process for the preparation of activated carbon from botanical sources. IN 2007CH00376 A 20081128.

Chapter 5
Biosorption of chromium (VI) by *Phanera vahlii* fruit biomass and carbons

5.1 Materials and methods

5.1.1 Preparation of Cr(VI) solution

A solution of 1000 ppm potassium dichromate was prepared by adding 2.828 g $K_2Cr_2O_7$ in 1 L deionized water. Working solution of 100 to 500 mg/L solutions were prepared by appropriate dilution of stock solution in deionized water.

5.1.2 Preparation of natural and activated carbon adsorbents

Phanera vahlii fruit biomass (PVF) was collected from Morni Hills, Panchkula, Haryana, India. The fruits were thoroughly cleaned with deionized water for the eradication of sand and dust followed by drying at 363 K for 24 h. Fruits were ground in a mixer-grinder and sieved into <300 µm particle size range. *Phanera vahlii* biochar (PVB) was prepared by incubating the PVF biomass at 473 K for 2 h. The yield of the PVB was 60%. *Phanera vahlii* phosphoric acid activated carbon (PVPAAC) was prepared by impregnating the PVF biomass with phosphoric acid in the ratio 1:4 (Weight: Volume) followed by incubation at 353 K for 24 h. The phosphoric acid impregnated PVF was incubated in a muffle furnace at 823 K for 1 h. The prepared activated carbon was washed with dilute HCl followed by washing with distilled water until the neutral pH was reached. The yield of the PVPAAC was 45%. *Phanera vahlii* zinc chloride activated carbon (PVZCAC) was prepared by impregnating the PVF biomass with zinc chloride in the ratio 1:4 (Weight: Weight) followed by incubation at 353 K for 24 h. The zinc chloride impregnated PVF was incubated in a muffle furnace at 823 K for 1 h. The remaining salt and impurities in the activated carbon were removed by dilute HCl followed by washing with distilled water until the pH became 7.0. The yield of the PVZCAC was 43%.

5.1.3 Characterization of biosorbent

The raw biomass, biochar and activated carbon were characterized for surface morphology by using Field emission scanning electron microscopy (FESEM) (Zeiss, Sigma, Germany). Energy dispersive X-ray spectrometry (EDX) (Zeiss, Sigma, Germany) was carried out for PVF, PVB, PVPAAC and PVZCAC for elemental analysis. Functional groups present on the PVF, PVB, PVPAAC and PVZCAC adsorbent were identified using Fourier transform infrared spectroscopy (FTIR) (Spectrum Two, PerkinElmer, USA) was done to identify different functional groups involved in Cr(VI) adsorption. Surface area and pore size of PVF, PVB, PVPAAC and PVZCAC were estimated by Surface area and Pore Size analyzer (Autosorb-IQ MP, Quantachrome,

USA). Thermal stability of the pristine biosorbent was analyzed by subjecting the biosorbent to temperatures in the range of 25°C to 800°C by increasing temperature at a rate of 10°C min^{-1} in N_2 atmosphere using High temperature DSC/TG system (TG) (STA449F3A00, Netzsch, Bavaria, Germany).

Biosorption parameter optimization experiments were performed in 250 mL conical flasks with working volume of 50 mL. All the experiments except temperature studies were carried out at 303 K using incubator shaker (Orbitek, Scigenics Biotech, India). The pH was adjusted by using 0.1 N HCl and 0.1 N NaOH solution. The chromium biosorption process was optimized for various parameters such as pH (2.0 - 7.0), biosorbent dose (0.5 - 5 g/L), Temperature (303 - 333 K) and initial Cr(VI) concentration (100 -500 mg/L). Residual Cr(VI) concentration was calculated by optical density (O.D.) after addition of 1, 5-Diphenyl Carbazide in acidic conditions at 540 nm wavelength in a UV-Visible spectrophotometer (GeneQuant 1300, GE, USA). The percentage removal of Cr(VI) was determined by using the equation:

$$\%\text{Removal} = \left(\frac{C_o - C_e}{C_o}\right) \times 100 \quad (1)$$

where, C_o represents the initial Cr(VI) concentration (mg/L), C_e depicts the equilibrium Cr(VI) conc. at time 't' (mg/L).

The adsorption capacity q_t of biosorbent was calculated by the equation

$$q_t = \frac{(C_o - C_e) \times \text{V}}{\text{m}} \quad (2)$$

where, C_t depicts the Cr(VI) concentration at any time 't' (mg/L), 'm' depicts the mass of biosorbent (g) and 'V' depicts the volume of Cr(VI) solution (mL).

5.1.4 Desorption and regeneration studies

Reuse studies were performed using 0.1 N NaOH as desorbing agent. The biosorbent was filtered after adsorption of Cr(VI) using Whatmann filter paper No. 1 and put in 50 mL of 0.1 N NaOH solution and residual Cr(VI) concentration was measured at regular intervals till maximum desorption occurred. The regenerated biosorbent was subjected to Cr(VI) adsorption studies to check the efficacy of used biosorbent. Desorption percentages were calculated using the following equation:

$$\%\text{Desorption} = \frac{C_{des}}{C_{ads}} \times 100 \quad (3)$$

where, C_{des} is the concentration of chromium desorbed at time 't' (mg/L), C_{ads} is the concentration of chromium adsorbed at the same time 't' (mg/L).

5.2 Results and discussion

5.2.1 Biosorbent characterization

BET analysis depicted in the Table 5.1 revealed that prepared biosorbents PVF, PVB, PVPAAC and PVZCAC have considerable surface area and pores suitable for metal binding. On activation of the biomass by zinc chloride, the surface area and pore size of the biomass increased considerably. The average pore diameter data suggested that all of the prepared biosorbents viz. PVF, PVB, PVPAAC and PVZCAC are microporous in nature.

Table 5.1. BET analysis of PVF, PVB, PVPAAC and PVZCAC

Parameters	PVF	PVB	PVPAAC	PVZCAC
Total pore volume	5.850×10^{-2} cc/g	1.148×10^{-2} cc/g	1.973 cc/g	1.496 cc/g
Surface area	28.56 m^2/g	6.882 m^2/g	1424.0 m^2/g	1673.0 m^2/g
Pore diameter	3.419 nm	3.234 nm	2.991 nm	3.123 nm
Average pore diameter	8.192 nm	1.148 nm	5.541 nm	3.577 nm

The Thermogravimetric analysis (Fig. 5.1) showed that with increase in temperature up to 197°C, the mass of the biosorbent declined primarily due to moisture reduction. On further increasing the temperature up to 369°C, the mass of the biosorbent decreased by the pyrolysis. From 369°C to 550°C, there was a relatively less sharp decrease in mass of biomass; however, a mass reduction of 16% occurred in this temperature range. From the thermogravimetric studies, the carbonization temperature was found as 550°C to obtain activated carbon for further studies.

FESEM micrographs of PVF (Fig. 5.2a) showed that the biosorbent surface is rough, irregular, striated with ridges and porous. Upon physical activation of PVF, the morphology and surface changed, however not considerably (Fig. 5.2b). Chemical activation of PVF with phosphoric acid and zinc chloride significantly increased the surface area as well as number of pores leading to increase in porosity and pore volume (Fig. 5.2c and 5.2d). The FESEM images of activated carbon suggest that the activated carbon promotes the removal of hexavalent chromium from wastewater. Similar observations have been made in several chemically activated plant based biosorbents like *Sterculia guttata* shell (Rangabhashiyam and Selvaraju, 2015) and Strychnine tree fruit shell (Nakkeeran and Selvaraju, 2017).

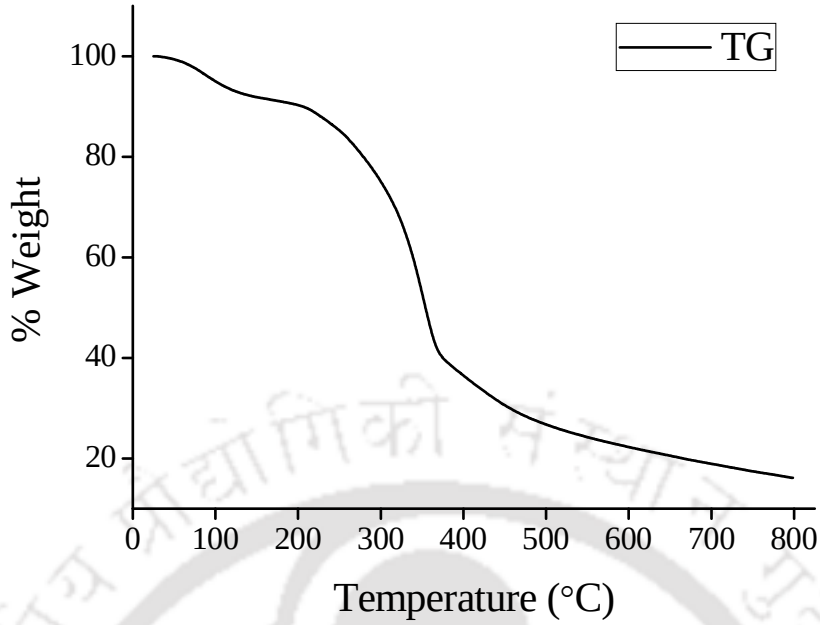

Figure 5.1. Determination of stability of the raw biosorbent (PVF) using TG in the temperature range of 25 to 800°C

EDX analyses (Fig. 5.2e, 5.2f, 5.2g and 5.2h) of Cr(VI) loaded PVF, PVB, PVPAAC and PVZCAC revealed the presence of peculiar peaks for Chromium at energy levels 0.57 KeV, 5.4 KeV and 5.9 KeV which confirmed that Cr(VI) was adsorbed on pristine biomass (PVF) as well as biochar and chemically activated carbon (PVB, PVPAAC and PVZCAC) attesting their applicability as a suitable biosorbent. The Cr(VI) biosorption capacity of PVZCAC was highest among all the prepared biosorbents as shown in the EDX spectra.

Surface functional groups of the biosorbent have been found to play important role in adsorption of Cr(VI). The FTIR spectrum of all prepared biosorbents was taken and analyzed for various peaks representing various functional groups present on the biosorbent surface. We find one broad peak at 3398 cm^{-1} which represents O-H stretching in the FTIR spectrum of PVF and PVB adsorbent (Fig. 5.3). Also, one peak was found at 2921 cm^{-1} which represents the asymmetric C-H stretching of methyl groups present in the PVF and PVB adsorbent. The peak found at 1730 cm^{-1} represented the C=O (stretching) involving the aldehyde or ketone group in both PVF and PVB adsorbent. Alkenes have been frequently reported by several researchers in various lignocellulosic biomass used for removal of heavy metals (Kuppusamy et al., 2016).

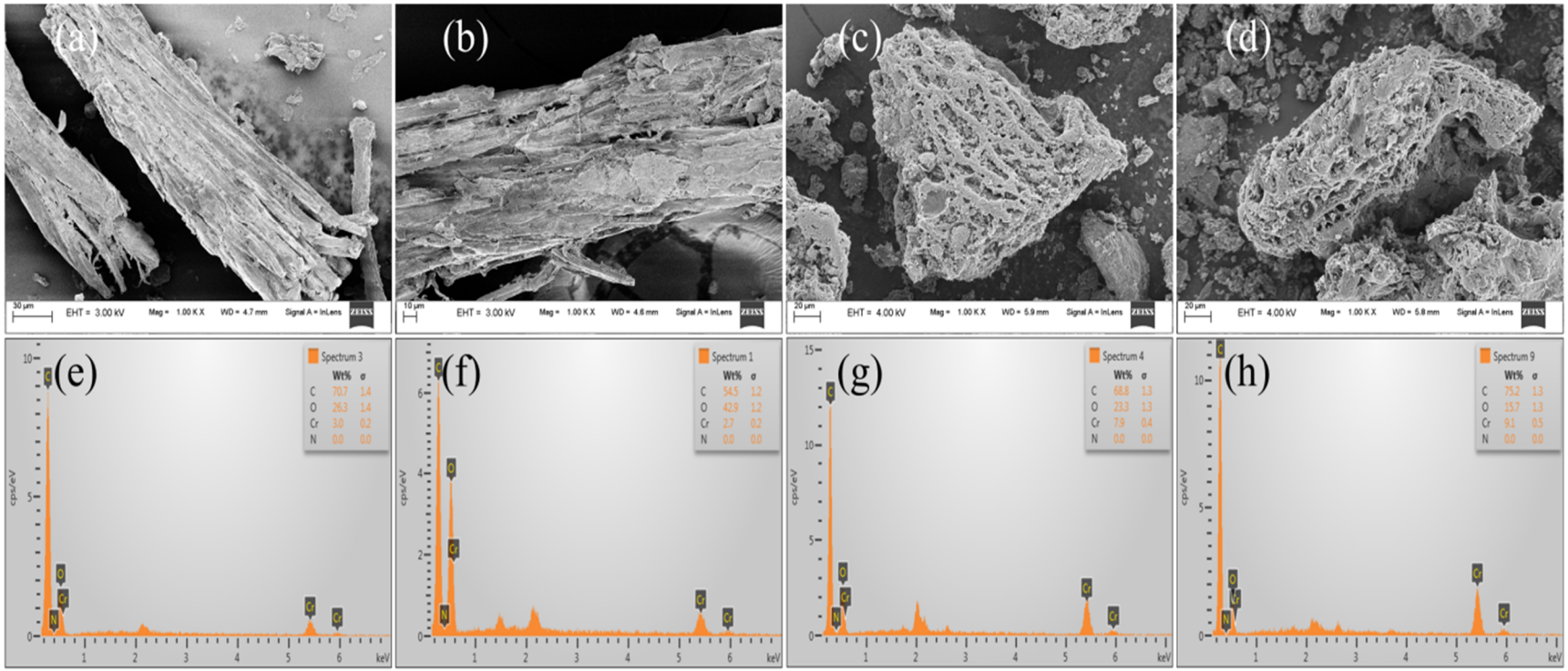

Figure 5.2. FESEM image of (a) *Phanera vahlii* fruit (PVF) particle size < 300 µm (x 1000), (b) *Phanera vahlii* biochar (PVB) particle size < 300 µm (x 1000), (c) *Phanera vahlii* phosphoric acid activated carbon (PVPAAC) and (d) *Phanera vahlii* zinc chloride activated carbon (PVZCAC). EDX image of (e) Chromium loaded *Phanera vahlii* fruit (PVF) particle size < 300 µm, (f) Chromium loaded *Phanera vahlii* biochar (PVB) particle size < 300 µm, (g) Chromium loaded *Phanera vahlii* phosphoric acid activated carbon (PVPAAC) particle size < 300 µm and (h) Chromium loaded *Phanera vahlii* zinc chloride activated carbon (PVZCAC) particle size < 300 µm

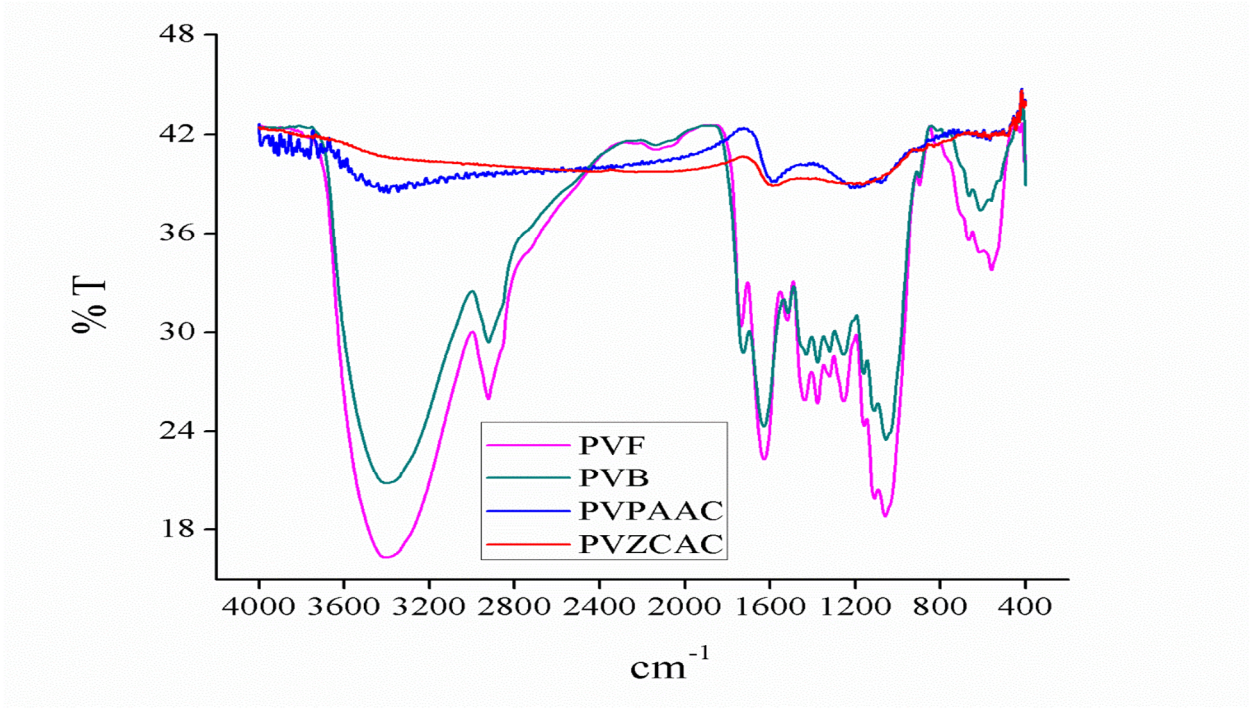

Figure 5.3. FTIR spectra of PVF, PVB, PVPAAC and PVZCAC

There were also peaks found at 1055.6 cm^{-1}, 1256.2 cm^{-1} and 1730.3 cm^{-1} which represented C-O (stretching), CN (stretching) and C=O. From the FTIR analysis done, the functional moieties interacting in the biosorption of Cr(VI) onto the surface of the prepared adsorbents may be hydroxyl, alkenes and alkyl groups. We also found that on chemical activation of PVF with phosphoric acid and zinc chloride; most of organic functional groups were lost which is in agreement with previous report (Domingues et al., 2017). This suggest that the mechanism of adsorption of chromium on PVPAAC and PVZCAC may be physisorption.

5.2.2 Influence of biosorbent dose

Influence of biosorbent dose was investigated by taking biosorbent in the range 0.5 g/L through 5.0 g/L of size less than 300 µm with 50 mL solution of 100 ppm initial chromium concentration kept at pH 2.0, temperature 303 K and agitation speed 120 rpm. Fig. 5.4. shows that the chromium percentage removal increased sharply with increase in the amount of *Phanera vahlii* fruit biomass and its activated carbon forms from 0.5 to 1.0 g/L and increased relatively less sharply afterwards till the complete removal of chromium. The increase in chromium percentage removal with increase in biosorbent dose may be explained by increase in surface area and more number of functional groups available for the biosorption of chromium. It was found that the *Phanera vahlii* zinc

chloride activated carbon was the best among all prepared biosorbents with the complete removal of chromium occurring at biosorbent dose of 1.0 g/L. The highest biosorption capacity was found for PVZCAC as 138.0 mg/g at biosorbent dose of 0.5 g/L. The decline in biosorption capacity of prepared biosorbents with increase in biosorbent dose may be explained by the relatively less available surface area per unit weight with increase in biosorbent dose.

5.2.3 Effect of pH

Influence of pH on Cr(VI) adsorption was examined in the pH range of 2.0 to 7.0 at 303 K with 100 mg/L of Cr(VI) solution, 0.5 g/L biosorbent dose. It was found that with PVF, PVB, PVPAAC and PVZCAC, maximum chromium adsorption occurred at pH 2.0 with magnitude of 89.19, 63.20, 125.4 and 150.2 mg/g, respectively. The adsorption capacity of all prepared biosorbents decreased with the increase in pH as shown in the Fig. 5.5. The main reason behind this pattern is that at lower pH negatively charged hydrogen chromate ($HCrO_4^-$), chromate (CrO_4^{2-}) and dichromate ($Cr_2O_7^{2-}$) ions in solution bind the positively charged functional groups present on the biosorbent through electrostatic interaction. At higher pH, the biosorbent surface becomes less protonated and hence repels off the anionic chromium ions (Labied et al., 2018).

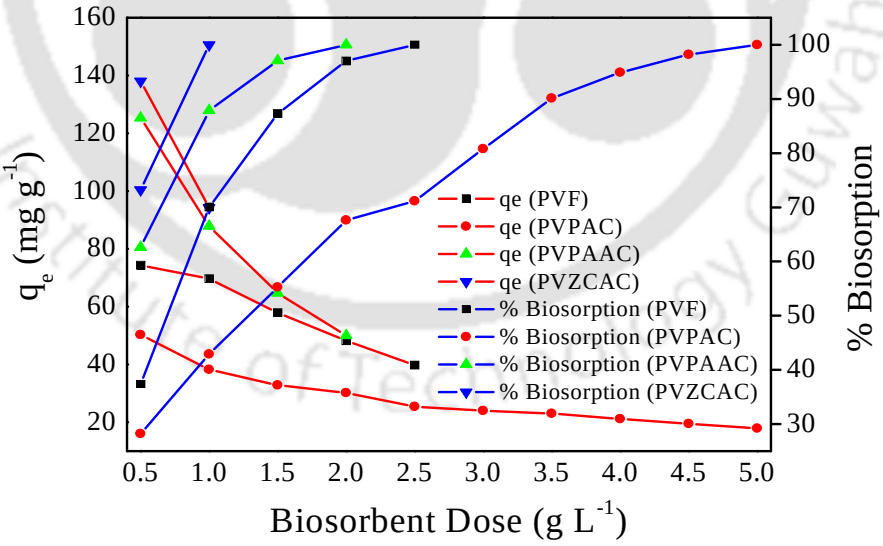

Figure 5.4. Plot showing influence of biosorbent dose on percentage removal and adsorption capacity (C_o 100 mg/L, contact time 3 h, agitation speed 120 rpm, pH 2.0, temperature 303 K)

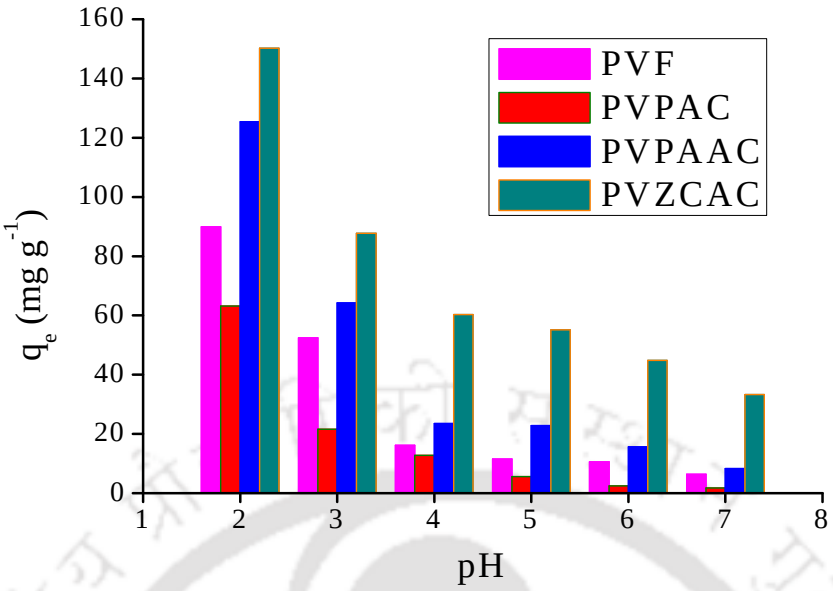

Figure 5.5. Influence of pH on Cr(VI) adsorption using PVF, PVB, PVPAAC and PVZCAC

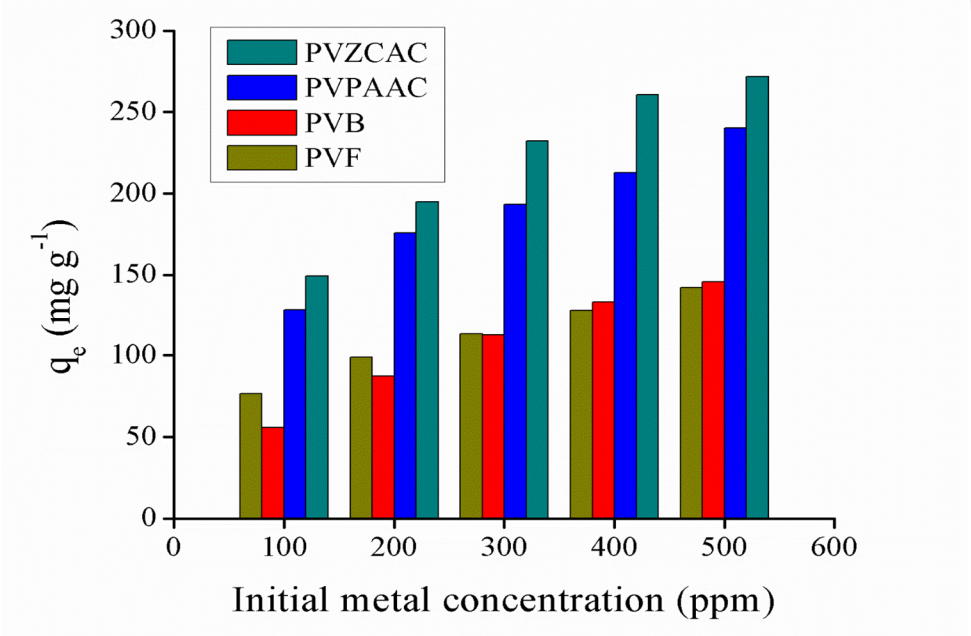

Figure 5.6. Influence of initial Cr(VI) concentration

5.2.4 Influence of initial Cr(VI) concentration

The effect of initial metal concentration was carried out in the range 100 mg/L through 500 mg/L for all prepared biosorbents at pH 2.0, 100 rpm and 303 K, contact time 3 h and biosorbent dose 0.5 g/L (Fig. 5.6). The adsorption capacity of PVF, PVB, PVPAAC and PVZCAC was found to increase from 76.43 to 142.1 mg/g, 55.85 to 145.7

mg/g, 128.6 to 240.1 mg/g and 149.2 to 271.9 mg/g, respectively. The increase in equilibrium adsorption capacity as the initial Cr(VI) concentration was increased may be due to the increased driving force of Cr(VI) which promoted the surface adsorption of chromium ions from the bulk solution (Moussavi and Barikbin, 2010).

5.2.5 Isotherm studies

Isotherm models informed regarding the nature of interaction between the biosorbent and chromium ions. Isotherm models based on two parameters such as Langmuir, Freundlich and Dubinin-Radushkevich models were applied to the experimental data at various initial Cr(VI) concentration.

5.2.5.1 Langmuir adsorption isotherm

Langmuir isotherm model considers attachment of ions over the surface of the biosorbent in a monolayer fashion with no interaction between the adjacent ions. Further, all ions have same affinity (Langmuir, 1918). The linear form of the Langmuir model is written as

$$\frac{C_e}{q_e} = \frac{1}{Q_0 K_L} + \frac{1}{Q_0} C_e \qquad (4)$$

where 'q_e' denotes the equilibrium adsorption capacity (mg/g), 'C_e' denotes the equilibrium concentration of adsorbate (mg/L), 'Q_0' represents the monolayer adsorption capacity (mg/g) and 'K_L' denotes the Langmuir isotherm constant (L/mg). The separation factor 'R_L' is estimated by the expression

$$R_L = \frac{1}{1 + K_L C_o} \qquad (5)$$

The nature of the adsorption process is concluded by the value of separation factor R_L. If R_L lies between 0 and 1, the adsorption may be favorable. If R_L is 1, adsorption is unfavorable and if R_L is 0, the adsorption is irreversible. Fig. 5.7a shows the isotherm plot of the ratio of equilibrium Cr(VI) concentration (C_e) and equilibrium adsorption capacity of PVF, PVB, PVPAAC and PVZCAC (q_e) vs. equilibrium Cr(VI) concentration (C_e). The regression coefficient values for PVF, PVB, PVPAAC and PVZCAC were calculated as 0.978, 0.991, 0.979 and 0.989, respectively, which are lower than regression coefficient values obtained for Freundlich isotherm model as well as Dubinin-Radushkevich isotherm. The monolayer adsorption potential of PVF, PVB, PVPAAC and PVZCAC was found as 166.9, 222.7, 259.7 and 297.6 mg/g, respectively. Lower value of

K_L, 0.0106, 0.0043, 0.019 and 0.024 for PVF, PVB, PVPAAC and PVZCAC respectively depicted good affinity between Chromium ions and the biosorbent. R_L value of 0.483 - 0.157, 0.696 – 0.314, 0.338 – 0.092 and 0.289 – 0.075 showed that and 0.375-0.107 for PVF, PVB, PVPAAC and PVZCAC respectively, for initial Cr(VI) concentrations of 100-500 mg/L showed that the adsorption process was favorable.

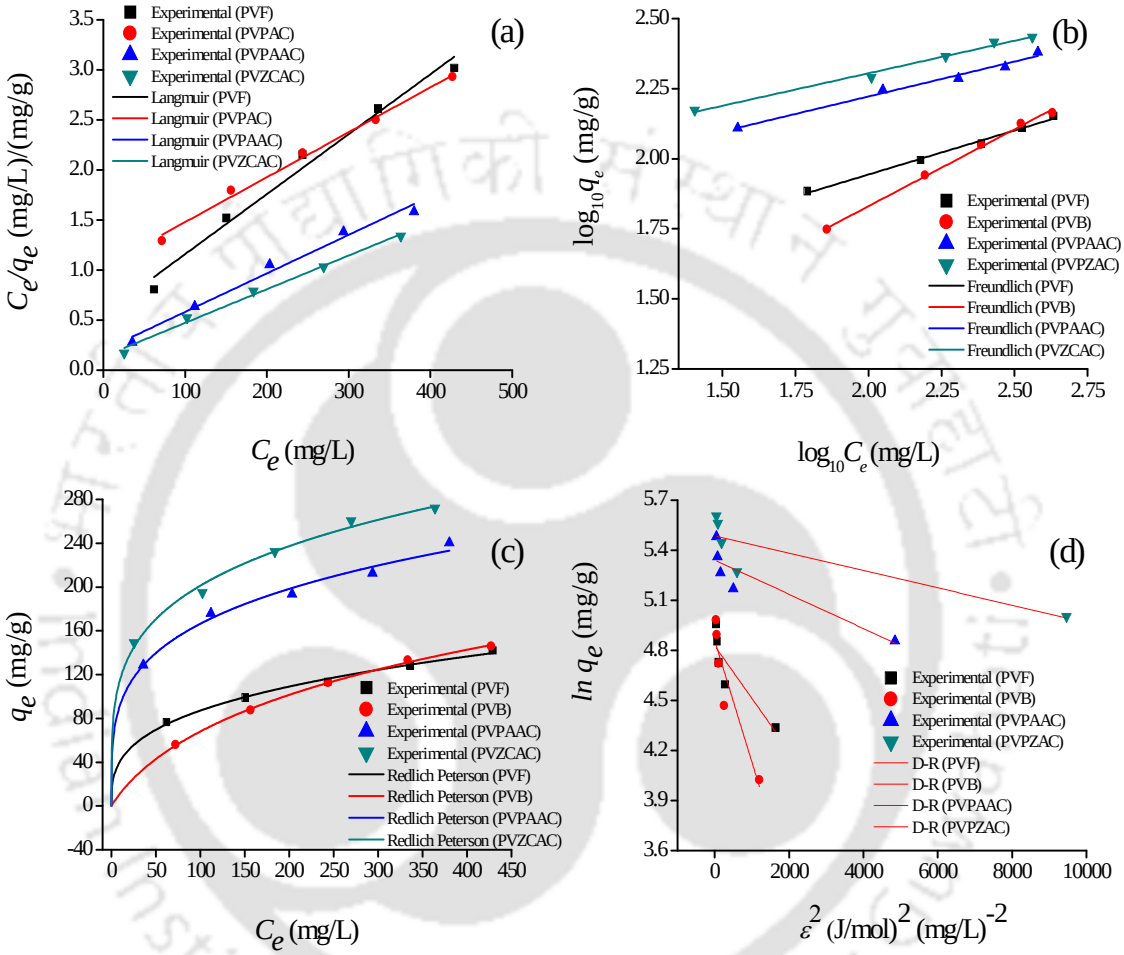

Figure 5.7. Isotherm plot of PVF, PVB, PVPAAC and PVZCAC for the adsorption of Cr(VI) solution at equilibrium Cr(VI) concentration (a) Langmuir isotherm (b) Freundlich isotherm (c) Redlich Peterson isotherm and (d) Dubinin-Radushkevich isotherm

5.2.5.2 Freundlich adsorption isotherm

Freundlich isotherm considers that the adsorption occurs in a multilayer fashion with heterogenous affinity towards the adsorbing ligands (Freundlich, 1907). The linear form of Freundlich isotherm model is expressed as

$$\log_{10} q_e = \log_{10} K_F + \frac{1}{n_F} \log_{10} C_e \qquad (6)$$

where, K_F and n_F represents the Freundlich isotherm constant (mg/g)(L/mg)$^{1/n}{}_F$ and Freundlich exponent (dimensionless) respectively. Freundlich constant (n_F) represents the degree to which adsorption deviates from linearity. From the linear isotherm (Fig. 5.7b), the value of K_F was found to be 20.64, 5.40, 52.87 and 69.28 for PVF, PVB, PVPAAC and

Table 5.2. Isotherm parameter of PVF, PVB, PVPAAC and PVZCAC for adsorption of Cr(VI)

Isotherm	Parameters	PVF	PVB	PVPAAC	PVZCAC
Langmuir	Q_o (mg/g)	166.9	222.7	259.7	297.6
	K_L (L/mg)	0.0106	0.0043	0.019	0.024
	R_L (100 – 500 mg/L)	0.483-0.157	0.696-0.314	0.338-0.092	0.289-0.075
	Goodness of fit				
	R^2	0.9784	0.9912	0.9797	0.9892
	Number of points	5	5	5	5
	Degrees of freedom	3	3	3	3
	Residual sum of squares	0.0501	0.0010	0.0173	0.0066
Freundlich	K_F (mg/g)(L/mg)$^{1/n}{}_F$	20.6	5.4	52.9	69.3
	n_F	3.18	1.82	4.01	4.30
	Goodness of fit				
	R^2	0.9917	0.9961	0.9813	0.9860
	Number of points	5	5	5	5
	Degrees of freedom	3	3	3	3
	Residual sum of squares	2.75E-3	3.24E-4	5.92E-4	4.75E-4
Redlich Peterson	α_{RP} (L/mg)	1.312E5	1.414	1.8E4	1.628E5
	β	0.6762	0.7303	0.7475	0.7622
	K_{RP} (L/g)	6689	0.03727	345.8	2419
	Goodness of fit				
	R^2	0.9975	0.9990	0.9938	0.9964
	Number of points	5	5	5	5
	Degrees of freedom	2	2	2	2
	Residual sum of squares	1.49E-3	5.93E-4	3.69E-3	2.11E-3
D-R	Q_m (mg/g)	124.9	128.9	208.9	241.6
	K (mol^2/J^2)	0.0003	0.0007	0.0001	0.0005
	E (kJ/mol)	0.0398	0.0261	0.069	0.0315
	Goodness of fit				
	R^2	0.7295	0.8344	0.7629	0.6924
	Number of points	5	5	5	5
	Degrees of freedom	3	3	3	3
	Residual sum of squares	0.0474	0.0739	0.0397	0.0555

PVZCAC, respectively. Lower value of $1/n_F$ viz. 0.314, 0.549, 0.249 and 0.232 for PVF, PVB, PVPAAC and PVZCAC, respectively, suggested that the adsorption of chromium over surface of all prepared biosorbents is favorable. Regression values of 0.991, 0.996, 0.981 and 0.986 for PVF, PVB, PVPAAC and PVZCAC, respectively (Table 5.2)

revealed Freundlich isotherm and Langmuir isotherm fitted to the experimental data equivalently that suggested that the adsorption process may be multilayer as well.

5.2.5.3 Redlich Peterson adsorption isotherm

Redlich Peterson model is the generalization of both Langmuir and Freundlich adsorption model taken together. Redlich Peterson model is described by the following equation.

$$q_e = \frac{K_{RP} C_e}{1 + a_{RP} C_e^{\beta}} \tag{7}$$

where, K_{RP} represents the Redlich Peterson model isotherm constant (L/g), a_{RP} is the Redlich Peterson model constant (L/mg). The exponent, β, lies between 0 and 1. The experimental data was fitted to the Redlich Peterson isotherm model. It was found that the experimental data fitted well to the Redlich Peterson model with a regression coefficient of 0.9975, 0.9990, 0.9938 and 0.9964 for PVF, PVB, PVPAAC and PVZCAC, respectively. The exponent β was found to be
significantly below 1 for all biosorbents which suggested that the adsorption process followed both Langmuir and Freundlich isotherm.

5.2.5.4 Dubinin–Radushkevich (D–R) adsorption isotherm

The DR isotherm model equation is represented by (Sing, 1985)

$$\ln q_e = \ln Q_m - K\varepsilon^2 \tag{8}$$

where, Q_m symbolizes the maximum adsorption capacity (mg/g), K symbolizes the activity coefficient (mol^2/J^2), ε denotes the Polanyi potential which is obtained by the equation

$$\varepsilon = \mathrm{RT}(\ln(1 + C_e^{-1})) \tag{9}$$

where, R represents the universal gas constant (J/mol K) and T represents the absolute temperature (K). Q_m values estimated by graph of $\log(q_e)$ vs. ε^2 were found to be 124.88, 128.92, 208.86 and 241.56 mg/g, respectively for PVF, PVB, PVPAAC and PVZCAC. K values were estimated as 0.00031, 0.0007, 0.0001 and 0.0005 mol^2/J^2 for PVF, PVB, PVPAAC and PVZCAC, respectively (Table 5.2). Apparent adsorption energy denoted by E (kJ/mol) is calculated by the expression

$$E = \frac{1}{\sqrt{2K}} \tag{10}$$

If $1<E<16$ kJ/mol, physical adsorption occurs between the adsorbate and adsorbent. If

E>16 kJ/mol, chemisorption occurs between the adsorbate and adsorbent. If 8<E<16 kJ/mol, the mechanism predominantly involves ion exchange (Aytas et al., 2011). The Dubinin-Radushkevich model was solved for various parameters and parameters are depicted in Table 5.2. The Apparent adsorption energy E for PVF, PVB, PVPAAC and PVZCAC was found as 0.039, 0.026, 0.069 and 0.031 kJ/mol, respectively which indicated that the physisorption occurred between the adsorbent and the adsorbate.

5.2.6 Kinetic studies

5.2.6.1 Pseudo-first order model

The Pseudo-first order kinetic model is represented by

$$\log(q_e - q_t) = \log q_e - \frac{k_1}{2.303} t \qquad (11)$$

where, k_1 denotes the Pseudo-first order rate constant (min^{-1}), q_e is the equilibrium adsorption capacity (mg/g) and q_t is the adsorption capacity (mg/g) (Lagergren, 1898). Table 5.3 depicts various parameters and regression values of the model. q_e values calculated from the plot of log(q_e-q_t) vs. t did not correlated well with the experimental values. The R^2 values of PVF, PVB, PVPAAC and PVZCAC obtained for Pseudo-first order model were found to be less than the R^2 values for other kinetic models which reveal that the adsorption of chromium upon PVF, PVB, PVPAAC and PVZCAC does not obey pseudo-first order reaction.

5.2.6.2 Pseudo-second order model

The Pseudo-second order kinetic model is represented by equation

$$\frac{t}{q_t} = \frac{1}{k_2 q_e^{\,2}} + \frac{t}{q_e} \qquad (12)$$

where, k_2 (g/mg/min) denotes the Pseudo-second order rate constant (Ho and McKay, 1999). The pseudo-second order kinetic model is shown in Fig. 5.8 at various initial Cr(VI) concentrations. The experimental q_e values correlated well with calculated q_e values with rise in the initial Cr(VI) concentration (Table 5.3). The R^2 values obtained for pseudo-second order model were better than the R^2 values for other kinetic models analyzed. Hence, the adsorption process of Cr(VI) by PVF, PVB, PVPAAC and PVZCAC followed Pseudo-second order kinetics with sharing of electrons between sorbent and sorbate.

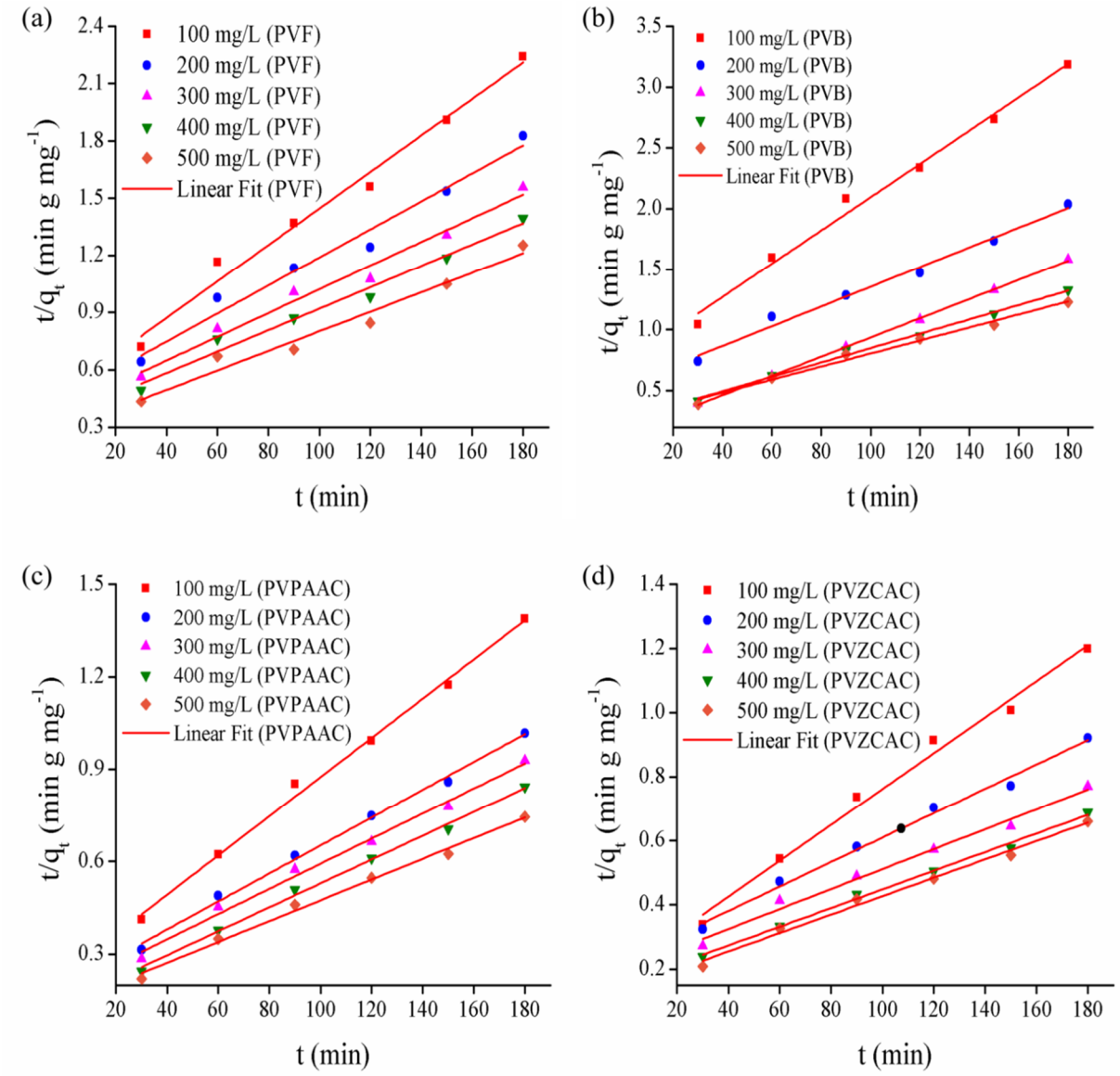

Figure 5.8. Pseudo-second order plot of (a) PVF, (b) PVB, (c) PVPAAC and (d) PVZCAC for the adsorption of Cr(VI) at equilibrium Cr(VI) concentrations

5.2.6.3 Intraparticle diffusion kinetic model

Intraparticle diffusion model is represented by equation

$$q_t = k_{id} t^{1/2} + C \qquad (13)$$

where, k_{id} denotes the intraparticle diffusion rate constant (mg/g/min$^{1/2}$), C denotes the intercept (Morris and Weber, 1964). The calculated q_e values did not correlate well with the experimental q_e values. R^2 values obtained from intraparticle diffusion model were lower than pseudo-second order and pseudo-first order kinetic models (Table 5.3).

Further, the plot between $t^{1/2}$ and q_t did not passed through the origin which suggested that multilinearity occurred which is depicted in the Fig. 5.9. It was inferred

Table 5.3. Kinetic studies of PVF, PVB, PVPAAC and PVZCAC for Cr(VI) removal

Biomass	C_0 (mg/L)	Pseudo-first order			Pseudo-second order			Intraparticle diffusion	
		k_1 (min^{-1})	q_e (mg/g)	R^2	k_2 (g/mg/min)	q_e (mg/g)	R^2	k_{id} ($mg/g/min^{1/2}$)	R^2
PVF	100	0.0642	121.2	0.939	0.0093	104.5	0.982	5.298	0.940
	200	0.0825	238.0	0.893	0.0066	136.0	0.972	7.176	0.924
	300	0.0826	356.1	0.870	0.0049	160.7	0.976	8.491	0.940
	400	0.066	227.9	0.936	0.0040	177.9	0.977	9.337	0.945
	500	0.098	443.1	0.929	0.0029	195.7	0.962	10.34	0.875
PVB	100	0.053	71.68	0.915	0.0198	72.94	0.987	3.658	0.981
	200	0.062	148.8	0.927	0.0088	123.1	0.984	6.471	0.963
	300	0.069	104.3	0.980	0.0023	126.6	0.999	4.603	0.868
	400	0.058	175.7	0.927	0.0030	169.5	0.993	8.260	0.966
	500	0.059	218.7	0.801	0.0020	186.9	0.985	9.198	0.986
PVPAAC	100	0.063	177.8	0.883	0.0030	157.0	0.995	7.311	0.962
	200	0.062	262.2	0.850	0.0018	220.7	0.994	10.71	0.977
	300	0.077	419.8	0.813	0.0015	245.7	0.990	12.03	0.968
	400	0.079	440.6	0.758	0.0011	259.1	0.995	11.98	0.968
	500	0.074	474.2	0.751	0.0009	297.6	0.991	14.03	0.980
PVZCAC	100	0.065	225.9	0.695	0.0022	178.5	0.988	7.911	0.978
	200	0.079	516.8	0.701	0.0017	262.4	0.989	7.511	0.979
	300	0.083	705.7	0.731	0.0012	321.5	0.984	16.77	0.973
	400	0.074	569.9	0.797	0.0009	344.8	0.995	17.69	0.966
	500	0.075	587.2	0.782	0.0008	349.6	0.988	17.32	0.976

that the process of Cr(VI) adsorption on the PVF, PVB, PVPAAC and PVZCAC surface may not be controlled by intraparticle diffusion (Morris and Weber, 1964).

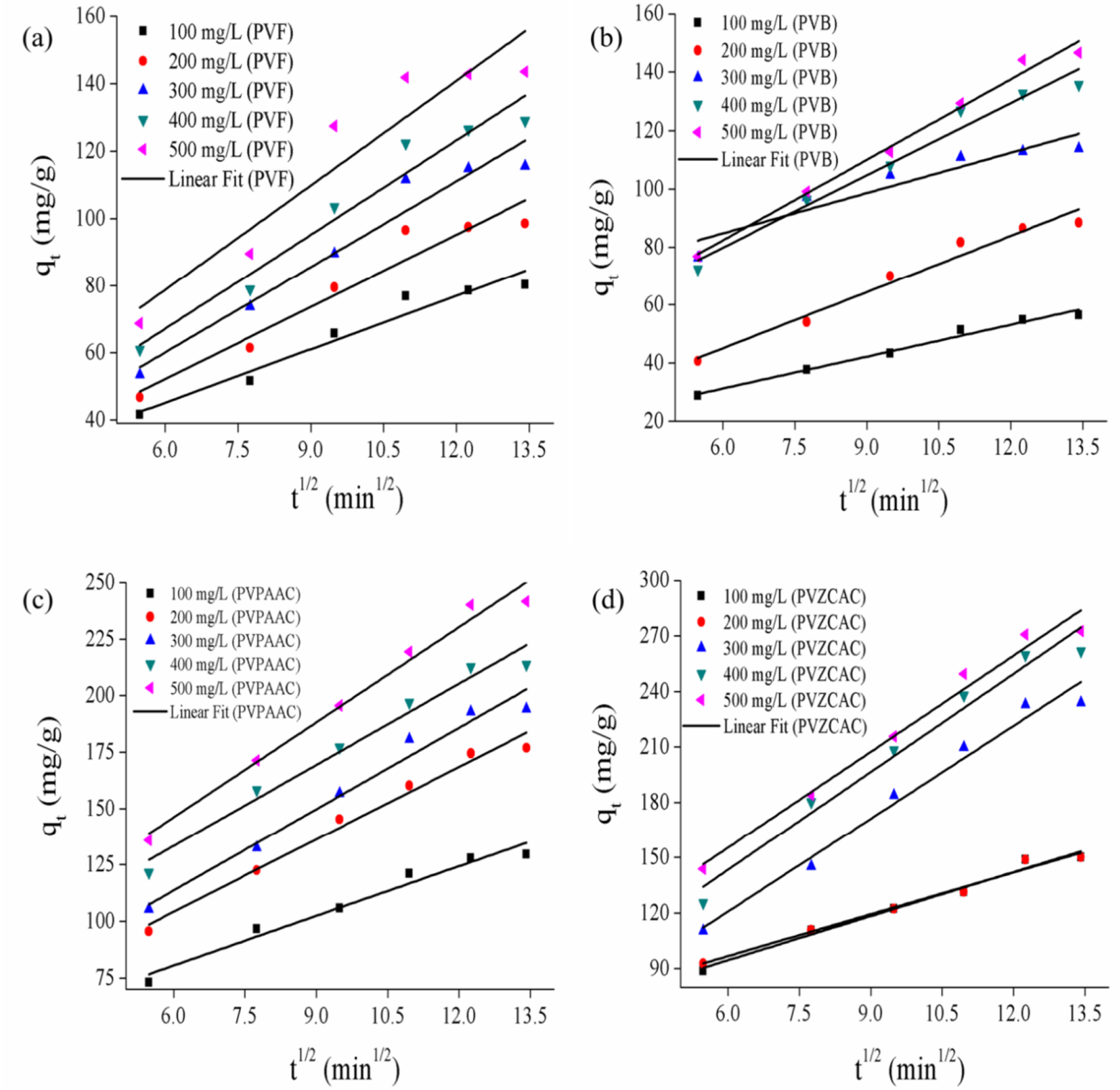

Figure 5.9. Intraparticle diffusion plot of PVF, (b) PVB, (c) PVPAAC and (d) PVZCAC for the adsorption of Cr(VI) at equilibrium Cr(VI) concentrations

5.2.7 Thermodynamic studies

Influence of temperature for various Cr(VI) concentrations was studied in the temperature range of 303 K through 333 K. The study was carried out by using different initial metal concentrations keeping the temperature constant. It was found that the adsorption capacity moderately increased with increase in both the initial Cr(VI) concentration and temperature. The increase in biosorption capacity might be due to the higher ion mobility and modification of functional groups present on the biosorbent

surface and the interaction between the functional groups and chromium ions increases with increase in temperature (Tran et al., 2016).

Gibbs free energy (ΔG°), enthalpy (ΔH°) and entropy (ΔS°) were determined by the following equations (Kumar and Jena, 2017)

$$\Delta G^o = -RT\ln K_C \quad (14)$$

where, 'T' represents absolute temperature (K) and 'R' is universal gas constant (8.314 J/mol/K) and K_C symbolizes the distribution coefficient as

$$\ln K_C = -\frac{\Delta H^o}{RT} + \frac{\Delta S^o}{R} \quad (15)$$

$$K_C = \frac{q_e}{C_e} \quad (16)$$

Table 5.4. Thermodynamic studies of PVF, PVB, PVPAAC and PVZCAC for Cr(VI) removal

Biomass	Initial metal conc. (mg/L)	ΔG° (kJ/mol) Temperature (K)				ΔH° (kJ/mol)	ΔS° (kJ/mol K^{-1})
		303	313	323	333		
PVF	100	1.421	0.642	0.503	-0.051	15.22	0.045
	200	3.536	2.998	2.830	2.865	10.22	0.022
	300	4.580	3.901	3.896	3.718	12.47	0.026
	400	5.106	4.601	4.643	4.709	8.655	0.012
	500	5.918	5.732	5.678	5.824	6.989	0.003
PVB	100	2.388	1.791	1.345	0.328	22.37	0.065
	200	3.217	3.086	2.807	2.344	11.95	0.028
	300	3.989	3.903	3.851	3.738	6.419	0.008
	400	4.479	4.306	4.347	4.313	5.870	0.004
	500	5.653	5.561	5.551	5.485	7.207	0.005
PVPAAC	100	-1.483	-1.700	-3.252	-4.522	30.76	0.105
	200	0.609	0.436	-0.379	-0.870	16.53	0.052
	300	1.873	1.705	1.178	1.003	11.41	0.031
	400	2.768	2.514	2.103	1.754	13.23	0.034
	500	3.636	3.331	2.995	2.646	13.65	0.033
PVZCAC	100	-2.569	-3.686	-4.422	-5.769	28.67	0.103
	200	0.249	-0.138	-0.873	-1.125	15.03	0.048
	300	1.288	0.940	0.511	0.273	11.84	0.034
	400	2.251	1.893	1.595	1.172	12.94	0.035
	500	3.137	2.867	2.354	1.947	15.50	0.040

ΔH° and ΔS° were estimated by calculating the slope and intercept from the linear plot of RlnK_c vs. -1/T. Table 5.4 depicts the thermodynamic parameters estimated from the temperature studies at various metal concentrations. ΔG° was found to be

positive and relatively less at various conditions which suggested that the adsorption phenomenon was non-spontaneous. Rarely, the ΔG° values were estimated as negative which indicated the spontaneity of biosorption process (Gao et al., 2008). The ΔH° values were positive which indicated endothermic nature of process. Further, ΔS° values were approximately zero under most conditions which revealed relatively stable bonding of Cr(VI) on PVF, PVB, PVPAAC and PVZCAC surface (Dakiky et al., 2002).

5.2.8 Desorption and reuse studies

Desorption studies were performed for a duration of 4 h using 0.1 N NaOH as desorption agent at 120 rpm and 303 K temperature. Maximum desorption was achieved in 3 h and no further increase in desorption was found. The regenerated sorbent was filtered followed by drying. Adsorption experiments were performed at optimized conditions of 100 mg/L initial metal concentration, 2.0 pH, 303 K and 120 rpm. These steps were repeated until no further considerable adsorption of Cr(VI) was attained. All the prepared adsorbents were found to have significantly reduced biosorption capacity in the 2nd regeneration (Table 5.5). The PVZCAC biosorbent was found to have the highest biosorption capacity amongst all the prepared biosorbents. The decline in the desorption and reuse capacity of biosorbent may be due to the irreversible modification of functional groups after exposure of desorbing agent and Cr(VI) solution. Tremendous decrease in the removal percentage post desorption was due to the unavailability of binding sites for chromium ions.

Table 5.5. Desorption and regeneration data of PVF, PVB, PVPAAC and PVZCAC using 100 ppm initial Cr(VI) concentration

Adsorbent	Cycle 1		Cycle 2	
	Chromium desorption (%)	Chromium adsorption (%)	Chromium desorption (%)	Chromium adsorption (%)
PVF	48.8	90.0	26.7	48.7
PVB	54.7	85.5	19.2	36.5
PVPAAC	59.7	85.6	33.2	16.4
PVZCAC	73.7	97.9	54.1	34.6

5.3 Conclusion

Phanera vahlii fruit biomass (PVF) and prepared activated carbon PVB, PVPAAC, PVZCAC were investigated for the removal of Cr(VI) from simulated solutions. Characterization of the pristine biomass as well as activated carbon biosorbent suggested that *Phanera vahlii* zinc chloride activated carbon has large surface area and

pore volume as compared to other prepared biosorbents available for the chromium ions to bind to the surface. The biosorption of Cr(VI) onto PVF, PVB, PVPAAC and PVZCAC was confirmed by FTIR, FESEM and EDX. The Cr(VI) removal was highest at an optimum initial solution pH 2.0, temperature 303 K, PVF, PVB, PVPAAC and PVZCAC dose of 0.5 g/L, contact time 180 min, initial chromium concentration of 500 mg/L and agitation of 100 rpm. Langmuir Adsorption isotherm and Freundlich adsorption isotherm equivalently fitted experimental data imply that the biosorption occurs in a monolayer fashion as well as multilayer fashion. PVF, PVB, PVPAAC and PVZCAC were found to have maximum biosorption capacity of 166.9, 222.7, 259.7 and 297.6 mg/g, respectively. Pseudo-second order kinetics model was found to fit the biosorption process. Thermodynamic studies revealed that the biosorption occurred in non-spontaneous, stable and endothermic manner.

References

Aytas, S., Turkozu, D.A., Gok, C., 2011. Biosorption of uranium(VI) by bi-functionalized low cost biocomposite adsorbent. Desalination 280, 354–362. https://doi.org/10.1016/j.desal.2011.07.023

Dakiky, M., Khamis, M., Manassra, A., Mer'eb, M., 2002. Selective adsorption of chromium(VI) in industrial wastewater using low-cost abundantly available adsorbents. Advances in Environmental Research 6, 533–540. https://doi.org/10.1016/S1093-0191(01)00079-X

Domingues, R.R., Trugilho, P.F., Silva, C.A., Melo, I.C.N.A. de, Melo, L.C.A., Magriotis, Z.M., Sánchez-Monedero, M.A., 2017. Properties of biochar derived from wood and high-nutrient biomasses with the aim of agronomic and environmental benefits. PLOS ONE 12, e0176884. https://doi.org/10.1371/journal.pone.0176884

Freundlich, H., 1907. Über die Adsorption in Lösungen. Zeitschrift für Physikalische Chemie 57U, 385–470. https://doi.org/10.1515/zpch-1907-5723

Gao, H., Liu, Y., Zeng, G., Xu, W., Li, T., Xia, W., 2008. Characterization of Cr(VI) removal from aqueous solutions by a surplus agricultural waste—Rice straw. Journal of Hazardous Materials 150, 446–452. https://doi.org/10.1016/j.jhazmat.2007.04.126

Ho, Y.S., McKay, G., 1999. Pseudo-second order model for sorption processes. Process Biochemistry 34, 451–465. https://doi.org/10.1016/S0032-9592(98)00112-5

Kumar, A., Jena, H.M., 2017. Adsorption of Cr(VI) from aqueous solution by prepared high surface area activated carbon from Fox nutshell by chemical activation with H_3PO_4. Journal of Environmental Chemical Engineering 5, 2032–2041. https://doi.org/10.1016/j.jece.2017.03.035

Kuppusamy, S., Thavamani, P., Megharaj, M., Venkateswarlu, K., Lee, Y.B., Naidu, R., 2016. Potential of *Melaleuca diosmifolia* leaf as a low-cost adsorbent for hexavalent chromium removal from contaminated water bodies. Process Safety and Environmental Protection 100, 173–182. https://doi.org/10.1016/j.psep.2016.01.009

Labied, R., Benturki, O., Eddine Hamitouche, A.Y., Donnot, A., 2018. Adsorption of hexavalent chromium by activated carbon obtained from a waste lignocellulosic material (*Ziziphus jujuba* cores): Kinetic, equilibrium, and thermodynamic study.

Adsorption Science & Technology 36, 1066–1099. https://doi.org/10.1177/0263617417750739

Lagergren, S.Y., 1898. Zur Theorie der sogenannten Adsorption gelöster Stoffe. Bihang till Kungliga Svenska Vetenskapsakademiens, Handlingar 24, 1–39.

Langmuir, I., 1918. The Adsorption of Gases on Plane Surfaces of Glass, Mica and Platinum. J. Am. Chem. Soc. 40, 1361–1403. https://doi.org/10.1021/ja02242a004

Morris, J.C., Weber, W.J., 1964. Removal of biologically-resistant pollutants from waste waters by adsorption, in: Southgate, B.A. (Ed.), Advances in Water Pollution Research. Pergamon, pp. 231–266. https://doi.org/10.1016/B978-1-4832-8391-3.50032-4

Moussavi, G., Barikbin, B., 2010. Biosorption of chromium(VI) from industrial wastewater onto pistachio hull waste biomass. Chemical Engineering Journal 162, 893–900. https://doi.org/10.1016/j.cej.2010.06.032

Nakkeeran, E., Selvaraju, N., 2017. Biosorption of chromium(VI) in aqueous solutions by chemically modified Strychnine tree fruit shell. Int J Phytoremediation 19, 1065–1076. https://doi.org/10.1080/15226514.2017.1328386

Rangabhashiyam, S., Selvaraju, N., 2015. Adsorptive remediation of hexavalent chromium from synthetic wastewater by a natural and $ZnCl_2$ activated *Sterculia guttata* shell. Journal of Molecular Liquids 207, 39–49. https://doi.org/10.1016/j.molliq.2015.03.018

Sing, K.S.W., 1985. Reporting physisorption data for gas/solid systems with special reference to the determination of surface area and porosity (Recommendations 1984). Pure Appl. Chem., PAC 57, 603–619. https://doi.org/10.1351/pac198557040603

Tran, H.N., You, S.-J., Chao, H.-P., 2016. Thermodynamic parameters of cadmium adsorption onto orange peel calculated from various methods: A comparison study. Journal of Environmental Chemical Engineering 4, 2671–2682. https://doi.org/10.1016/j.jece.2016.05.009

Chapter 6
Column studies on adsorption of chromium (VI) by *Phanera vahlii* zinc chloride activated carbon

6.1 Materials and methods

6.1.1 Synthesis of Cr(VI) solution

2.828 g of potassium dichromate was dissolved in 1 L double distilled water to prepare 1000 mg/L $K_2Cr_2O_7$ solution. Corresponding dilutions of 100 to 500 ppm were made by appropriately diluting stock solution in double distilled water. The pH of the solutions was adjusted using 0.1 M NaOH and 0.1 M HCl. All chemicals were of high quality.

6.1.2 Preparation of *Phanera vahlii* zinc chloride activated carbon

Phanera vahlii fruit biomass (PVF) was collected from Morni Hills, Panchkula, Haryana, India. The fruits were thoroughly cleaned with double distilled water followed by drying at 363 K for 20 h. Fruits were crushed using a grinder and sieved to get particles of size <300 μm. *Phanera vahlii* zinc chloride activated carbon (PVZCAC) was produced by impregnating the PVF biomass with zinc chloride in the ratio 1:4 (Weight: Weight) followed by incubation at 353 K for 24 h. The zinc chloride impregnated PVF was kept in a heating furnace at 823 K for 1 h. The obtained carbon was treated with dilute HCl for the removal of impurities superseded by washing with distilled water until the pH became 7.0. The yield of the PVZCAC was 43%.

6.1.3 Estimation of hexavalent chromium

Hexavalent chromium was estimated using already established method. Hexavalent chromium under acidic conditions react with 1,4 Diphenylcarbazide to give purple-pink complex which is estimated quantitatively by taking absorbance at 540 nm in a UV-Visible spectrophotometer (GeneQuant 1300, GE, USA) (Stover, 1928).

6.1.4 Packed bed column experiment

Continuous column studies were performed to estimate the capacity of the PVZCAC to eliminate hexavalent chromium under various conditions in continuous mode. For conducting continuous column studies, glass column of internal diameter 2 cm and height 50 cm was prepared. The diagrammatic representation of the packed bed column is shown in Fig 6.1. Peristaltic pump (PP-20-EX, Miclins, India) was used to pass the hexavalent chromium through the column. The flow was kept upward to avoid channeling. Various parameters influencing the biosorption of hexavalent chromium such as bed height, initial metal concentration and flow rate were studied. The effect of bed height was studied by considering bed height 2 cm, 4 cm, 6 cm and 8 cm. The influence

of flow rate was investigated by using flow rate 5 mL/min, 10 mL/min and 15 mL/min. The effect of initial metal concentration was examined by using 50 ppm, 100 ppm, 150 ppm and 200 ppm hexavalent chromium. While doing the experiments, the bed height was kept constant at 4 cm, initial metal constant was kept constant at 50 ppm and flow rate was kept constant at 5 mL/min.

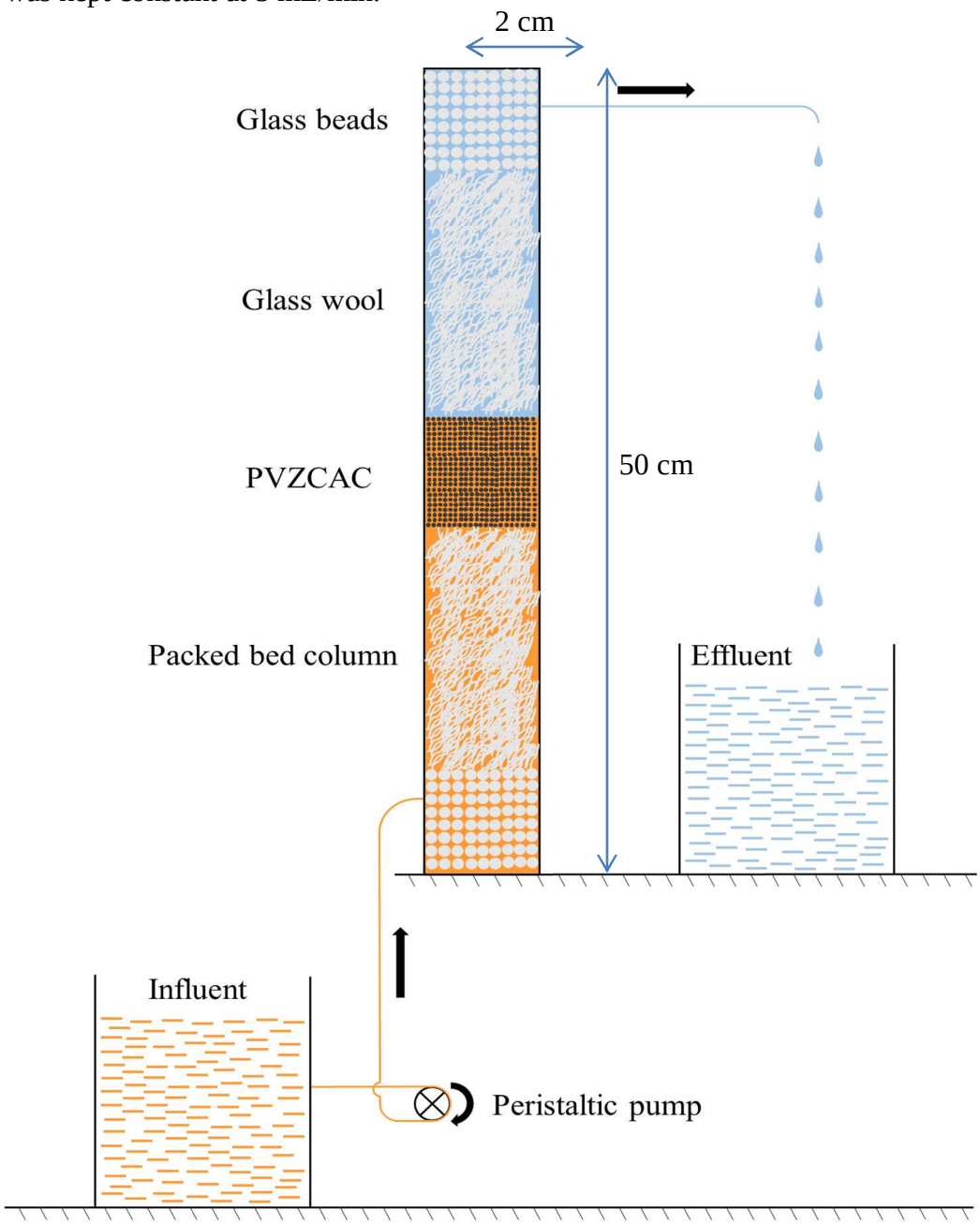

Figure 6.1. Schematic representation of Packed bed column

6.1.5 Theoretical formulae

The total amount of chromium ions that were introduced into the column (m_{total}) is estimated by the expression

$$m_{total} = \frac{C_o F t_{total}}{1000} \quad (1)$$

where C_o is the initial metal concentration (mg/L), F is the flow rate in mL/h and t_{total} is the total time for which the column was run before the adsorbent got saturated with hexavalent chromium.

The amount of chromium ions adsorbed by the adsorbent in the column experiment (q_{total}) (mg) is estimated by the multiplication of flow rate (F) (mL/h) with initial metal concentration (C_o) (mg/L) and the area above the curve (h) in the breakthrough plot of C_t/C_o vs. t (h). The expression (Vieira et al., 2008) is given as

$$q_{total} = \frac{C_o F}{1000} x \left(t_{total} - \int_{t=0}^{t=t_{total}} \frac{C_t}{C_o} dt \right) \quad (2)$$

where, F is the flow rate (mL/h), t_{total} is the total time taken for the saturation of adsorbent with hexavalent chromium ions (h), C_o is the initial metal concentration (mg/L).

The percentage removal of Cr(VI) (Y(%)) is calculated from the ratio of the amount of chromium ions adsorbed (q_{total}) to the total amount of chromium ions introduced into the column (m_{total}) (mg) (Gokhale et al., 2009). It is written as

$$Y(\%) = \frac{q_{total}}{m_{total}} x100 \quad (3)$$

The maximum biosorption capacity in column studies ($q_{e\,(exp)}$) is estimated by the ratio of amount of chromium ions adsorbed by the adsorbent (q_{total}) (mg) by the weight of adsorbent used for the experiment (W) (g) (Chauhan and Sankararamakrishnan, 2011).

$$q_{e(exp)} = \frac{q_{total}}{W} \quad (4)$$

Dead volume is the total of column volume and tubing volume. Dead volume (200 mL) was compensated while doing all the calculations of the continuous column studies.

6.2 Results and discussion

6.2.1 Bed height studies

Bed height studies were carried out at 2 cm, 4 cm, 6 cm and 8 cm at a constant flow rate of 5 mL/min and initial metal concentration of 50 ppm. It was found that with

increase in bed height, the volume required for saturation of bed as well as the time required for breakthrough increased (Fig 6.1) Further, total time was also observed to rise with rise in bed height. With increase in bed height from 2 cm to 8 cm, there was an increase in percentage chromium removal from 52.5 to 63.6% (Table 6.1). This increase might be due to the more amount of biosorbent and correspondingly more number of sites available for adsorption (Singh et al., 2017).

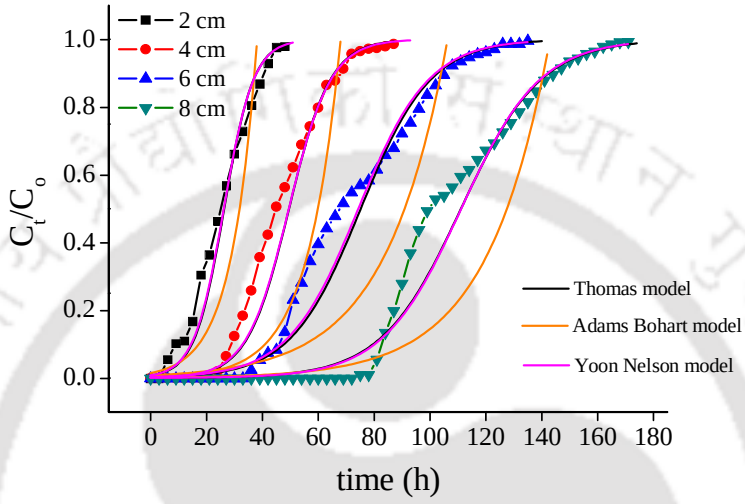

Figure. 6.2. Influence of bed height on breakthrough curve

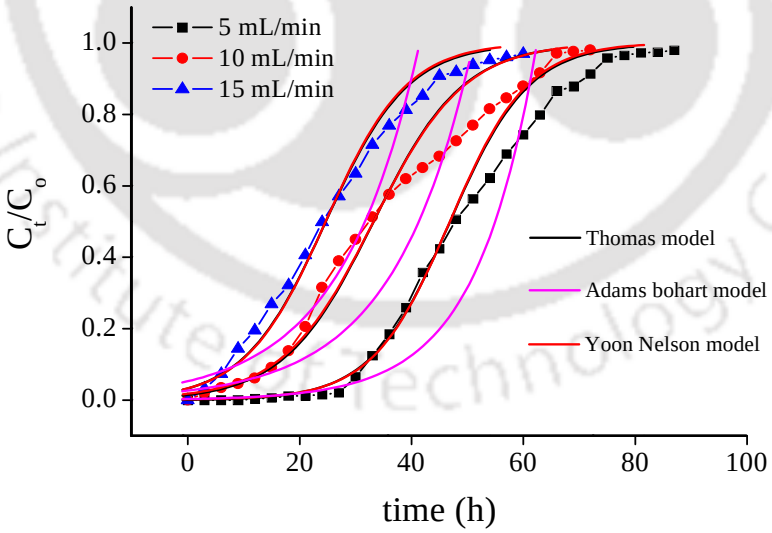

Figure. 6.3. Effect of flow rate on breakthrough curve

6.2.2 Flow rate studies

Flow rate was investigated for the adsorption of hexavalent chromium at 5 mL/min, 10 mL/min, 15 mL/min at a constant bed height of 4 cm and initial metal

concentration of 50 ppm. We found that breakthrough time as well as total time reduced with increase in flow rate (Fig. 6.2). Further, with increase in flow rate, there was decrease in volume of chromium solution required for saturation of bed. The percentage chromium removal too decreased with rise in flow rate. The chromium biosorption capacity rose from 186.4 mg/g to 288.3 mg/g with elevation in the flow rate from 5 mL/min to 15 mL/min (Table 6.1). This was due to increased exposure of adsorbent to chromium ions in less time with increase in flow rate (Bhaumik et al., 2013).

6.2.3 Initial metal concentration studies

Initial metal concentration studies were performed for 50 ppm, 100 ppm, 150 ppm and 200 ppm keeping bed height and flow rate constant at 4 cm and 5 mL/min, respectively. Total time as well as breakthrough time decreased with elevation in initial metal concentration from 50 mg/L to 200 mg/L (Fig 6.3). On elevating the initial metal concentration, the amount of chromium ions adsorbed by bed and the biosorption capacity of the bed increased. This might be owing to the elevated driving force between the chromium ions and the functional groups present on the surface of adsorbent as a result of increased initial metal concentration (Rangabhashiyam et al., 2016).

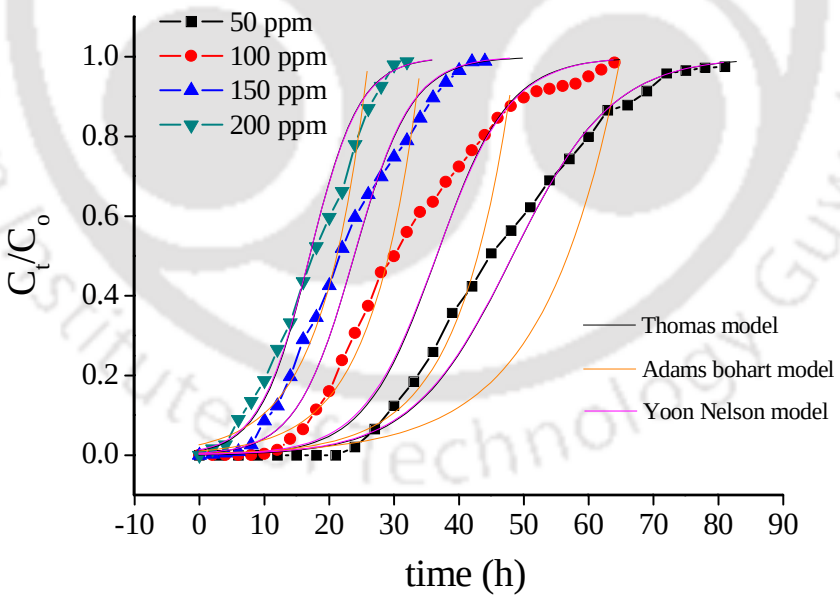

Figure. 6.4. Influence of initial metal concentration on breakthrough curve

6.2.4 Theoretical analysis of column experiments

Various column models were considered for the theoretical studies of column studies. Thomas model, Adams-Bohart model and Yoon-Nelson models were the main

theoretical models used for the present studies. In addition, Bed Depth Service time model was also studied to justify the correlation between the bed height and the total time needed for saturation of column.

Table 6.1. Evaluation of column data at various conditions for adsorption of Cr(VI) removal using PVZCAC

u (cm/min)	Z (cm)	F (mL/min)	Co (mg/L)	t_{total} (h)	m_{total} (mg)	q_{total} (mg)	$q_{e(exp)}$ (mg/g)	V_{eff} (L)	Y (%)
1.59	2	5	50	48	720	378.0	189.0	14.4	52.50
1.59	4	5	50	87	1305	703.8	175.9	26.1	53.93
1.59	6	5	50	135	2025	1091.0	181.8	40.5	53.87
1.59	8	5	50	171	2565	1631.8	203.9	51.3	63.61
1.59	4	5	50	81	1215	702.0	175.5	24.3	57.78
1.59	4	5	100	64	1920	974.0	243.5	19.2	50.73
1.59	4	5	150	44	1980	1021.9	255.4	13.2	51.61
1.59	4	5	200	32	1920	1041.6	260.4	9.6	54.25
1.59	4	5	50	87	1305	745.9	186.4	26.1	57.15
3.18	4	10	50	72	2160	1063.5	265.8	43.2	49.23
4.77	4	15	50	60	2700	1153.2	288.3	54.0	42.71

6.2.4.1 Thomas model

Thomas model is a popular theoretical model used for column data analysis and for anticipation of breakthrough curves. Thomas model is based on the assumptions of Langmuir isotherm model and second order kinetic model (Thomas, 1944). Maximum adsorption capacity and adsorption rate constant was estimated from the Thomas model for continuous column studies.

The Thomas model is expressed as

$$\ln\left(\frac{C_o}{C_t} - 1\right) = \frac{k_{TH} Q_o W}{F} - k_{TH} C_o t \qquad (5)$$

where, k_{TH} represents the adsorption rate constant and C_o depicts the maximum adsorption capacity. W is the weight of the adsorbent used in the column experiment. C_o/C_t is the ratio of the effluent to the inlet initial metal concentration. k_{TH} and Q_o were calculated from the linear plot between $\ln(C_o/C_t - 1)$ and t.

Table 6.2 shows the various Q_o and k_{TH} values obtained from the Thomas model for various combinations of bed height, initial Cr(VI) concentration and flow rates. We find that the Q_o increased and k_{TH} decreased with increase in flow rate from 5 mL/min to

15 mL/min. Further, with increase in initial metal concentration, the value of Q_o and k_{TH} elevated and declined, respectively. With increase in bed height as well, Q_o and k_{TH} increased and decreased, respectively. We found that Thomas model fitted the experimental data well with a correlation coefficient value of more than 0.9 in most of conditions. Maximum adsorption capacity was found to be 314.4 mg/g at a bed height, initial metal concentration and flow rate of 4 cm, 50 ppm and 5 mL/min, respectively.

6.2.4.2 Adams-Bohart model

The Adams-Bohart model is based on the assumption that the adsorption capacity is directly proportional to the residual capacity as well as the initial metal concentration (Bohart and Adams, 1920). The mathematical form of the model is

$$\ln\left(\frac{C_t}{C_o}\right) = k_{AB} C_o t - k_{AB} N_{AB}\left(\frac{Z}{u}\right) \quad (6)$$

where, N_{AB} represents the saturation concentration (mg/L), k_{AB} depicts the kinetic constant (L/mg min) and u represents the linear velocity (cm/min). Z represents the bed height (cm). N_{AB} and k_{AB} were estimated from the linear plot between $\ln(C_t/C_o)$ and t. We find that with elevation in bed height from 2 cm to 8 cm, the value of N_{AB} and k_{AB} decreased. However, with increase in initial metal concentration from 50 ppm to 200 ppm, N_{AB} increased while k_{AB} got decreased. We also found that as the flow rate was increased from 5 mL/min to 15 mL/min, the N_{AB} got increased from 1376.7 mg/L to 2764.7 mg/L while k_{AB} got decreased from 0.17 to 0.13 mL/mg min. We find that Adams-Bohart model was the least fitted model with the experimental data among all studied model with a correlation coefficient value of not more than 0.899 for all conditions.

6.2.4.3 Yoon-Nelson model

The Yoon-Nelson model considers that the probability of adsorption of each molecule is directly proportional to the probability of adsorbate adsorption and the probability of adsorbate breakthrough on the adsorbent (YOON and NELSON, 1984). The mathematical form of the Yoon-Nelson model is expressed as

$$\ln\left(\frac{C_t}{C_o - C_t}\right) = k_{YN} t - k_{YN}\tau \quad (7)$$

where, k_{YN} represents the Yoon-Nelson rate constant and (L/min) and τ depicts the time required for 50% adsorbate breakthrough (min). k_{YN} and τ were estimated from the linear plot between $\ln(C_t/(C_o-C_t)$ and t. We observed that k_{YN} values decreased with elevation in

bed height while τ elevated owing to more number of adsorption site with increase in bed height. Further, we find that with increase in initial metal concentration, the values of k_{YN} and τ increased and decreased, respectively which is due to the lesser time required for 50% breakthrough with increase in initial metal concentration. We also found that with increase in flow rate from 5 mL/min to 15 mL/min, the values of both k_{YN} and τ decreased which may be due to the lesser time required for 50% breakthrough as the flow rate was increased. Yoon-Nelson model fitted the experimental data well with the correlation coefficient values same as that for Thomas model which is due to similarity in mathematical expression of both models.

6.2.4.4 Bed Depth Service Time model

The prediction of service time of bed is a vital parameter in the design of the packed bed column adsorption system. Optimum bed height of the adsorbent can be predicted using Bed Depth Service Time model at constant inlet initial metal concentration. The BDST model is based on the assumption that a linear relation exists between the bed height (Z) and the service time of the column (t). Further, this model assumes that the intraparticle diffusion and external mass transfer resistance is insignificant. BDST model was put forward by Hutchins by the modification of Adams-Bohart model (Hutchins, 1973).

The mathematical form of the model is

$$t = \left(\frac{N_o Z}{C_o u}\right) - \left(\frac{1}{C_o K_a}\right) \ln\left(\frac{C_o}{C_t} - 1\right) \quad (8)$$

where, t is the service time (min) at breakthrough time, u represents the linear flow velocity (cm/min), N_o depicts the adsorption capacity of the bed (mg/L). The bed height is represented by Z and the rate constant is represented by (L/mg min). For the BDST model, the breakthrough point (C_t/C_o) was considered as 0.95. N_o and K_a were estimated from the linear plot between bed height (Z) and the service time (t). Various parameters associated with the BDST model are shown in the Table 6.3. The BDST model was found to fit well with the experimental data and the correlation coefficient was found to be 0.995. The rate constant for PVZCAC was found to be 1.43 x 10^{-2} L/mg min which is relatively less and indicates that large bed is required to avoid breakthrough. BDST model can also be used for scale-up process irrespective of inlet initial metal concentration.

Table 6.2. Various models for column data for Cr(VI) removal using PVZCAC

Column parameters			Thomas model			Adams-Bohart model			Yoon-Nelson model		
Z (cm)	F (mL/min)	C_o (mg/L)	Q_o (mg/g)	k_{TH} (L/mg h)	R^2	N_{AB} (mg/L)	k_{AB} (L/mg h)	R^2	k_{YN} (1/h)	τ (h)	R^2
2	5	50	197.2	0.0038	0.926	1518.6	0.0022	0.696	0.1875	26.25	0.926
4	5	50	185.7	0.0027	0.976	1353.7	0.0017	0.817	0.1331	49.53	0.976
6	5	50	188.0	0.0016	0.982	1410.2	0.0009	0.835	0.0795	74.44	0.981
8	5	50	208.3	0.0014	0.957	1421.8	0.0009	0.899	0.0710	111.26	0.957
4	5	50	181.5	0.0026	0.985	1294.5	0.0017	0.866	0.1291	48.40	0.985
4	5	100	275.1	0.0018	0.908	1942.9	0.0012	0.723	0.1757	36.68	0.908
4	5	150	269.7	0.0015	0.960	2053.4	0.0009	0.765	0.2261	23.97	0.960
4	5	200	256.8	0.0013	0.975	2089.2	0.0007	0.842	0.2558	17.12	0.975
4	5	50	195.7	0.0026	0.985	1376.7	0.0017	0.863	0.1324	52.16	0.985
4	10	50	279.6	0.0023	0.930	2260.6	0.0013	0.701	0.1128	37.27	0.930
4	15	50	314.4	0.0025	0.896	2764.7	0.0013	0.592	0.127	27.94	0.896

Table 6.3. BDST model for adsorption of hexavalent chromium PVZCAC

Column parameters			Bed depth service model		
u (cm/min)	C_o (mg/mL)	C_o/C_t	N_o (mg/L)	K_a (L/mg min)	R^2
1.591	50	1.013	1654.54	0.0143	0.995

6.3 Conclusion

In this work, we have identified *Phanera vahlii* zinc chloride activated carbon as an efficient adsorbent for the removal of hexavalent chromium in continuous mode. The adsorption process was found to be influenced by parameters such as bed height, flow rate and initial metal concentration. Lower initial metal concentration and flow rate and higher bed height were found to be beneficial for the adsorption capacity of the adsorbent. Thomas model, Yoon Nelson model and Bed depth service time model fitted well to the experimental data.

References

Bhaumik, M., Setshedi, K., Maity, A., Onyango, M.S., 2013. Chromium(VI) removal from water using fixed bed column of polypyrrole/Fe_3O_4 nanocomposite. Separation and Purification Technology 110, 11–19. https://doi.org/10.1016/j.seppur.2013.02.037

Bohart, G.S., Adams, E.Q., 1920. Some aspects of the behavior of charcoal with respect to chlorine. J. Am. Chem. Soc. 42, 523–544. https://doi.org/10.1021/ja01448a018

Chauhan, D., Sankararamakrishnan, N., 2011. Modeling and evaluation on removal of hexavalent chromium from aqueous systems using fixed bed column. Journal of Hazardous Materials 185, 55–62. https://doi.org/10.1016/j.jhazmat.2010.08.120

Gokhale, S.V., Jyoti, K.K., Lele, S.S., 2009. Modeling of chromium (VI) biosorption by immobilized *Spirulina platensis* in packed column. Journal of Hazardous Materials 170, 735–743. https://doi.org/10.1016/j.jhazmat.2009.05.005

Hutchins, R.A., 1973. New method simplifies design of activated carbon systems. Chemical Engineering 133–138.

Rangabhashiyam, S., Nandagopal, M.S.G., Nakkeeran, E., Selvaraju, N., 2016. Adsorption of hexavalent chromium from synthetic and electroplating effluent on chemically modified *Swietenia mahagoni* shell in a packed bed column. Environ Monit Assess 188, 411. https://doi.org/10.1007/s10661-016-5415-z

Singh, D.K., Kumar, V., Mohan, S., Bano, D., Hasan, S.H., 2017. Breakthrough curve modeling of graphene oxide aerogel packed fixed bed column for the removal of Cr(VI) from water. Journal of Water Process Engineering 18, 150–158. https://doi.org/10.1016/j.jwpe.2017.06.011

Stover, N.M., 1928. Diphenylcarbazide as a test for chromium. J. Am. Chem. Soc. 50, 2363–2366. https://doi.org/10.1021/ja01396a007

Thomas, H.C., 1944. Heterogeneous Ion Exchange in a Flowing System. J. Am. Chem. Soc. 66, 1664–1666. https://doi.org/10.1021/ja01238a017

Vieira, M.G.A., Oisiovici, R.M., Gimenes, M.L., Silva, M.G.C., 2008. Biosorption of chromium(VI) using a Sargassum sp. packed-bed column. Bioresource Technology 99, 3094–3099. https://doi.org/10.1016/j.biortech.2007.05.071

YOON, Y.H., NELSON, J.H., 1984. Application of Gas Adsorption Kinetics I. A Theoretical Model for Respirator Cartridge Service Life. American Industrial Hygiene Association Journal 45, 509–516. https://doi.org/10.1080/15298668491400197

Chapter 7
Conclusions and Recommendations

7.1 Conclusions

With depleting water sources and increasing water pollution, there is considerable interest and attention towards the recycling of wastewater by elimination of pollutants. Hexavalent chromium, a proven Category A carcinogenic substance is being used and released in enormous quantities owing to urban and industrial activities of human. Adsorption is a relatively unexplored method which is eco-friendly, cheap, involves less or no chemicals. The present work focuses on the removal of hexavalent chromium from synthetic wastewater by the use of lignocellulosic plant materials in their raw form and activated carbon form through the adsorption process.

Pinus kesiya cone biomass (PKB), *Senna siamea* seed pods (SSSP) and *Phanera vahlii* fruit biomass (PVF) were used in their raw form and activated carbon form namely *Senna siamea* zinc chloride activated carbon (SSAC), *Phanera vahlii* biochar (PVB), *Phanera vahlii* phosphoric acid activated carbon (PVPAAC) and *Phanera vahlii* zinc chloride activated carbon (PVZCAC). Qualitative techniques such as FESEM, EDX revealed the adsorbents have large pores for the adsorption of hexavalent chromium. FTIR analysis was done to determine the functional groups present on the surface of raw adsorbents and involved in adsorption of hexavalent chromium as hydroxyl, alkenes and alkyl groups. FTIR analysis revealed the absence of functional groups on the surface of activated carbons namely SSSP, PVPAAC and PVZCAC. BET analysis suggested that the adsorbents had large surface area with enormous number of pores conferring the materials with high porosity. Among the materials investigated, *Phanera vahlii* zinc chloride activated carbon was found to highest surface area as well largest pores of magnitude 1673.0 m^2/g and 3.123 nm, respectively. Thermogravimetric analysis indicated that the materials investigated were stable and followed two phase pattern for depletion in mass. Various vital parameters influencing the adsorption process were modulated for determining the maximum biosorption capacity such as pH, biosorbent dose, temperature, initial metal concentration and contact time. The optimized parameters were determined as pH 2.0, biosorbent dose 0.5 g/L, 303 K temperature, 500 mg/L initial metal concentration and 180 min contact time. Theoretical studies were carried out by fitting various adsorption isotherms namely Langmuir, Freundlich, Redlich Peterson and Dubinin-Radushkevich to the experimental data. Langmuir and Freundlich adsorption isotherms were found to agree well with the experimental data. Kinetic models were fitted to the experimental data to find out the mechanism of adsorption process. It was

found that the mechanism of adsorption for all the materials followed Pseudo-second order rate kinetics. Thermodynamics studies were performed and revealed few materials to have spontaneous, exothermic nature of adsorption process while for some materials, adsorption process was non-spontaneous, endothermic in nature. Desorption and reuse studies suggested all the materials to be reusable, however, PVZCAC was found to have high reusability among the investigated materials. Langmuir adsorption isotherm revealed that PVZCAC possessed the maximum adsorption capacity among all the investigated adsorbents with a magnitude of 297.6 mg/g. A comparison table comprising of biosorption capacity of all biosorbents investigated in this work is given below.

Table 7.1. Comparison of biosorption capacity of various biosorbents used in this work

Biosorbent	**Maximum biosorption capacity** Q_o (mg/g)
Pinus kesiya cone biomass (PKB)	73.96
Senna siamea seed pod biomass (SSSP)	119.18
Senna siamea activated carbon (SSAC)	139.86
Phanera vahlii fruit biomass (PVF)	166.9
Phanera vahlii biochar (PVB)	222.7
Phanera vahlii phosphoric acid activated carbon (PVPAAC)	259.7
Phanera vahlii zinc chloride activated carbon (PVZCAC)	297.6

Continuous column studies were conducted by preparing packed bed of *Phanera vahlii* zinc chloride activated carbon adsorbent. Variables influencing the adsorption process were optimized by considering the bed height as 2 cm, 4 cm, 6 cm and 8 cm, initial metal concentration as 50 ppm, 100 ppm, 150 ppm and 200 ppm, flow rate as 5 mL/min, 10 mL/min and 15 mL/min. The operating condition of 8 cm bed height, 5 mL/min flow rate and 50 ppm initial metal concentration was found to be the best for the continuous column mode operation. Under these conditions, the breakthrough time, total time and amount of chromium adsorbed was maximum with magnitude of 80 h, 171 h and 1631.8 mg, respectively. Various theoretical models viz. Thomas model, Yoon Nelson model, Adams Bohart model and Bed depth service time model were applied to the experimental data. Thomas model and Yoon Nelson models were found to have

similar and better fit with the experimental data as compared to the Adams Bohart model. Bed depth service time model fitted well with the experimental data and confirmed the linear relationship between the service time and bed height of the packed bed.

We found that the adsorbent *Phanera vahlii* zinc chloride activated carbon (PVZCAC) is capable of abatement of hexavalent chromium from wastewater with high magnitude of adsorption capacity both in batch mode as well continuous mode. Further, the adsorption process was found to be eco-friendly, inexpensive, less laborious, rapid method for the elimination of hexavalent chromium by the use of raw lignocellulosic materials or the activated carbon prepared from them.

7.2 Recommendations for future work

Biosorption has potential for the abatement of various metal impurities including hexavalent chromium from effluent. Various natural and synthetic biosorbents have been investigated for the removal of hexavalent chromium including the ones investigated in our study. From our studies on lignocellulosic biosorbents, we concluded that lignocellulosic biomass being conveniently available in huge quantities, biodegradable, non-toxic have great potential for the treatment of various impurities such as heavy metals, dyes etc. including hexavalent chromium.

The future scope of the present work is as follows.

- The investigated novel adsorbents can be tested for adsorption of other metal, dye pollutant either individually or in combination.
- The used lignocellulosic materials can be developed into more efficient activated carbon and more activation methods can be developed using these materials subsequently.
- The used novel adsorbents can be further probed for determination of adsorption mechanism.
- Investigation of the adsorbent (PVZCAC) for removal of hexavalent chromium at a larger scale in continuous mode than the present scale.

List of Publications and Communications

1. **Abhishek, A**., Saranya, N., Chandi, P., Selvaraju, N., 2018. Studies on the remediation of chromium(Vi) from simulated wastewater using novel biomass of *Pinus kesiya* cone. Desalination Water Treat. 114, 192–204. https://doi.org/10.5004/dwt.2018.22321

2. **Ajmani, A**., Shahnaz, T., Narayanan, S., Narayanaswamy, S., 2019. Equilibrium, kinetics and thermodynamics of hexavalent chromium biosorption on pristine and zinc chloride activated *Senna siamea* seed pods. Chem. Ecol. 35, 379–396. https://doi.org/10.1080/02757540.2019.1584614

3. **Ajmani A.**, Shahnaz, T., Subbiah, S., Selvaraju, N., 2019. Hexavalent chromium adsorption on virgin, biochar and chemically modified carbons prepared from *Phanera vahlii* fruit biomass*:* Equilibrium, kinetics and thermodynamics approach. Environ. Sci. Pollut. Res. Int. 26, 32137–32150. https://doi.org/10.1007/s11356-019-06335-z

4. **Ajmani A.**, Patra, C., Subbiah, S., Selvaraju, N., 2020. Packed bed column studies of hexavalent chromium adsorption by zinc chloride activated carbon synthesized from *Phanera vahlii* fruit biomass. J. Environ. Chem. Eng. 8, 103825. https://doi.org/10.1016/j.jece.2020.103825

5. Saranya, N., **Ajmani, A**., Sivasubramanian, V., Selvaraju, N., 2018. Hexavalent Chromium removal from simulated and real effluents using *Artocarpus heterophyllus* peel biosorbent - Batch and continuous studies. J. Mol. Liq. 265, 779–790. https://doi.org/10.1016/j.molliq.2018.06.094

Vitae

The author was born on January 19, 1988 in Ambala, Haryana, India. He completed High School examination conducted by Central Board of Secondary Education, Delhi in 2003. He completed Senior Secondary School examination conducted by Central Board of Secondary Education, Delhi in 2005. He had done B.Tech Biotechnology from University Institute of Engineering and Technology, Kurukshetra University, Kurukshetra in 2009. He completed M.Tech Biotechnology from University Institute of Engineering and Technology, Kurukshetra University, Kurukshetra in 2012.

Mr. Abhishek Ajmani joined the Ph.D. program in July 2014 at the Department of Biosciences and Bioengineering, Indian Institute of Technology Guwahati, Guwahati, Assam, India. He successfully completed his coursework with 7.5/10 Cumulative Point Index (CPI). He completed his Ph.D. on 18-03-2020.